Study AC loss of 2G HTS for future electric aircraft propulsion

PhD Thesis

Tian Lan

Applied Superconductivity Group
Institute for Energy and Environment
Department of Electronic and Electrical Engineering
University of Strathclyde, Glasgow

Dec 22th, 2022

Declaration

This thesis is the result of the author's original research. It has been composed by the author and has not been previously submitted for examination which has led to the award of a degree.

Signed: 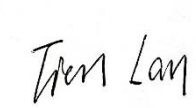

Date: 22/12/2022

Acknowledgement

First of all, I would like to express the sincerest gratitude to my supervisor, Prof. Min Zhang. For all these years, she has provided me with valuable guidance at every research stage. If it were not for the assistance she has offered to me, what I have achieved during my PhD study would not have been possible. I would also like to convey my regards to her for supporting me at various conferences and also encouraging me to take an active part in other research projects in the lab. All of this has helped me to establish myself as an independent researcher and has also given me confidence to continue my future work in the respective field.

I'm very grateful to my second supervisor Prof. Weijia Yuan for academic support during my PhD. I would like to thank Prof. Graeme Burt and Richard Munro. I truly appreciate the great work environment they offer and the expert technical support they have provided throughout my PhD.

I would also like to acknowledge the support of my colleagues in the Applied Superconductivity Group at the University of Strathclyde. I would like to express my gratitude to all my lab mates, especially Dr Fangjing Weng, Dr Muhammad Zulfiqar Ali, Muhammad Haseeb Iftikhar, Felix Huber, Abdelrahman Elwakeel, and Hengpei Liao for their continuous support throughout my PhD study.

Many thanks to Fujikura Ltd for providing me with the HTS samples, which helped me to acquire a lot of useful experimental data for this thesis.

Last but not least, I would also like to thank all my friends for their companionship and encouragement, and my parents for having always loved me unconditionally and being extremely supportive financially and mentally over the years.

Publications during PhD

1. Lan Tian, Liao H., Muhammad Iftikhar., Yuan W., Cole A., Abdouh R. and Zhang Min. (2022). Multi-filament HTS cables to reduce AC loss: proof-of-concept experiments and simulation. *IEEE TAS*. (Accepted)
2. Weng, F., Zhang, M., Lan, T., Wang, Y., & Yuan, W. (2020). Fully superconducting machine for electric aircraft propulsion: study of AC loss for HTS stator. *Superconductor Science and Technology*.
3. Weng, F., Zhang, M., Elwakeel, A., Lan, T., Mcneill, N., and Yuan, W. (2021) Transient test and AC loss study of a cryogenic propulsion unit for all electric aircraft. *IEEE Access*.

Abstract

Superconductor technologies have attracted increasing appealing over the past decades, owing to advancements made in the material manufacturing technology and the reduction of cost. As a result, superconducting materials have received large interest and hence been widely investigated in many applications including power industries and aerospace, of which one of the most promising and popular applications is the electric machine, which plays an essential role in power generation and consumption. The second-generation (2G) high temperature superconducting (HTS) materials show great potential in situations of high magnetic field and high current density, benefiting from high energy efficiencies. Therefore, they have become a focus of superconducting research and are believed to usher in a period of development opportunities. However, there still exist many challenges related to the efficiency, cost-effectiveness, reliability, and safety of HTS machines, and the alternating current (AC) loss of HTS remains one of the most critical issues. Over the years, superconducting technology applications in electric machine have been developed and put into practice due to their significant advantages of higher efficiency and power density compared to conventional technology, which meet the requirements for future electrical aircraft propulsion. However, as the technology currently stands, the AC loss of HTS armature windings is hindering the improvement of overall machine efficiency. It has been an established understanding that the AC loss of 2G HTS windings must be accurately identified and minimized for fully HTS machine applications, in order to lower the constraint on the cryogenic cooling demand and ensure long term operation.

Aiming to push the HTS machine towards commercial use in power applications, this thesis studies the interpretation and understanding of AC loss of 2G HTS using both experimental and numerical methods, especially proposing several methodologies for AC loss reduction in 2G HTS cable. It provides a thorough study on exploring effective ways to minimize the AC loss of 2G HTS for future electric aircraft

propulsion. This thesis is divided into three parts. The first part is Chapter 1, which provides a foundation for this thesis through a review of the theory of superconductivity and AC loss, and AC loss reduction challenges for a fully HTS machine. The second part consists of Chapters 2, 3 and 4, which form the core of this thesis, and include the experimental and numerical study of the AC loss of 2G HTS coils based on several proposed AC loss reduction strategies. The third part is Chapter 5, which illustrates the AC loss measurement mechanism at temperatures lower than 77 K, including a detailed cryostat design of the HTS machine demonstrator and helium cooling system working protocol.

To sum up, this thesis discusses very interesting and useful aspects of 2G HTS AC loss reduction strategies. It is expected that this thesis will contribute to the loss quantification and minimization of 2G HTS in electric machines, providing a valuable reference for the design optimization of fully HTS machines.

Contents

List of Figures

List of Tables

Glossary of Abbreviations

1G	First generation HTS
2G	Second generation HTS
3S	Soldered-stacked-square
AC	Alternating current
B	Magnetic flux density
BCS	Bardeen-Cooper-Schrieffer
Bi-2212	Bismuth strontium calcium copper oxide superconductor ($Bi_2Sr_2CaCu_2O_{8+x}$)
Bi-2223	Bismuth strontium calcium copper oxide superconductor ($Bi_2Sr_2Ca_2Cu_3O_{10+x}$)
BSCOO	Bismuth strontium calcium copper oxide superconductor
CC	Coated conductor
CF	ConFlat
CORC	Conductor on round core
DAQ	Data acquisition
F	Flow rate
FEM	Finite element method

GM	Gifford-McMahon
GdBCO	Gd-Ba-Cu-O ($GdBa_2Cu_3O_{7-\delta}$)
H	Magnetic field
HTS	High-temperature superconductors
I_c	Critical current
J_c	Critical current density
J_e	Engineering critical current density
LaBaCuO	Lanthanum barium copper oxide
LN_2	Liquid nitrogen
LTS	Low-temperature superconductors
MgB_2	Magnesium diboride
MW	Megawatt
NbTi	Niobium–titanium
NdFeB	Neodymium iron boron magnets
NI coil	No-insulation coil
p	Machine pole pair number
P&ID	Piping and instrumentation diagram
PIT	Powder-in-tube

PM	Permanent magnet
PTFE	Polytetrafluoroethylene $(C_2H_4)_n$
R	Resistance
ReBCO	Rare-earth barium copper oxide
SLPM	Standard litres per minute
Tl-Ba-Ca-Cu-O	Thallium barium calcium copper oxide
V	Voltage
YBCO	Yttrium barium copper oxide ($YBa_2Cu_3O_{7-x}$)

Chapter 1

Introduction

1.1 Background

With the rapidly increasing demand for power worldwide, new solutions are needed for development in areas such as power transportation, power distribution, and electric machines. Superconductivity can be the key to these new challenges, especially in solving problems for electric aircraft propulsion. A superconductor has zero resistivity in its superconductive state, meaning it has zero energy loss and is therefore particularly useful in situations where there is a requirement for high current transmission as there is no energy or power loss across them. One of the main advantages of superconducting cables is their ability to carry high currents compared to conventional cables with the same diameter. This advantage is beneficial to electric machines for aircraft propulsion which demand high power density, however, they cannot lower the weight and size of the associated cooling system. The power density in superconducting machines can be significantly increased compared to conventional machines with copper windings. Hence, owing to their decreased volume and weight, superconducting machines can play a paramount role in many electrical applications.

In 1986, the high temperature superconductor (HTS) ($T_c > 77$ K) was discovered by a group of IBM researchers [1]. They succeeded in inducing superconductivity in a lanthanum barium copper oxide (LaBaCuO) at a temperature of 35 K. This discovery opened the door to the discovery of more high-temperature materials and other superconducting applications. High temperature superconductors (HTS) have shown great potential in many electrical applications over low temperature superconductors (LTS). They can be operated at relatively higher temperatures while still having large

current densities, thereby tremendously increasing the machine power density and improving the overall efficiency. The commercialization of HTS conductors began in the 1990s, with initial focus on bismuth strontium calcium copper oxide (BSCCO), the so-called first generation (1G) HTS [2]. BSCCO was the first HTS material to be used for making practical superconducting wires. The manufacturing process of 1G conductors requires silver, which makes up the majority of the cost. The second generation (2G) HTS yttrium barium copper oxide (YBCO) was discovered in 1987 [3]. 2G HTS conductors can carry high current densities in external magnetic fields and exhibit superior mechanical performances. Compared to 1G HTS conductors, the preparation of 2G HTS conductors does not require a noble metal, so the manufacturing process is more cost-effective. Since 2005, long lengths of 2G HTS conductors have become commercially available. Their potential operation at relatively high temperatures makes them good candidates for power applications, including HTS magnets [4], HTS electrical machines [5], HTS cables [6], and HTS energy storage systems.

However, using superconducting technologies for future electric aircraft propulsion requirements is still being investigated and desperately requires more research. Due to the heavy cooling penalty, AC loss in the HTS stator has become one of the key topics in HTS machine design. Based on this, one of the biggest challenges facing superconducting technologies is how to accurately estimate and reduce AC losses for armature windings that use HTS coils in AC electrical machine environments. The changing currents and magnetic fields inside 2G HTS coils lead to heat dissipation, which is considered as the AC loss of 2G HTS coils. These AC losses are difficult to remove at low temperatures, thus adding an extra burden to the aircraft cooling system. To address these challenges, both experimental [7];[8];[9] and numerical methods [10];[11];[12] have been investigated by researchers around the world.

1.2 Report structure and purpose

This thesis focuses on the interpretation and understanding of studying AC loss of 2G HTS using both experimental and numerical methods, especially proposing several methodologies for AC loss reduction of 2G HTS cable. It provides a thorough study on exploring effective ways to minimize the AC loss of 2G HTS for future electric aircraft propulsion, which addresses the aforementioned challenges and enables systemic optimization of machine design. By means of the electrical and calorimetric measurement methods, the AC loss reduction achieved by different strategies for 2G HTS coil used as armature windings can be characterized, thus contributing to optimizing HTS machine design and improving overall efficiency for aircraft propulsion applications.

Chapter 1 provides an introduction to superconductivity and describes the AC loss theory, as well as the reasons why fully HTS machine should be applied for electric aircraft propulsion. The fundamental principle of superconductivity and AC loss is introduced through a review of major theories in the history of superconductivity research. The fully HTS machine concepts are illustrated through specific examples proposed by major aircraft companies and worldwide institutions.

Chapter 2 introduces the HTS coil experiments. It starts by selecting the insulation materials for 2G HTS coils, then continues to the experimental measurements of critical current and AC loss. Both the electrical and calorimetric methods are used to characterize the AC loss performance of 2G HTS coils under self-field conditions as well as real machine environments.

Chapter 3 proposes three different AC loss reduction strategies, investigating the AC loss reduction rate based on each methodology. It gives a detailed comparison

between different strategies through experimental measurement results, offering possibilities to improve the cable performance and optimize the motor armature winding design.

Chapter 4 introduces the 2D H-formulation modelling of HTS coils. It describes the modelling of superconducting coils using the finite element method in detail, including validation of the experimental transport loss results for tested coils and further extended exploration based on empirical data to evaluate the proposed AC loss reduction strategies. The impact on total transport AC loss of the presence of the soldering stack in multi-filament coils is also presented by numerical modelling.

Chapter 5 describes AC loss measurement at operating temperatures lower than 77 K based on the methodology employing helium gas as coolant. It starts by introducing the cryostat design for a novel fully HTS demonstrator as a background information. Then, it illustrates the testing set-up procedures, and the calibration method and measurement principles for the machine system. Last, the challenges of estimating the AC losses from a 2G HTS coil at temperatures lower than 77 K are also described.

Chapter 6 summarizes this thesis and describes future work.

1.3 Thesis contributions

The main contributions from this thesis can be summarized as follows:

1. Three effective AC loss reduction strategies are proposed: 3S coil, striated coil, and multi-filament coil. They are experimentally tested and then validated using FEM models based on the numerical modelling method using COMSOL software. All of these methodologies can contribute to minimizing the AC loss of 2G HTS coils as

stator armature windings for a fully HTS machine. Different reduction rates for 2G HTS coils obtained from self-field transport loss and total loss under a 0.45 T rotational magnetic field are presented and compared. Therefore, it can provide a significant reference for HTS machine motor design and improve the overall machine efficiency.

2. A novel way to develop multi-filament HTS coils is proposed, mainly focusing on suppressing the coupling losses by reducing the contact resistivity within the HTS coils. Heat shrink tubes are used to directly insulate narrow HTS filaments into a cable structure. Using the calorimetric boiling-off of liquid nitrogen, the total loss measurement in a peak 0.45 T rotational magnetic field is characterized for this new multi-filament coil. According to the results, the total AC losses of HTS stator windings with multi-filament coil show considerable loss reduction up to around 50% compared to standard 4 mm coil, since employing heat shrink tubing mostly eliminates the eddy losses and coupling losses originating from the soldering stack connections, leading to lower AC losses. This method can therefore be highly competitive for future aircraft prolusion applications. Also, this method can be further applied to a thinner multi-filament coil, which can be expected to achieve greater AC loss reduction.

3. Design of a novel HTS machine demonstrator using helium gas circulation system. The full details are presented for the design of a 200 kW fully HTS machine demonstrator. Using helium gas as the coolant, the temperature of the key positions of the HTS machine can achieve less than 30 K, which can further improve the performance and power density of the machine.

1.4 Introduction to superconductivity

1.4.1 Basic characteristics of superconductivity

Superconductivity is widely perceived to be a phenomenon of zero electrical resistance. In a superconductor the resistivity drops abruptly to zero when the material is cooled below its critical temperature. Another way to demonstrate this property is by inducing a persistent current in a circuit loop. An electric current flowing through a loop of superconducting wire can persist for a long time without a power source. More precise measurement reveals that the resistance of a superconductor is smaller than $10^{-25}\,\Omega\cdot\mathrm{m}$ [13]. For reference, the resistance of copper is $10^{-8}\,\Omega\cdot\mathrm{m}$ at room temperature, and 10^{-10} Ω·m at 77 K liquid nitrogen temperature. This property is traditionally named zero-resistance or ideal conductivity.

Most superconducting devices own the fundamental property that they are able to carry current without energy dissipation. This feature only exists when the current density is below a certain value, which is called the critical current, I_c. If the current density exceeds I_c, the superconductivity disappears, known as quench. The critical current I_c is characterized by the current at which the electric field E_c reaches a certain value. A value of 1 μV/cm or 0.1 μV/cm is commonly used. A typical E-I curve is presented in Figure 1.1. Unlike a traditional conductor, depicted by the linear Ohm's law, the change of voltage with the current in a superconductor is highly non-linear. For a superconductor, it is usually described using the E-J power law [14]:

$$E = E_0\left(\frac{J}{J_c}\right)^n \tag{1.1}$$

where E_0 is defined as $10^{-4}\ \mu\mathrm{V/m}$, J_c is the critical current density measured when the electric field reaches E_0, and n is a particular characteristic of the HTS dependent on the material properties and its microstructure, which determines the stiffness of the E-J curve, normally 20–30 for Type II superconductors.

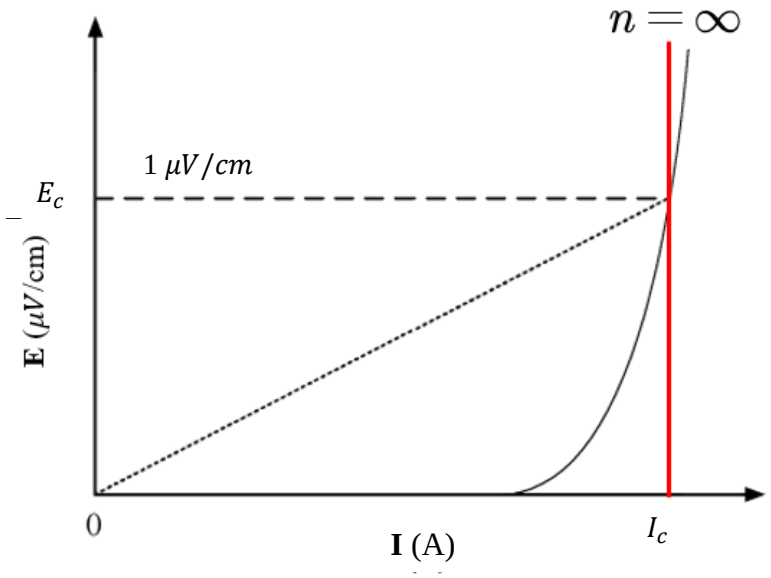

Figure 1. 1. *Typical E-I curve of superconductors*

Except for zero-resistance as a straightforward way to define superconductors, another criterion for characterizing superconductivity is the Meissner Effect [15]. A superconductor cooled below its superconducting transition temperature expels the magnetic field and does not allow the magnetic field to penetrate inside it. This phenomenon in superconductors is called the Meissner Effect, which describes the ideal diamagnetism of a superconductor. It was discovered in 1933 by the German physicists Walther Meissner and Robert Ochsenfeld. They noticed that superconducting tin and lead samples cancelled nearly all interior magnetic fields when the temperature was below a critical temperature.

The Meissner Effect is similar to diamagnetism in other normal materials. The difference is that superconductors can expel the magnetic flux completely, showing that they are perfect diamagnetic materials. Ideal diamagnetism means that the material expels the entire magnetic flux from its interior (B = 0 inside the sample), while ideal conductivity means that the material conserves its interior magnetic field (dB/dt = 0). When a magnetic field is applied after cooling the sample below its critical temperature, no difference can be observed between a superconductor and an

ideal conductor, since the magnetic fields inside the sample remain unchanged (zero) for both. When the magnetic field is applied before the sample is cooled down, however, an ideal diamagnet will expel the entire magnetic field from its interior, while an ideal conductor will conserve the magnetic field. Figure 1.2 illustrates the difference between an ideal conductor and a superconductor in terms of expelling a magnetic field.

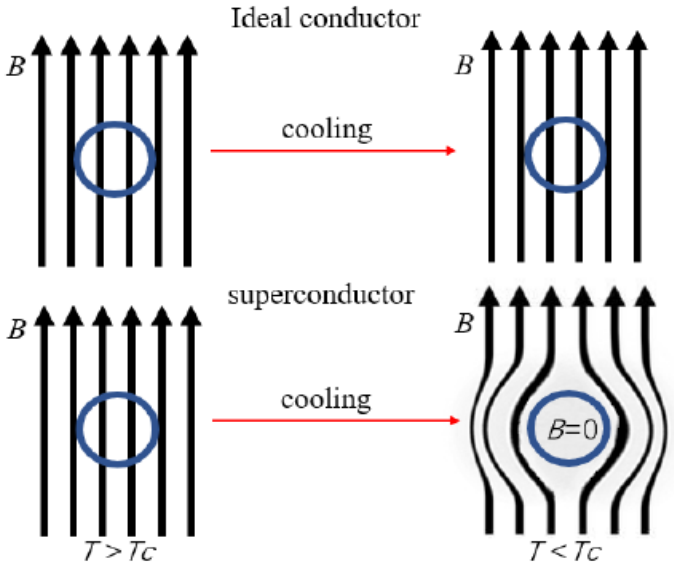

Figure 1. 2. *Illustration of the Meissner Effect under field cooling conditions*

The existence of superconductivity is highly dependent on the surrounding physical conditions, which can be defined by three typical major parameters: temperature, magnetic field, and current density. Each parameter has its own critical value, defined by the superconducting/normal transition process, denoted by T_c, H_c and J_c. For example, the critical temperature of certain superconductors marks the emergence of superconductivity when the conductor is continually cooled. The relationship between critical temperature, critical magnetic field, and critical current is very complex as shown in Figure 1.3, in which the marked area describes the superconducting region. The characteristics of superconductivity can only be present if the conductor's current density, temperature and magnetic field lie within this area.

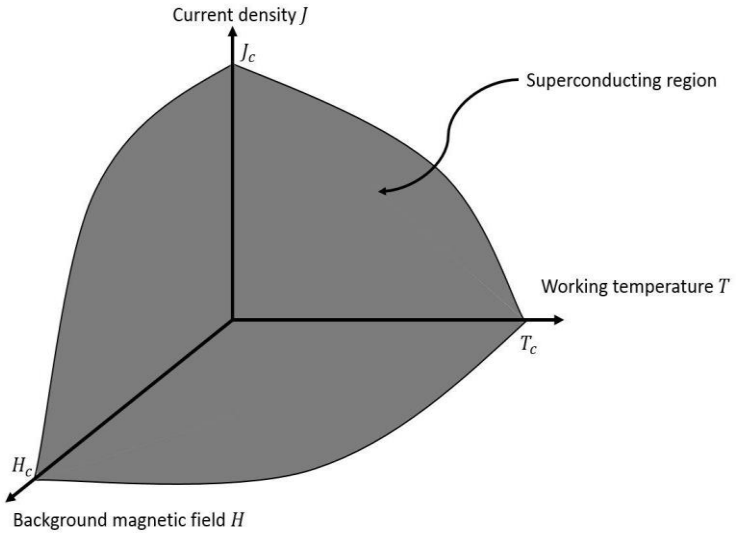

Figure 1. 3. *The critical surface of T-H-J for superconductors. The marked zone within the surface is the superconducting region, and the remainder of the zone is the normal region*

- Critical temperature T_c

The critical temperature of a superconducting material is the temperature at which the material changes from the normal conducting state to the superconducting state. This transition from the normal conducting state to the superconducting state is sudden and complete. Hence, we can know that superconducting materials work in two different states: the superconducting state and the normal state. The characteristics of superconductivity only appear when the temperature T is below the critical temperature T_c of the materials. The value of the critical temperature differs from one material to another.

- Critical magnetic field H_c

When a superconductor is placed in an external magnetic field, where if it exceeds a certain value, the superconductor will lose its superconductivity. Therefore, the magnetic field strength that causes the superconductor to lose superconductivity is defined as the critical magnetic field strength, denoted by H_c.

- Critical current density J_c

In spite of the fact that superconductors are able to carry current with zero resistance,

their current capacities are limited to some degree. As the current increases, the superconductivity will disappear above a certain current value. The current value at which the superconductor loses its superconductivity is defined as the critical current density, denoted by J_c, which is given by I_c divided by the cross-sectional area S of the superconducting region: $J_c = \frac{I_c}{S}$. In practical applications, however, the engineering critical current density J_e is more often used as a vital quantity of superconductors, since superconductors normally consist of several layers not just superconducting layer, which is described in detail in section 1.4.5. This value is obtained by dividing I_c using the cross-section of the whole wire, including the superconducting area and the normal conductor area [16].

1.4.2 Low temperature superconductor (LTS) and High temperature superconductor (HTS)

Superconductors can be classified in different ways. According to their critical temperature, superconductors can be categorized into low temperature superconductors (LTS) and high temperature superconductors (HTS). The general idea of defining an LTS material is to see whether it follow the classical Bardeen-Cooper-Schrieffer (BCS) theory or not. The BCS theory was first proposed by John Bardeen, Leon N Cooper and John R Schrieffer in the year 1957 [17]. The basic conceptual element of the BCS theory is the coupling of electrons into Cooper pairs against Coulomb repulsion under a certain temperature, typically below 30 K [18]. Most LTS have low critical temperatures, no higher than 30 K. One exception, however, is the binary compound MgB_2, which has a critical temperature around 39 K. The outstanding discovery of high-temperature superconductivity by J.G Bednorz and K.A. Mueller in 1986 indicated that the worldwide research of superconductivity had officially entered a new age [1]. High-temperature superconductivity was first found in a series of materials with critical temperature ranges from 35 K to 40 K. Later, in

1987, following the footsteps of Bednorz and Muller's work, yttrium barium copper oxide (YBCO) with a transition temperature of 93 K was discovered. This transition temperature is obviously above the boiling point of liquid nitrogen (77 K) [19]. The ReBCO family was the first to be found with T_c values higher than 77 K. The rare earth elements, having similar atomic structures to yttrium, are substituted for Y and are referred to as rare-earth barium copper oxide (ReBCO). In 1988, the Bi-Sr-Ca-Cu-O (BSCCO) system was discovered by Maeda and Tallon with an even higher transition temperature of T_c = 120 K for BSCCO-2223 [20];[21]. In the same year, Z. Z. Sheng and A.M. Hermann found that the Tl-Ba-Ca-Cu-O system reaches a transition temperature of 125 K [22]. By far, the highest T_c value among all materials is obtained in the Hg-Ba-Ca-Cu-O system. In 1993, A. Schilling found superconductivity in Hg-1223 at around 133 K under ambient pressure. This value reaches around 160 K under high pressure [23].

Usually, a low operating temperature requires highly costly cryogenic systems. Liquid helium is used as the coolant for LTS, which is very expensive; while HTS, especially copper oxides, can employ liquid nitrogen as coolant, which greatly saves on cost. Compared to LTS, HTS superconductors can operate at higher magnetic field ambience and operate over a broader temperature range. All of these are the reasons why high temperature superconductors have become the focus of engineering applications.

1.4.3 Type I and Type II superconductors

From the perspective of applied magnetic field, superconductors are divided into two types. All superconductors enter a Meissner state in an external magnetic field. However, as the external field increases, the Meissner Effect breaks down. Some superconductors return to a normal state, while others enter a mixed state. Type I refers to superconductors which have only superconducting state and the normal state; while Type II superconductors have three states: the superconducting state, the mixed

state and the normal state. Figure 1.4 shows Type I and Type II superconductors in the three different states [24].

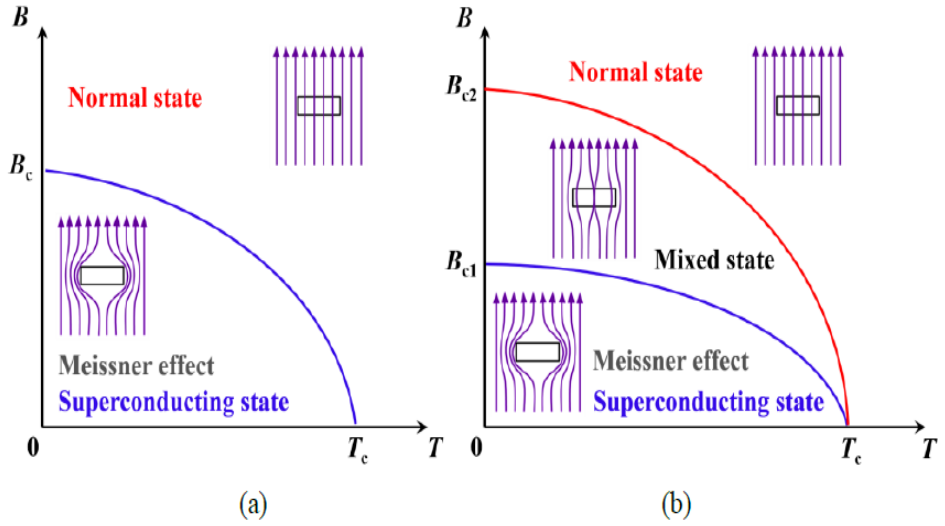

Figure 1. 4. *State transition of Type I (a) and Type II (b) superconductors with varying temperature and magnetic field*

Type I superconductors usually have a very small value for the critical field B_c and are mostly metals and metalloids, such as Hg, Al, Sn, and In. As shown in Figure 1.5 [25], Type I superconductors remain perfectly diamagnetic below the critical magnetic field (B_c), and the superconductors enter a normal state suddenly when the external field exceeds B_c.

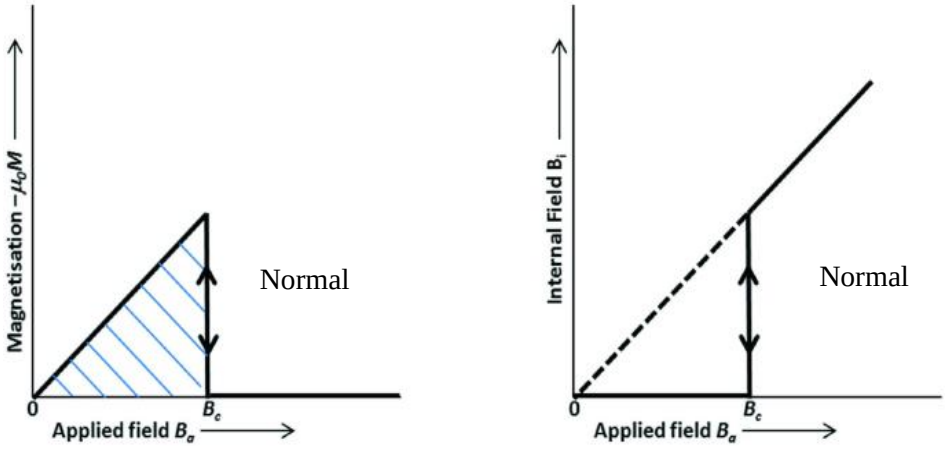

Figure 1. 5. *The magnetisation characteristics of Type I superconductors*

In comparison with Type I superconductors, Type II superconductors are cable of carrying larger amounts of current in higher magnetic fields, and they have two critical magnetic fields: an upper critical field B_{c2} and a lower critical field B_{c1}. The magnetisation characteristics of Type II superconductors are shown in Figure 1.6 [25]. When the magnetic field is lower than B_{c1}, Type II superconductors are in the superconducting state. The state involving partial penetration of magnetic flux is called the mixed state, which occurs when the magnetic field is lower than B_{c2} and higher than B_{c1}. In the mixed state, the magnetization of the type II superconductor decreases monotonically with an increasing applied field, until the applied field reaches the upper critical field. When the magnetic field is over B_{c2}, Type II superconductors enter into a normal state.

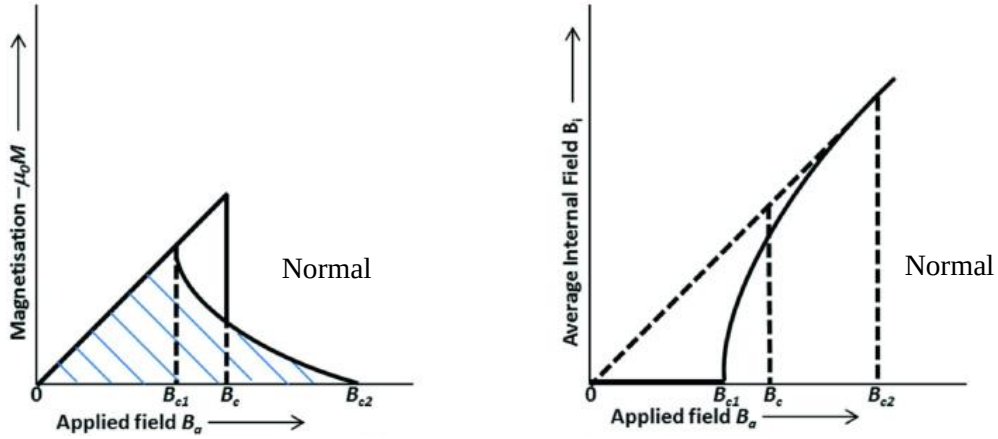

Figure 1. 6. *The magnetisation characteristics of Type II superconductors*

Examples of type II materials are alloys and compounds, such as Nb_3Sn, NbTi, MgB_2, and all high temperature cuprates. The critical fields B_c for type I superconductors are relatively low, usually not more than 100 mT (at a temperature of 4.2 K, B_c is 41 mT for mercury, 80 mT for pure lead), which means even a self-field can destroy the superconducting state. Applications of Type I superconductors are therefore limited. On the other hand, the upper critical fields B_{c2} of type II superconductors can be very high (at a temperature of 4 K, B_{c2} is 12 T for NbTi, 27 T for Nb_3Sn, 15 T for MgB_2,

and normally more than 100 T for YBCO and Bi-2223 [26]), indicating their promise for use in large-scale power applications. Moreover, all HTS materials are Type II superconductors. Hence, this thesis primarily focuses on type II superconductors.

1.4.4 Vortex and flux pinning in Type II superconductors

Inside a superconductor, the magnetic flux density does not penetrate in a homogenous way but locally in disconnected volumes called vortices [27]. Type II superconductors have some impurities and crystalline defects such as dislocations, voids, grain boundaries, etc., so that flux vortices are prevented from moving within the bulk of the superconductor, and the magnetic field lines are "pinned" to those locations. This phenomenon is known as flux pinning [28], and the impurities or crystalline defects are named as “pinning centres” [29]. In principle, every inhomogeneity of the material that is less advantageous for superconductors would act as a pinning centre, and the vortices attempt to occupy the most energetically favourable locations.

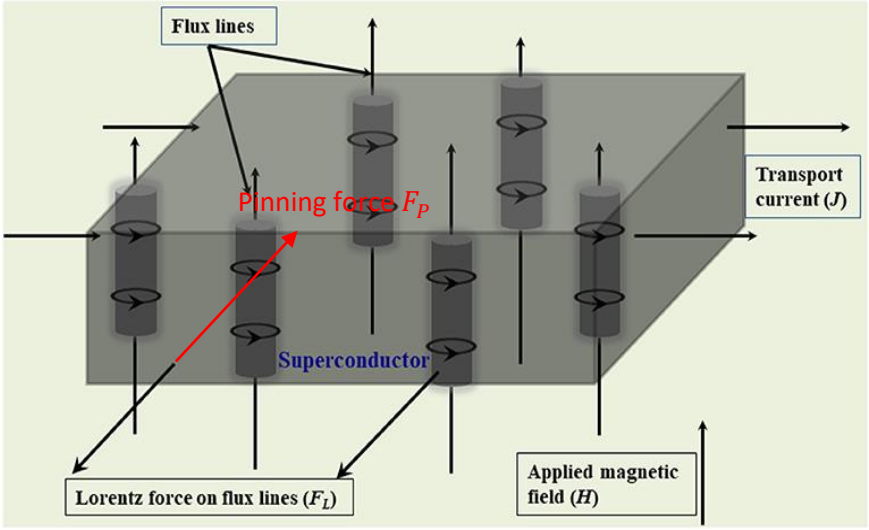

Figure 1. 7. *Magnetic flux starts penetrating the sample in the form of small “tubes” (vortices). Lorentz force* $\boldsymbol{F_L}$ *and pinning force* $\boldsymbol{F_P}$ *on the vortex in Type II superconductors [30]*

In most engineering applications, Type II superconductors rely upon the mixed state, in which they are able to carry large currents in strong magnetic fields. In the mixed state, when a Type II superconductor is placed under a transverse field and a transport current, the vortices will be subjected to Lorentz Forces $\mathbf{F_L}$ according to $\mathbf{F_L} = \mathbf{J} \times \mathbf{B}$. Due to the influence of this Lorentz force, the vortices start to move in a direction perpendicular to the directions of both the transport current and the applied magnetic field, as illustrated in Figure 1.7 through a schematic representation of this situation. The force which resists the motion of the vortices under the influence of the Lorentz force is called the pinning force $\mathbf{F_P}$. In order to avoid the movement of the vortex in the direction of the Lorentz force, the pinning force $\mathbf{F_P}$ should be greater than the Lorentz force $\mathbf{F_L}$. In this case, current is capable of flowing without heat dissipation.

For a large enough Lorentz force, the vortices become de-pinned and move in the direction of the force with velocity $\mathbf{v}$. This vortex movement generates an electric field $\mathbf{E} = \mathbf{B} \times \mathbf{v}$, which is parallel to the current, so that the superconductors have electrical resistance. These forces will induce vortices displacement and then energy dissipation inside the material, which is due to two fundamental processes. The first loss is associated with the appearance of local electric fields generated by the moving vortices. This local electric field can accelerate the unpaired electrons, delivering energy from the electric field to the lattice, and thereby generating heat [24]. The second loss is caused by the spatial variation of the Cooper pair density in a vortex, which increases from its value of zero in the vortex centre toward the outside [31].

The pinning effect can also be understood simply considering the perspective of energy, meaning that the pinning centres are surrounded by an energy barrier which the pinned vortex must climb before it can move. The Lorentz force effectively lowers this barrier and when the pinning force is balanced by the Lorentz force, the critical current density J_c of a superconductor would reach [30]. Therefore, the critical current density J_c of Type II superconductors can be defined as a measure of $\mathbf{F_P}$, when $\mathbf{F_L}$ produced by the J_c equals the pinning force $\mathbf{F_P}$. Provided the current exceeds J_c, vortices start to move, and thereby electrical resistance appearing.

1.4.5 1G HTS and 2G HTS

Currently, two types of HTS conductors have been available to the worldwide market for use in making different HTS devices for many applications. They are known as first generation 1G HTS, usually referring to BSCCO (Bi-2212 and Bi-2223) made with powder-in-tube (PIT) methods, and second generation 2G HTS referred to ReBCO, which comprises multiple coatings on a base material or substrate. Figure 1.8 shows the basic structure comparison between 1G HTS and 2G HTS tapes.

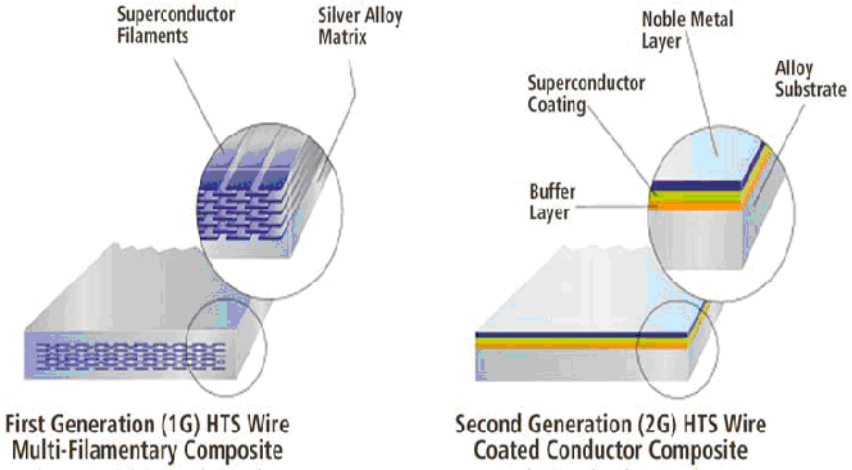

Figure 1. 8. *First generation (1G) versus second generation (2G) HTS tape [32]*

Whilst the manufacturing technology of BSCCO wires is well developed and high-quality BSCCO tapes are available commercially in kilometre lengths with critical current up to 150 A [33], BSCCO wires are still probably not suitable for the large-scale replacement of conventional power equipment with HTS counterparts. The main reason is the prohibitive cost of BSCCO compared to conventional copper or aluminium conductors, and the need for considerable increase in the critical current (I_c) and the engineering current density (J_e) of the superconducting wire, since BSSCO tapes are fabricated using a powder-in-tube (PIT) technique followed by a sintering process. Due to the limitations of the PIT method, there is no control over

the grain alignment, leading to poor inter-grain electrical conductivity, requiring the sheath material to be a good electrical conductor to provide the low resistance inter-grain electrical contact. This makes the BSCCO dependent on silver, removing any further scope for cost reduction. As a result, the costly wire affects the large-scale industrial application and commercial use of HTS seriously. The anisotropy of BSCCO tapes is an additional concern, especially in applications with magnetic fields having a non-negligible perpendicular component, in which the BSCCO wires demonstrate a faster decay of the critical current in the perpendicular magnetic field compared with the ReBCO wires [34]. Last but not least, the alloy sheath is used in order to effectively increase the strength of Ag-sheathed BSCCO (Bi-2223) tapes. However, it also thus caused the J_c value of alloy sheathed tapes not high enough since the undesired reaction to form impurity phases and the change in formation rate of Bi-2223 were disturbed by the microstructure of the filaments [35]. According to the experimental results on Ag-sheathed BSCCO (Bi-2223) tapes, due to the lowering of the critical current density, there is a drastic increase in transport losses caused by external transverse magnetic fields [36];[37]. Therefore, the loss level in AC applications for BSCCO tapes is also a significant issue that needs to be taken into account. To sum up, in consideration of the anisotropy of BSCCO tapes in perpendicular magnetic field, the AC loss problem due to the relatively low I_c, and particularly the unavoidable high cost, BSCCO tapes still remain critical challenges to be utilized for the large-scale industrial applications and commercial use.

On the other hand, YBCO tapes are manufactured using a coated conductor (CC) technology, resulting in a large degree of control over the orientation of crystals on the tape surface leading to high current densities. YBCO superconducting tape is generally composed of a base layer, a transition layer, a superconducting layer, and a protective layer [38], as shown in Figure 1.8. It has a higher critical magnetic field and current density than 1G HTS. The main components of 2G HTS are cheap metals such as Hastelloy, stainless steel or copper, and YBCO thin film. The production process requires only a minimal amount of silver (usually 1–3 μm thick) and no other

expensive metals. Hence, compared to 1G HTS, 2G HTS has more advantages in reducing tape cost and is expected to satisfy commercial use widely. This thesis therefore only emphasizes the investigations of 2G HTS tape.

1.5 Fully superconducting machine concepts

1.5.1 Introduction to fully HTS machine

To push the electrical machine toward the high-power density applications, both stator and rotor windings can be replaced with HTS coils, producing an HTS machine. The current density in stator windings can be significantly increased due to the HTS coils increasing the operating current. The size and weight of rotor windings can be considerably reduced compared to a conventional copper coil or permanent magnet because the iron core is removed. While the best permanent magnets can have a magnetization of up to 1.3 T [39], HTS permanent magnets made from HTS bulks or HTS stacked tapes are capable of providing much higher magnetic fields, in which a silver-doped Gd-Ba-Cu-O (GdBCO) bulk with a stainless steel ring as a reinforcement has achieved a 17.6 T trapped field [40], and the highest magnetic field achieved by HTS stacked tapes is 17.7 T [41]. By using a smaller volume of field winding owing to the high-current-carrying capability of superconductors, it is possible to generate much higher air-gap field strength, thus being able to exceed 1.3 T, which can solve the problem that the magnetic field strength in the air gap of conventional machines is limited by the saturation of iron teeth on the rotor and stator [42].

Generally, HTS machines can be divided into two categories, referring to partially superconducting machines and fully superconducting machines. The majority of technology demonstrations to date have been with partially superconducting technology for wound field winding synchronous topology, since it is straightforward to use and can achieve higher efficiency and lower weight than using copper field winding in conventional machines [42]. In a partially superconducting machine, the

armature windings remain unchanged conventional copper-based coils whilst the rotor windings are replaced with superconducting materials. Many industries and research institutes have successfully demonstrated partially superconducting machines in which superconducting windings are used solely on the rotors, where the transport current is DC, and the background field is stationary relative to the rotor in the synchronous machine. Partially superconducting machines have the potential for increased specific power with complete elimination of ferromagnetic components and higher operating flux density, due to more matured HTS materials capable of high fields at high temperatures, and composite structures developed to replace the relatively heavy vacuum vessels and torque tubes [42]. It has already been confirmed that a partially superconducting machine can achieve a very high-power density and high efficiency (99%), however, most power dissipation is from the copper armature windings. This could be further reduced by using HTS coils in the stator.

To date, most projects regarding superconducting machines have focused on a superconducting rotor combined with a conventional copper stator winding [43]. The major drawback of this design is that the thick cryogenic shell between the “cold” rotor and the “warm” stator greatly increases the air gap, which reduces the magnetic field in the stator winding. A fully superconducting machine, enabled by a superconducting stator winding, is a much better solution in terms of coupling the rotor and stator to produce a stronger magnetic field [44]. When superconducting windings are used for both stator and rotor windings, the machine is referred to as a fully superconducting machine. A fully superconducting machine has the potential to attain the highest efficiency as the superconducting windings can minimize the power dissipation in both rotor and stator. To attain these levels of losses, however, significant achievements must be made for acceptable superconductors. Since partially superconducting machines are already projected to achieve 99% efficiency with most losses occurring in the conventional copper windings, to obtain superior efficiency, the AC losses in a superconducting armature must be significantly less than 0.1% of the machine rating to keep the required refrigeration reasonable, since 0.1% of losses

on a high-power machine is still a very large amount of losses for a cryogenic system [45]. This has to be achieved by a minimized AC loss design on the stator windings for fully superconducting machines, in order to be competitive with partially superconducting machines. Due to the stator windings operating in an AC magnetic field and carrying AC current, both magnetization loss and transport loss exist in them. Therefore, in this case, these losses must be appropriately evaluated and quantified for improving the machine design.

Superconducting windings can be designed with either LTS field windings or HTS field windings. Three possible conductors are being considered for armature windings: BSCCO, YBCO, and MgB_2. Various standard machine topologies can be used in superconducting machine design: wound-field-synchronous machine, PM synchronous machine, HTS bulk magnet machine, etc. For a synchronous machine, topologies can be either axial flux or radial flux. Different fully superconducting machine prototypes have been successfully developed by many research institutes worldwide. A fully superconducting machine for an electric vehicle [46] and a liquid nitrogen-cooled fully superconducting machine for ship propulsion [47] were built in Japan. A fully superconducting prototype with YBCO stator coils operating in liquid nitrogen bath was developed in Cambridge, UK [48] and a fully superconducting machine cooled by iron conduction was built in China [49]. Fully superconducting machines have also been proposed for offshore wind turbine applications [50]. Figure 1.9 shows an example of a fully superconducting machine configuration.

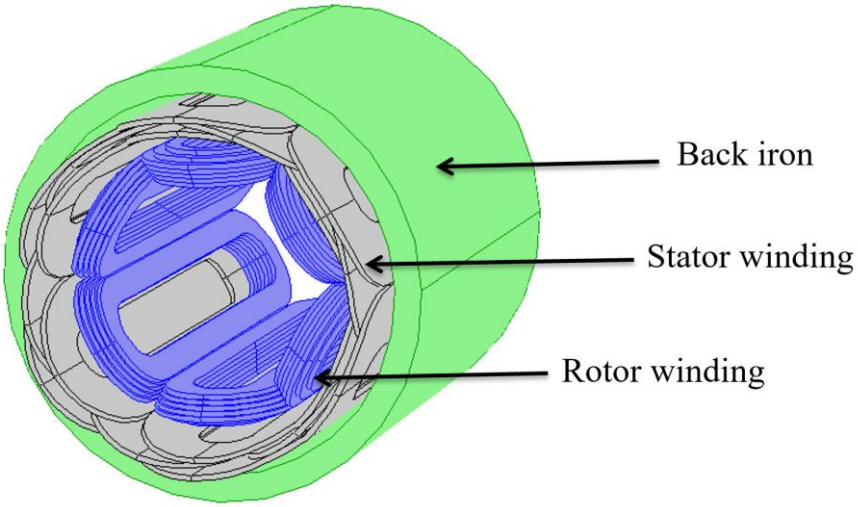

Figure 1. 9. *An example of a fully superconducting machine configuration [51]*

1.5.2 Road map of the superconducting machine

Superconducting technology applications in electric machines have been developed and put into practice over recent decades due to their significant advantages of higher efficiency and power density over conventional technology. Many HTS machine prototypes or machine testing rigs have been successfully demonstrated by many research institutions around the world. However, commercial adoption has been very slow in spite of the many successful technology demonstrations, presumably because the limitation for value versus cost and technology risk has not yet been crossed, especially for the full-size MW-class machine. Currently, HTS tape is still quite expensive for commercial uses. Additionally, although liquid nitrogen is favourable in terms of ease of availability and cheap price, and suitable for use in HTS device testing, the operating temperature of liquid nitrogen cooled power devices is limited to 77 K. Cryogenic systems that need to operate at temperatures lower than 77 K still require highly costly coolant. The other factor is stability: HTS material is a ceramic material, and very fragile and easy to damage through either coil quench or mechanical shock, and a commercial operating environment is usually complex

compared to the laboratory environment. Thus, no significant progress has been achieved, especially in terms of using HTS machines in commercial applications. To use HTS machines in engineering, more research is deemed necessary to evaluate the viability of future HTS systems [42];[52]. Table 1.1 shows some past superconducting machine demonstrations developed by a variety of research institutes.

Table 1. 1: Superconducting machine demonstrations

Year	**Speed (rpm)**	**Power (kW)**	**Conductor type**	**Cryogenic cooling**	**Efficiency (%)**	**Application**	**Developer**
1978	3600	20000	NbTi	Liquid He	99.3	Utility	GE [53]
1978	3600	1200000	NbTi	Liquid He	99.6	Utility	Westinghouse [54]
1980	7000	20000	NbTi & Nb_3Sn	Liquid He	99.5	Air force	GE [55]
1997	3600	78700	NbTi	Liquid He	NA	Utility	Super-GM (Japan) [56]
2001	1800	3725	BSCCO	Neon boil-off	97.7	Industrial	AMSC [57]
2001	1500	400	Bi-2223	Ne-Thermosiphon	97	Demo	Siemens [58]
2004	3600	4000	BSCCO	Ne-Thermosiphon	98.7	Generator	Siemens [59][60]
2007	120	36500	NA	Gaseous He	NA	Marine	AMSC [61]
2008	10000	1300	BSCCO	Neon boil-off	98	Aerospace	GE [62]
2012	214	17000	BSCCO	He gas	NA	Hydro	GE (Converteam)
2019	6000	10000	Nb_3Sn	Conduction	NA	Aerospace	Illinois [63]
2020	10	10000	MgB_2	Gaseous He	98	Wind	Kalsi GPS [64]
2020	120	40000	BSCCO & MgB_2	Gaseous He	99.4	Marine	Kalsi GPS [64]
2020	10	12000	YBCO	Gaseous He	98	Wind	Changwon National University [65]

Currently, some good progress for the commercial use of HTS machines has been achieved by industry in recent years, including manufacturing HTS conductors up to 100 m in length, basically achieving quasi-industrial production, allowing critical current at lower temperatures and moderate magnetic fields, acquiring a steeper U-I curve (n-value), improved pinning, and decreasing the cost ($/kAm). However, further progress is still needed in these aspects:

- Implement the use of kilometre-level HTS tape lengths
- Improve the mechanical properties of HTS coils
- Optimize the AC loss reduction technologies
- Increase the critical current of HTS tape in higher operating temperatures and higher magnetic fields
- Enhance the HTS performance in a complex magnetic field environment
- Achieve more dedicated cooling technology
- Boost the mechanism of coil quench detection and protection
- Reduce the cost of HTS materials and the cryogenic systems
- Optimize the design of machine's structure in engineering

Over the following decades, more research in engineering will push HTS machines in scalable power to reduce product cost. It should be realized that product cost is also strongly related to the market size. Larger markets will help drive down the cost of superconductor technology and cryogenic systems. Supply chains of superconductors and other components for mass production need to be developed and improved for commercial applications employing superconducting technology. Additional operational prototypes for industrial applications should be implemented to prove performance reliability. It is also essential to make sure enough funding is available to mitigate the risks of validating the technology for industrial commercial applications.

1.5.3 Why use a fully superconducting machine for future aircraft propulsion

Electric propulsion is an age-old idea, which can achieve lower emissions, diminished noise, and reduced fuel burn, thus being able to potentially reduce operating costs for aircraft operators. However, due to the poor specific power density of electrical machines, cables, switchgear, and the resultant electrical propulsion network, it has received less academic and industrial interest. Challenges to the use of electric propulsion in commercial aviation are many and range from the batteries and motors to the wiring and cooling system. Therefore, electrical propulsion is yet to be achieved in larger and commercial aircraft, despite significant interest from major aircraft companies [66];[67]. Nonetheless, with the advancements in the field of superconductivity, many power applications which were deemed not to be plausible two decades ago are now becoming a reality [68]. Given the potential of superconductivity in power applications, considerable research is taking place to develop commercial superconducting motors with far superior power densities to conventional motors [69]. However, one of the major challenges of scaling up electric propulsion to larger aircraft is the power-to-weight ratio. In other words, today's electrical systems simply do not meet the necessary power requirements without adding extra weight to the aircraft. However, HTS technologies are emerging as a promising solution to this technical conundrum, notably by increasing power density in the propulsion chain while significantly lowering the mass of the distribution system.

According to IATA's goals from "Aircraft Technology Roadmap to 2050" [70], new aircraft must be configured to reduce fuel burn and carbon dioxide emissions, which is called electric propulsion aircraft. Although electricity is not currently emissions-free, it can be expected that the life-cycle carbon emissions will reduce considerably. Electricity can be generated by clean energy to reduce the emissions further.

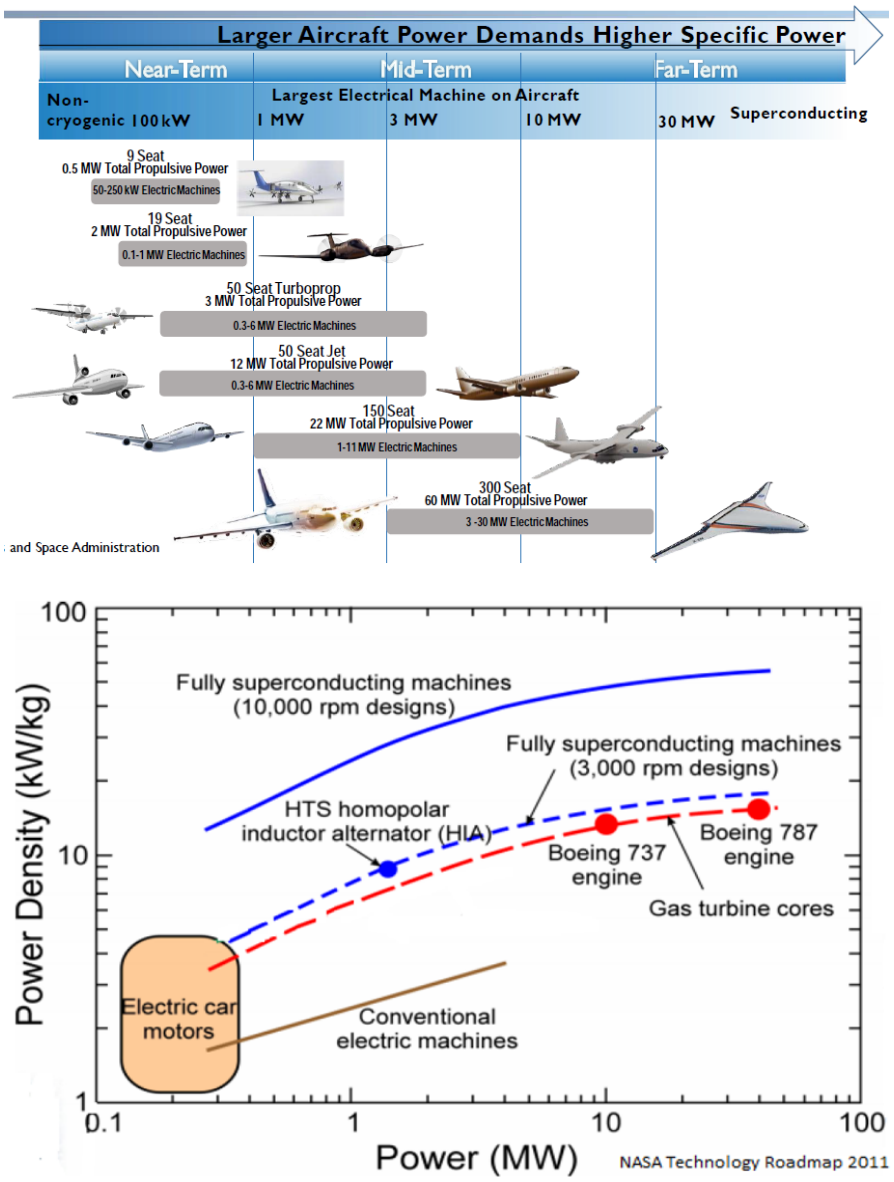

Figure 1. 10. *NASA estimates that power densities could reach above 15 kW/kg excluding the cooling systems*

Aircraft architectures with electrical networks need to be incorporated using high power density machines. For electric aircraft applications, NASA has proposed a distributed propulsion concept, estimating that power densities could reach above 15-kW/kg excluding the cooling systems, thereby reducing fuel burn to around 70%

[71];[72];[73], as shown in Figure 1.10. NASA's concept is challenging and requires advanced technology in motors, generators, power cables, and energy storage systems. The power density of a conventional copper-based machine is usually lower than 1-kW/kg, which cannot be able to meet the requirement of distributed electrical propulsion systems. It is obvious that superconducting machines hold potential for the extreme reduction in machine size and weight [42]. Thus, two large superconducting turbogenerators are set at the wingtip in NASA's design concept, and thrust is provided by 15 superconducting motors. Table 1.2 lists the specific parameters of required generators and motors.

Table 1. 2: Electrical machine requirement for turboelectric-aircraft design concept [72]

	Generators	**Motors**
Number of units	2	15
Power level	22.4 MW	3 MW
Weight	1000 Kg	236 Kg
Efficiency	99.3 %	99 %
Power density	22.4 kW/kg	12.7 kW/kg

A major breakthrough in electric propulsion for long-range aircraft could soon be on the horizon. Alongside superconducting technologies, the presence of a cold source in the form of liquid hydrogen promises to unlock new possibilities. In 2021, a project named the ASCEND demonstrator by Airbus UpNext aims to mature these technologies to significantly boost the performance of electric and hybrid-electric propulsion systems in future low-emissions aircraft, as shown in Figure 1.11 [74]. This project proposes to show that an electric or hybrid-electric propulsion system complemented by cryogenic and superconducting technologies can be more than 2 to 3 times lighter than a conventional system through a reduction in cable weight and a limit of 30 kW/kg in power electronics, without compromising a 97% powertrain efficiency. To achieve this objective, ASCEND features a 500-kW powertrain consisting of the following components: a superconducting distribution system,

including cables and protection item; cryogenically cooled motor control unit; a superconducting motor; and a cryogenic system. The ASCEND demonstrator is expected to adapt ground-based cryogenic and superconducting technologies to a fully electric powertrain to confirm their potential for use in aircraft.

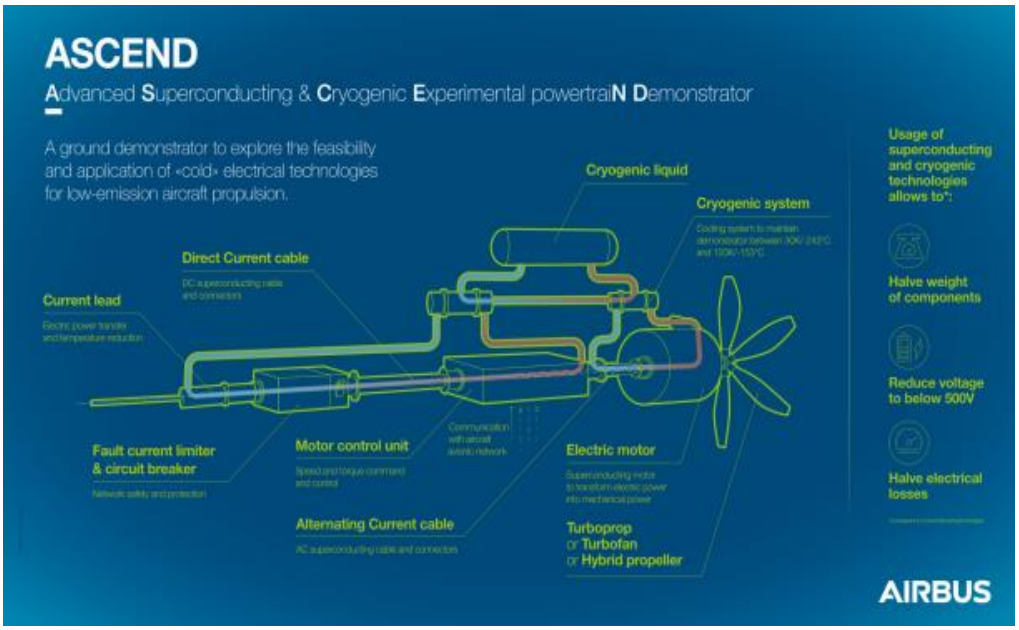

Figure 1. 11. *ASCEND: The mechanism of applying cryogenic and superconducting technologies to enhance electrical propulsion*

Therefore, to sum up, high power density machines at MW-class are considered extremely necessary for future electric aircraft. Currently, the majority of HTS machines are designed based on conventional topologies, replacing copper-based rotor windings with superconductor materials. A partially superconducting machine with an HTS rotor and copper-based stator can reach an efficiency of 99%, in which most power dissipation is still in the conventional copper-based stator windings. A fully superconducting machine using HTS windings in both rotor and stator will have the potential to reach the highest efficiency, as the power dissipation is minimized in both rotor and stator. However, the AC losses introduced in fully superconducting

machines are particularly difficult to remove at low temperatures, and these losses become compounded in high frequency situations [75]. As a result, fully superconducting machines are known to be suited for low frequency applications, however in higher speed cases, it is not as clear. Conversely, the electric propulsion system demands high speed since it can achieve the reduction of the system weight for a given magnitude of power conversion, thereby reducing fuel burn and emissions. Therefore, studying AC losses becomes a significant challenge for fully superconducting machines, and it is of paramount importance to appropriately evaluate and quantify the AC loss considering the system design optimization.

1.6 AC loss in HTS superconductors

Alternating magnetic fields and transport currents cause dissipation of energy in type-II superconductors. The energy dissipation is called AC loss. The resistance in ordinary type II superconductors arises due to flux flow and creep, typical of electrical power applications at low frequencies. Owning the capability of carrying more current in a larger magnetic field makes Type II superconductors attract a lot of technological interest and academic investigation, however, losses are induced accordingly as the existence of electric fields inside the superconductors [76]. It is essential to study AC losses in HTS, in consideration of optimizing the design for applications that make use of superconductors and improve overall efficiency. The completeness of the theory can be checked by comparing experimental data with theoretical values. Each potential electrical power application of superconductivity needs to be evaluated separately due to the different devices encountering different time-varying currents and magnetic fields.

1.6.1 AC loss types

According to the AC source that provides the energy, AC losses can generally be divided into two categories: magnetization loss and transport current loss [77];[78]. Both of these losses can be involved in superconducting applications. The two types of AC loss in superconductors are described below.

Magnetization loss is the power dissipated in the superconductor when an alternating magnetic field is applied to the superconductor, normally including hysteresis loss, coupling loss, and eddy current loss. This energy originates purely from the source of the external magnetic field without transport current. For the calculations of transport AC losses in this research, it is assumed that the superconductor-related losses are dominant, so the eddy current loss is ignored and will not be considered for the following analysis regarding to our experiment results. However, eddy current loss could be dominant at higher frequencies, which must be considered for the design of practical HTS devices. More details related to this will be discussed in section 3.5.2.

Transport current loss is the power delivered by the power supply that enables a transport current to flow through the superconductor in the absence of an external magnetic field, usually consisting of hysteresis loss and flux flow loss. The voltage along the sample can be used as a measurement for the dissipated power. In this thesis, for the investigations on AC loss measurement of 2G HTS coils, we only apply small transport currents with respect to the critical current, so the flux flow loss is not considered in our work. Since the self-field dominates at small transport currents, the flux flow loss contribution is insignificant and can be neglected.

1.6.1.1 Hysteresis loss

The AC losses in a single superconducting filament or bulk are mainly from hysteresis losses. Hysteresis loss is caused by the penetration and movement of the magnetic flux in the superconducting material [79], which can be considered as a result of irreversibility caused by vortex pinning [76]. As addressed in Section 1.4.4, due to

flux pinning in Type II superconductor, the flux has entered the superconductor does not leave in precisely the same way by which it entered, so these losses are called hysteresis losses, which is deemed as one of the essential factors impeding the commercial application of 2G HTS coils.

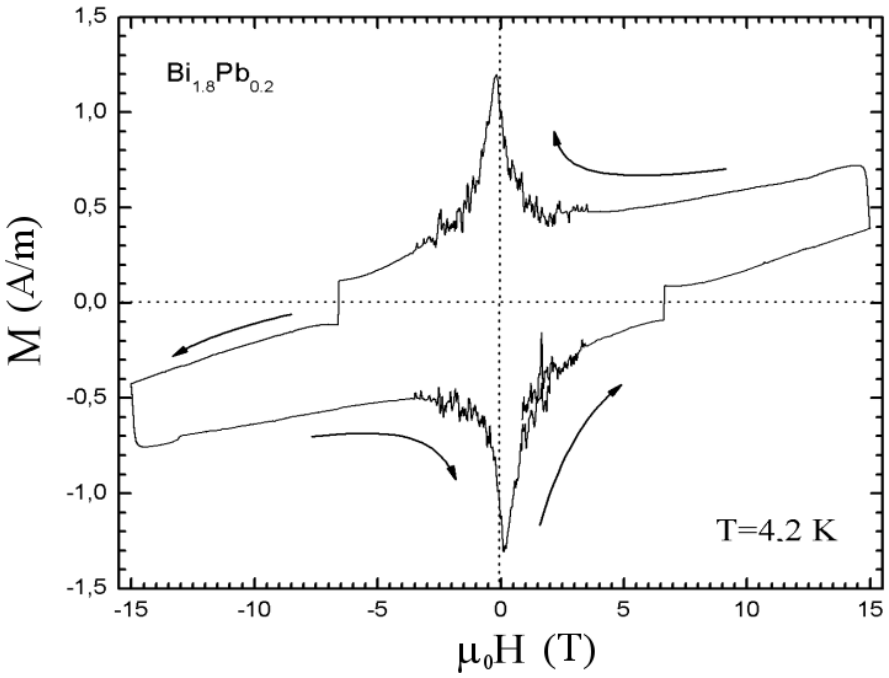

Figure 1. 12. *A Hysteresis loop of the magnetization curve in high magnetic field for HTS superconductor* $Bi_{1.8}Pb_{0.2}Sr_2Ca_2Cu_3O_{10}$ *composition as a function of applied magnetic induction (arrows indicate the direction of variation of applied magnetic field) [81]*

An example of a hysteresis loop is shown Figure 1.12, which is traversed once per cycle and illustrates the relationship between the magnetic field H and the magnetic induction M. The area of the hysteresis loop shows the energy required to complete a full cycle of magnetizing and de-magnetizing, and the energy loss per cycle is proportional to the area of this loop [77]. Such hysteresis losses are dissipated as heat and the loss becomes higher for stronger pinning. In order to achieve practical purposes, Type II superconductors must be capable of carrying a large critical current, which leads to a large Lorentz force, so a strong pinning force is required to act

against the Lorentz force and prevent the vortices from moving. Materials with a strong pinning force are therefore referred to as hard superconductors. And the larger the critical current of a hard type II superconductor, the larger the hysteretic losses [80].

Normally, the hysteresis loss can be generated either by an external magnetic field or transport current. Even if there is no external magnetic field, with an alternating transport current, the alternating self-field (a transport current in a superconductor generates a magnetic field around the conductor) penetrates the superconductor during each current cycle, and the variation of the self-field inside the material can still cause a hysteresis loss, which is called self-field loss. In transport current losses, the hysteresis losses account for relatively large portion, which is quite significant.

1.6.1.2 Coupling loss

There are two main contributions to the coupling losses in superconducting structures with filaments, strands, stripes or striations: between neighbouring (adjacent) strands or filaments, and between strands crossing on the opposite sides [82]. Whilst striation reduces the hysteretic loss in comparison with a single tape, due to the coupling between separate filaments, the new introduced loss in the form of coupling loss could be a significant problem in multi-filament conductors, even tremendously more than the self-field loss in an uncoupled tape carrying the same current. For BSCCO conductors consisting of multiple superconducting filaments within a silver sheath [77];[83], the coupling loss could be dominant and difficult to eliminate. For YBCO conductors, if the tapes are striated into filaments, it will also be a problem as large coupling losses are induced by filaments coupling together. An eddy current induced by the varying magnetic field flows partly through the superconductor and also through the silver between the filaments. When currents flow from one filament to another, they can couple the filaments together into a single large magnetic system, which encounters a resistance along the current path through the silver matrix. This ohmic loss in the metal matrix is often called the coupling loss [78];[84]. The power

dissipated by the coupling currents is given by the following equation:

$$P = \frac{1}{\rho_t}(L \cdot \frac{dB}{dt})^2 \quad (1.2)$$

where ρ_t is the effective transverse resistivity of the strand, dB/dt is the variation rate of the external magnetic field, and L is the length of the superconductor.

In order to effectively reduce the coupling loss for multi-filament conductors, ideally, twisting the filaments into strands as well as the substructures of the cable is adopted. However, the requirement for stability against electromagnetic perturbations does not allow the use of matrix materials with very high resistivity. Hence, the compromise solution is to manufacture cables in more stages of twisting and cabling process. Coupling loss is a major issue investigated in this thesis, since we propose a new AC loss reduction strategy which mainly focusing on suppressing the coupling losses for multi-filament coils. In that case, heat shrink tubing is employed as insulation, so narrow HTS strips will be directly stacked without soldering, as a result, the coupling losses originating from the soldering stack connections can be effectively reduced.

1.6.2 AC loss calculations

The amount of electromagnetic energy converted into heat in one AC cycle has been considered as one of the most important parameters characterising the electromagnetic performance of a superconducting wire/coil used for AC applications. This quantity, generally called the AC loss, can be perceived from two perspectives. From one side it is the heat dissipated in conductors. This can be calculated by double-integrating the product of the local electrical field with the local density of electrical current, called the electric method [85]. An electric field is induced by an applied time-varying magnetic field. A screening current begins to flow and there is a local non-zero product of voltage and current. The product $\mathbf{E} \cdot \mathbf{J}$ is integrated spatially over the conductor cross-sectional area and with respect to time over the magnetic field cycle yields to give the loss in per unit volume per field cycle (J/cycle/m^3) by the following

equation:

$$Q = \frac{1}{S}\int_0^{1/f}\int_S \mathbf{E}\cdot\mathbf{J}\,dS\,dt \tag{1.3}$$

The applied magnetic field is $\mathbf{B} = u_0(\mathbf{H} + \mathbf{M})$. If the value of the magnetic field is taken at a considerable distance from the superconductor, then the influence of the screening currents in the superconductor is negligible in this case, and $\mathbf{B} = u_0\mathbf{H}$. If the applied magnetic field is larger than the lower critical magnetic field B_{c1}, then the Meissner state can be neglected.

On the other side, the AC loss per cycle in a superconducting wire can also be estimated by integrating Poynting's vector $\mathbf{E} \times \mathbf{H}$ on a closed surface surrounding the wire over a period T of alternating electromagnetic environment, where E is the electric field, H is the magnetic field, and V is the volume of the specimen surrounded by the surface [85]. The AC loss per unit volume per field cycle in J/cycle/m^3 in a volume V enclosed by a surface S is given by:

$$Q = \frac{1}{V}\int_0^{T}\int_S (\mathbf{E}\times\mathbf{H})\cdot\mathbf{n}\,dS\,dt \tag{1.4}$$

Equation 1.4 does not depend on the origins of the AC loss in the specimen, but instead gives a basis for measurement methods for the AC loss. Similar to ferromagnetic materials, the non-linear voltage-current relationship suggests that the magnetic behaviour of the superconductor is predominantly hysteretic in nature. The magnetisation curve encloses an area that represents the magnetisation loss per unit volume per field cycle [78]. In this case, the loss can be interpreted by an equation that is derived from Equation 1.4, where **M** is the magnetisation of the superconductor, as the following equation shows:

$$Q = \oint \mathbf{M}\cdot d\mathbf{B} \tag{1.5}$$

1.6.3 Technical importance of AC loss

Superconductors are developed for use in high-power devices such as transformers, power-transmission cables, motors, and generators. As mentioned previously, a high critical current and a low-cost price are the two key parameters for superconductors to meet, in order to compete with the presently used normal conductors. In addition, the AC loss should be low enough to justify the extra investment in the superconductor and highly costly refrigeration system. Usually, due to financial considerations, using superconductors in electrical power devices for industry applications is ultimately based on the following aspects: energy costs, superconducting material costs (including the extra production steps intended to reduce the AC loss), cooling system costs, maintenance, and reliability [87].

Under the same circumstances, the AC loss in a superconductor is usually much lower than the resistive loss in a normal conductor. The energy is dissipated as heat in a low-temperature environment, which has to be removed by a cooling system that consumes a multiple of the dissipated energy. Usually, the total power consumption of a typical device operating at 77 K is approximately 10–20 times the AC loss in the superconductor [87]. For instance, the most famous regenerative cryocoolers are Gifford-McMahon (GM) and Stirling types [88]. According to [89], the Carnot efficiency of Stirling cryocoolers is in the range of 4% to 30%, and for GM cryocoolers is about 1% to 9%. The penalty factor of the GM cryocoolers is typically about 15 to 20 at 77 K. It means that for extracting 1 W out of the cryostat at 77 K, 15 to 20 W should be consumed in cryocooler. On the other hand, for extracting 1 W heat by a Stirling cryocooler, there is a need for 18.3 W of electrical power at temperatures around 77 K [90];[91]. Therefore, it is of paramount importance to accurately predict and minimize the AC losses in order to lower the heavy cooling penalty. Ideally, the use of HTS over LTS greatly reduces the problem of heat removal, due to the higher operating temperature, but it does not completely eliminate it. In the case of a superconducting machine, the armature windings need to be carefully designed so that the smaller size and lighter weight advantages realized by using superconductors are

not diminished by the requirement of a large cooling system [92].

In certain motor and generator designs, there is an AC winding located in the stator and a DC field winding located on the rotor, which is the most common configuration, although the two winding locations are interchangeable. The rotor has a DC winding that carries a constant or slowly varying current in a nearly constant magnetic field, while the stator has an AC winding that carries an alternating current and is subjected to the rotating magnetic field of the rotor. This generates AC losses, which potentially increases the size and weight of the machine cooling system. Due to the rotation of the magnetic field, the tapes in the AC winding are subjected to a perpendicular magnetic-field component, whose amplitude is equal to the total magnetic-field strength of the device. The AC loss in tapes is dominated by variations in the magnetic-field component perpendicular to the tape. These variations are largest in the AC winding of a motor, large in a transformer, small in a power transmission cable, and smallest in the DC winding of a motor. Therefore, from the perspective of AC loss, the construction of a fully superconducting machine faces greater challenges than a transformer, and a transformer faces greater challenges than a cable [87].

1.6.4 AC loss reduction challenges for fully superconducting machine

Commercial electric aviation targets demand higher power density (>20 kW/kg) motors with higher efficiency to leverage the weight benefits of electric propulsion [93];[94]. Fully superconducting machines meet the requirements to achieve these high-power density targets by increasing electric and magnetic loading without losing efficiency to ohmic heat losses. However, as mentioned before, studying AC losses still remain a significant challenge for fully superconducting machines due to the high-speed requirement of electric propulsion. In a fully superconducting machine, both rotor and stator windings are replaced with superconducting materials. Thus, fully superconducting machines are expected to reach a higher efficiency than

partially superconducting machines since the armature power loss is greatly reduced compared to conventional copper-based windings. Theoretically, after being replaced with superconducting windings, the ohmic losses in the stator will be significantly reduced, however, the armature windings carry an AC current and operate in an AC magnetic field. In this case, both transport current loss and magnetization loss are present in HTS armature windings, and must be studied carefully. Conversely, HTS rotor windings carry a DC current below the critical current and operate in a complex magnetic field, including a fundamental base field and higher-order harmonic field. As such, the magnetization loss needs to be investigated for rotor design. Moreover, HTS conductors capable of operating in a high frequency field (~200–2000 Hz) are not yet available, since the contribution of eddy current loss to total loss increases with frequency, which must be taken into account when considering the design of practical HTS devices [95], and minimizing the use of metallic components for reducing mass still remains unsolved [42]. Therefore, to address the challenges above and improve the overall machine efficiency, more work needs to be carried out and the AC losses need to be appropriately evaluated and quantified to improve the machine design.

Of the many challenges hindering the development of a fully HTS machine, the most critical is the investigation of AC losses in armature windings. The development of HTS coils with relatively low AC losses has aroused renewed interest in the investigation of superconducting stator windings. The relative economy of using liquid nitrogen as the coolant gives the promising prospect for the development of practical HTS stator windings, and research projects are ongoing across the world. The development of an HTS coil with lower AC losses is desperately needed for fully HTS machine armature windings, otherwise the size and weight of the cooling system will not be acceptable. Ideally, the HTS coil needs to be twisted into narrow filaments to reduce AC loss. However, currently, there are no wire technologies available to achieve the feasibility and effectiveness of the HTS stator for commercial use. Some wire concepts, e.g., Rare-earth barium copper oxide (ROEBEL) cable [96] and

Conductor on round core (CORC) cable [97], have been studied by many researchers as to their feasibility and effectiveness for small scale use, however, they have not yet been proven for large scale commercial use due to various existing drawbacks. Reasons for this are discussed in detail in Chapter 3 when illustrating the AC loss reduction strategies.

To sum up, in machine design, a minimized AC loss design need to be considered, with efficiency an essential parameter for evaluating the design of high-power density HTS machines for the sake of saving economic cost. For HTS coils in the machine, AC losses are critical issues in engineering. Firstly, the AC losses provide data for cryogenic systems design, so that the cooling power can be matched with the machine accordingly. Secondly, both magnetization AC loss and total AC loss need to be identified separately to properly evaluate the different HTS materials or coil structures. These data can play an essential role in large-scale machine design. Finally, high AC losses may cause unavoidable heat inside the coil, thus leading to the temperature increasing over the critical temperature of the HTS tape, and eventually give rise to the HTS coil quenching at the weak point or even being damaged totally.

In this study, a new HTS machine platform is developed to measure AC losses of the stator windings. This platform is able to provide the AC losses values of the HTS stator coil in a rotational magnetic field machine environment. Based on the calorimetric method of boiling-off liquid nitrogen, both magnetization AC loss and total AC loss can be identified and measured in this machine. Using the proposed AC loss reduction strategies, the newly made multi-filament HTS coils based on each methodology can be tested in this platform. Hence, this act can be used to improve the machine design, thus significantly reducing the machine size and weight, contributing to lowering the cost of cooling system and increasing the machine efficiency.

The following research will be focused on the operating temperatures of HTS lower than 77 K, which can be achieved by the newly developed fully HTS machine demonstrator using a helium gas circulation system. With temperatures cooled down lower than 77 K, the HTS machine can operate at much higher currents, and achieve

the possibilities to become more compact and lightweight when operated at lower temperatures. Using helium gas as the coolant, the temperature of the key positions of the HTS machine can achieve less than 30 K, hence it can further improve the performance and power density of the machine.

1.7 Conclusion

This chapter began by explaining the fundamental principles of superconductivity. It first introduced the basic properties and theories, focusing on their macro aspects. In brief, superconductivity can be interpreted as ideal conductivity combined with ideal diamagnetism. However, a superconductor is much more complicated than either a perfect conductor or diamagnet, and the different classifications of superconductors were introduced in the following part including LTS and HTS, Type I and Type II superconductors, and 1G HTS and 2G HTS. In the second section, the fully HTS machine concepts were presented, to illustrate the clarifications of HTS machine, the road map of HTS machine development, and discuss the importance of fully HTS machines for enabling the electric propulsion of aircraft. Finally, special attention was paid to the AC losses in HTS superconductors. Significant contributions from various worldwide institutes have already pushed forward the area of AC loss analysis, modelling, measurement, and control in superconductors. This section describes some basic AC loss principles including AC loss types, the equations used for AC loss calculation, and the technical importance of AC loss. Additionally, it opens up the challenges that need to be addressed for the design of fully HTS superconducting machines, delivering a helpful guideline for future research efforts.

Chapter 2

AC loss experimental measurement

Superconducting electrical machines will be widely used in many modern transport applications in the near future. Their great features such as high efficiency, high torque density, high power density, and lighter weight make them an excellent fit for electric aircraft and marine applications. Meanwhile, the application of 2G HTS coils for fully superconducting machines has become a promising research focus over recent decades [98];[99];[100]. Not only could it provide the high-power density required for future electric aircraft propulsion, but it will also push for the reduction of AC losses to lower the constraint on the cryogenic cooling system. However, the AC losses generated in superconducting windings in AC electrical machine environments are difficult to entirely remove at low temperatures, thereby adding an extra burden to the aircraft cooling system. Due to the heavy cooling penalty, it is essential to study AC losses in the HTS stator in consideration of optimizing HTS machine design and improving overall efficiency. In order to understand and estimate the total AC loss of HTS coils as armature windings for electrical machines, in this chapter we designed and performed both electrical and calorimetric measurements for different 2G HTS coils. The AC loss measurements were based on the electrical transport method and calorimetrically boiling-off liquid nitrogen. Both the total AC loss and magnetisation loss in the HTS stator were measured in a rotational magnetic field condition. These measurements are essential to characterize AC losses in the HTS stator to seek ways to reduce the AC loss and maximize the efficiency of fully HTS machines for future aircraft propulsion applications.

2.1 Overview of methodology

In order to study the AC loss of 2G HTS coils for future electrical machines, it is necessary to establish experimental measurement techniques. A number of studies have been done to identify AC losses in HTS coils or cables [8];[12];[100]. Aircraft applications require high power density and high transport current, therefore higher cryogenic cooling power is required. At cryogenic temperatures, the power dissipation caused by AC loss has been a heavy burden to cryogenic systems [101]. In this thesis, the reasons why we should study and investigate the AC loss is to appropriately identify and quantify the AC losses in stator windings, focusing on investigating the AC loss reduction achieved by different strategies for improving overall machine efficiency, as well as to estimate the cooling power required, and hence design an appropriate cryogenic system for aircraft propulsion applications.

In general, there are three methodologies to measure the AC losses of HTS coils: electric, magnetic, and calorimetric methods [102]. The electrical method is based on measurement of the component of the voltage in-phase with the current to determine the AC loss. The magnetisation method to measure losses can be achieved by integrating signals from pick-up coils wound around or Hall probes placed close to the sample [103]. The calorimetric method determines the loss indirectly by measuring the temperature rise or the amount of gas boil-off. Table 2.1 compares the three different measurement methods. However, the magnetic method is typically applied in static measurements and for short samples. Thus, to study AC loss in HTS machines, only the electric method and the calorimetric method are discussed in detail in the following sections.

Table 2. 1: Comparison between different AC loss measurement methods [104]

Measurement Methods	Main purpose	Advantages	Disadvantages
Electrical method	Transport current loss; Total AC loss	High sensitivity; high accuracy; able to measure low AC loss	Compensation coil needed; lock-in amplifier can only work with pure sinusoidal signals; easy introduction of harmonics
Magnetic method	Magnetization loss	High sensitivity; high accuracy; able to measure low AC loss	Limited to static measurement; pick-up coils easily interfered with by external magnetic fields
Calorimetric method	Total loss	Disregarding object shape; disregarding working conditions; able to measure large scale specimens	Poor sensitivity; weak accuracy; long time consumption; possible disturbance from thermal effects of non-superconductors

2.2 4 mm HTS sample coil preparation

2.2.1 Selection of insulation materials

In fully electric aircraft, most of the windings are built out of 2G HTS wires which work at cryogenic temperatures. In applications utilizing HTS under high mechanical loads as high-field magnets, or field coils of generators and motors for high-power electric machines, HTS coils are placed in a rotating machine environment, as a result, they will be unstable due to mechanical disturbances caused by the magnetic fields and the rotational vibration of the rotor [105][106]. Therefore, the wires in windings have to be insulated or impregnated with proper material in order to achieve high heat transfer, thermal stability, and to be electrically insulated. Currently, it is commonly accepted that effective ways to solve the problem above include epoxy insulation or paraffin impregnation, and these insulation methods have been actively studied in many studies [107];[108]. However, these methods might easily cause critical current

degradation because of radial stress and cleavage stress. Additionally, sometimes while the insulating material itself shows an acceptable performance in insulating the wire and having a good thermal conductivity, because of thermal contraction and shrinkage it would not last long in proper shape at cryogenic temperature. Moreover, applying epoxy insulation materials is most likely to increase the turn-to-turn contact resistance for No-Insulation (NI) coils [109]. An alternative feasible method such as using non-epoxy insulation might be an effective way to achieve the purpose of providing insulation for HTS tapes or coils. For example, heat shrink tubing or Kapton tape have been considered effective options [100];[110]. However, one disadvantage of using Kapton tape as insulation is that the helical winding technique could result in an uneven surface of the 2G HTS tape, and there also exists limited research regarding to whether employing heat shrink as insulation will lead to critical current degradation of the tape. Therefore, in order to investigate the insulation method, as well as to decide the most suitable insulation materials for HTS tapes used as armature winding coils, first of all, we need to explore the feasibility of different insulation materials for non-insulated tapes.

4 mm wide 2G HTS tapes supplied by Shanghai Superconductor Technology Co. Ltd. (SHSC) were investigated in our work. Having cut them into identical lengths, voltage taps were soldered onto the upper surface of the tapes with 10 cm gaps in between. Choosing the best type of insulation materials as well as the optimal thickness of insulation are not straightforward, and it requires technical knowledge and experience depending on factors such as the voltage level, operating temperature, number of turns in coils and windings, thickness of superconductor, as well as thermal expansion coefficient and thermal conductivity of insulation materials [111]. In our work, we only focus on six epoxy and two non-epoxy insulation materials, as shown in Figure 2.1, in consideration of their good mechanical properties and high thermal and chemical resistance. Table 2.2 shows the specific mixture ratio and cure conditions for the epoxy insulation materials. Specifications of the non-epoxy insulation materials used, including Kapton tape and heat shrink tubing, are listed in Table 2.3.

Table 2. 2: Epoxy insulation materials

Resin component		Mix Ratio (Weight)	Cure time
Cryogenic glue 7110	Part A: Grey Part B: Clear	10 1	Recommended cure: 2 h, 80℃
Cryogenic glue H20E	Part A: Silver Part B: Sliver	1 1	Recommended cure: 1h, 150℃
Stycast 2850KT Blue	Part A: Stycast blue Part B: LOCTITE CAT 24LV	100 4	8 to 16 hours @ 25°C 2 to 4 hours @ 45°C 30 to 60 minutes @ 65 °C
Stycast 2850KT Black	Part A: Stycast black Part B: LOCTITE CAT 23LV	100 7.5	16 to 24 hours @ 25°C 4 to 6 hours @ 45°C 2 to 4 hours @ 65°C
Araldite 2020	Part A: 2020 A Part B: 2020 B	100 30	16 h, 23℃
Polyurethane Resin ER2220	Part A – Resin (grey) Part B – Hardener (black)	20.81 1	24 h, 23℃

Table 2. 3: Specifications of non-epoxy insulation materials

Parameter	Heat shrink tubing	Kapton tape
Size	Avg ID 0.16" Avg Wall 0.005"	Width 5 mm Overall thickness 0.06 mm
Temperature range	-196°C (-320.8°F) – 135°C (275°F)	-269°C (-452°F) – 400°C (752°F)
Melting point	235°C (455°F)	None
Colour	Clear	Amber
Dielectric strength	> 4000 V/mil	6000 V/mil
Thermal conductivity	0.19–0.25 W/m·K	0.75 W/m·K
Insulation resistance	Volume resistivity: $>10^{18}$ Ohm-cm Surface resistivity: $>10^{14}$ Ohm/square	Volume resistivity: 2.3×10^{16} Ohm-cm Surface resistivity: 3.6×10^{16} Ohm/square

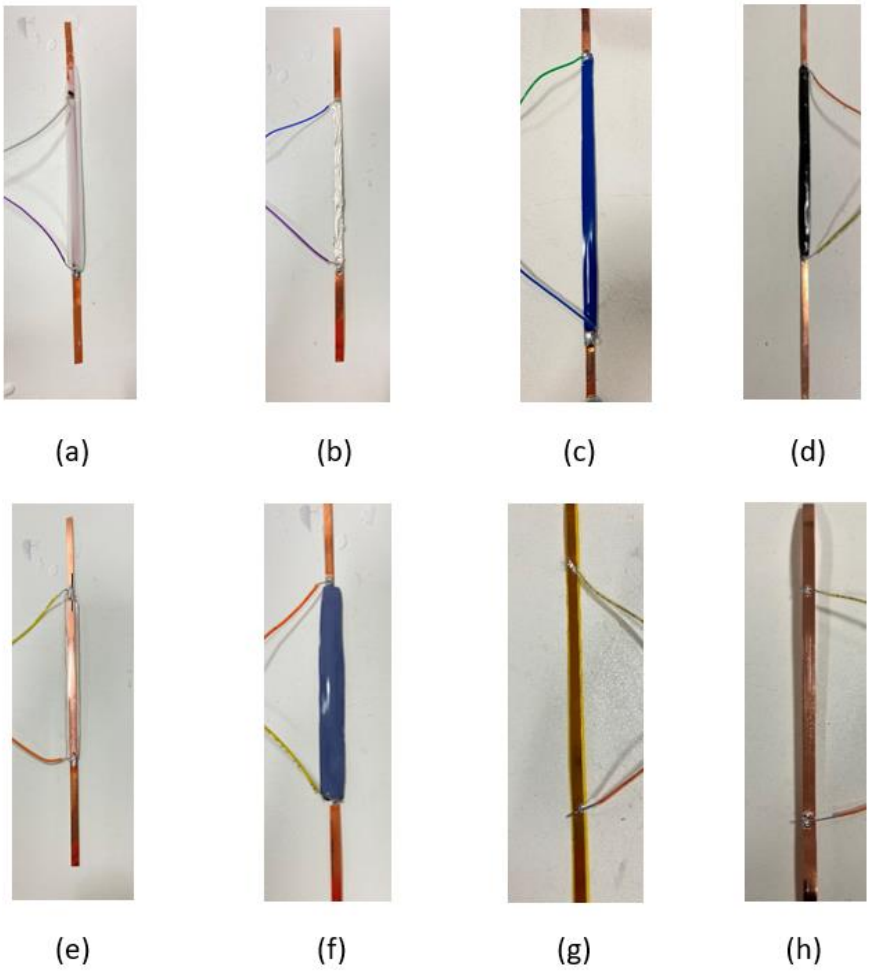

Figure 2. 1. *Prepared samples with different insulation materials (a) Cryogenic glue 7110; (b) Cryogenic glue H20E; (c) Stycast 2850KT – Blue; (d) Stycast 2850KT – Black; (e) Araldite 2020; (f) Polyurethane Resin-ER2220; (g) Kapton tape; (h) Heat shrink tubing*

Before insulation coating, the self-field critical currents at 77 K for the bare samples were measured using the four-point method. Each sample was selected from a self-field critical current around 136 A within range $\pm$ 0.5 A. Prepared samples were then placed on the thin film which can prevent tape from adhering to other surface as Figure 2.2 (a) shows, applying different epoxy insulation materials separately, and waiting for them to cure at room temperature. For non-epoxy insulations, as shown in Figure 2.2 (b), Kapton tape insulation is directly adhered to the HTS tape surface, and

can be firmly attached very well with appropriate external tension force. To apply the heat shrink tubing insulation, the HTS tape is inserted into the tube, and evenly heated up to around 422 K for a few seconds until the tube shrinks and firmly attaches to the HTS tape [100]. Finally, all samples were successfully prepared, and then they were put into the critical current testing platform to measure their critical currents. All the results are plotted in Figure 2.3 to summarize the critical current degradation of each tape corresponding to the different insulation materials.

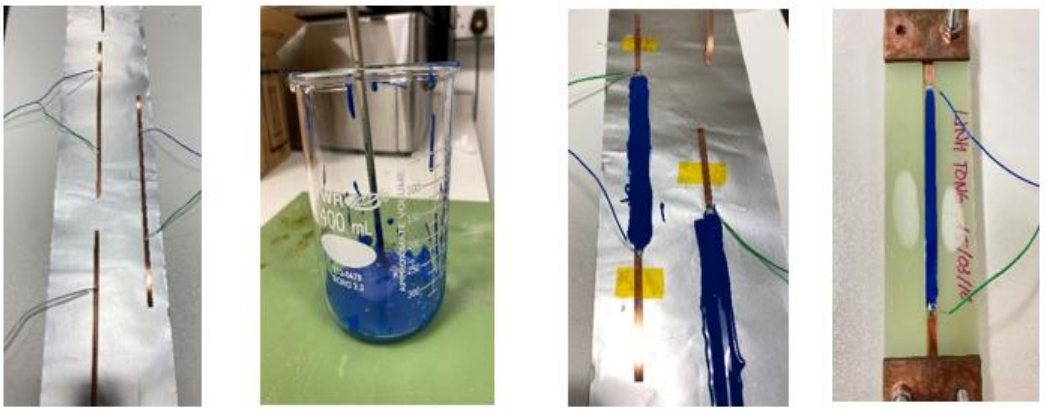

(a) Epoxy insulation method

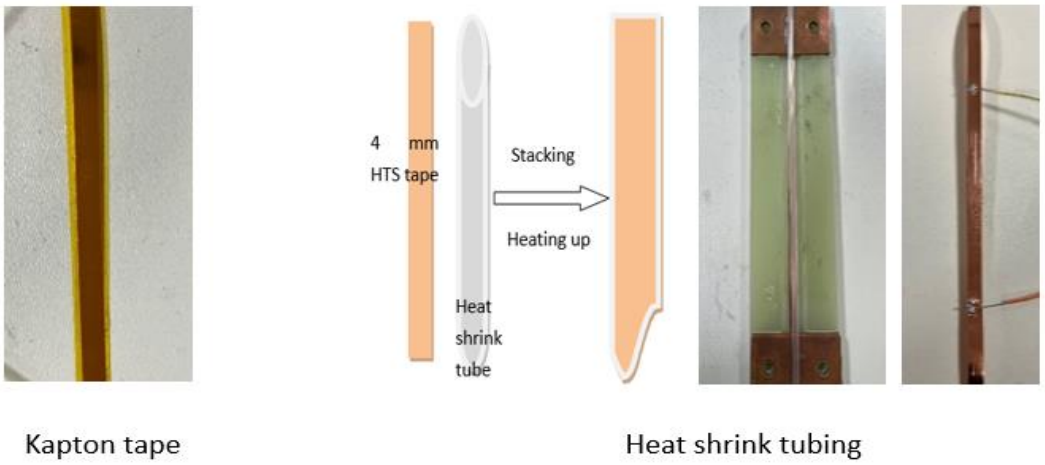

(b) Non-epoxy insulation method

Figure 2. 2. *Insulation process for epoxy and non-epoxy insulation methods*

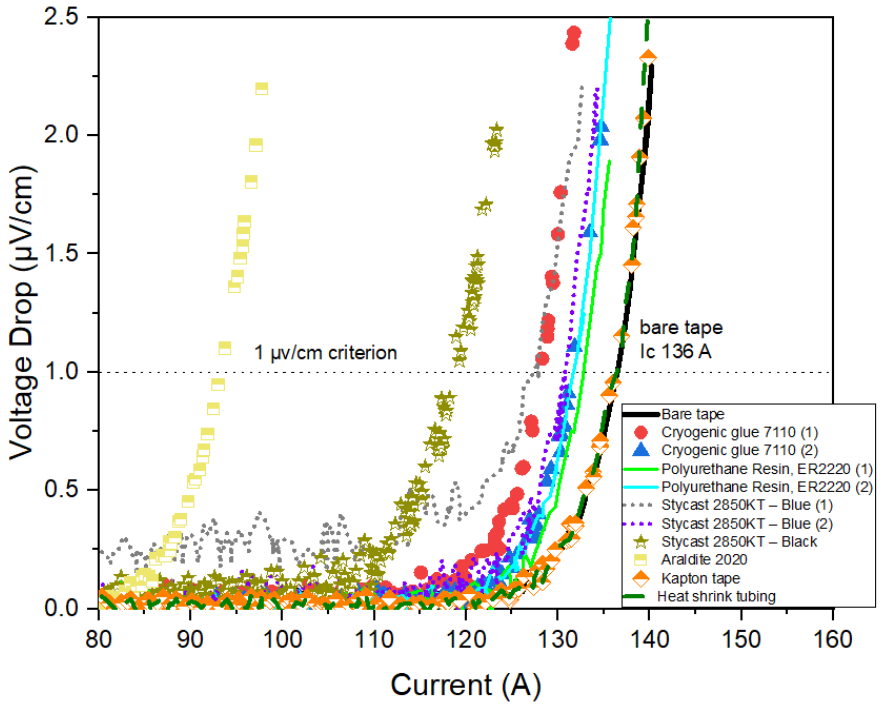

Figure 2. 3. *E-I curves with different insulation materials*

Due to cracks in the cryogenic temperature for tapes insulated with Cryogenic glue H20E, only the results of other seven insulation materials are plotted in Figure 2.3 for comparison. Both Araldite-2020 and Stycast-2850KT(Black) showed substantial critical current degradation at different levels, corresponding to a drop in I_c from 136 A to 93 A and 118 A, respectively. The degradation was closely related to the mismatch in thermal expansion. As for other tapes including insulation with Cryogenic glue-7110, Stycast-2850KT(Blue), and Polyurethane Resin-ER2220, as shown in the E-I curves of the samples, the critical currents of the insulated tapes degraded to a reasonable scale. Conversely, Kapton tape and heat shrink tubing insulation barely degraded the critical currents of the HTS tapes, since the E-I curves almost overlap together in the figure.

Thermal cycling tests were then carried out to check the stability of insulated samples and their ability to endure cyclical exposures to extreme temperature. This test was performed between liquid nitrogen temperature (77 K) and room temperature (around

296 K) using 30 min long as a cycle and 10 cycles in total. According to the testing results, for epoxy insulated tapes, some small cracks were observed in the middle for tapes insulated with Cryogenic glue-7110, and tapes with Stycast-2850KT(Blue) insulation were obviously degraded. Only the tapes insulated with Polyurethane Resin-ER2220 showed good performance and continuous stability without visible critical current degradation after 10 thermal cycles. For the non-epoxy insulated tapes, the tubing material and Kapton tape both worked perfectly at the temperature of liquid nitrogen, and no degradation of the insulation itself was observed during or after the thermal cycling test. Table 2.4 lists the critical current degradation results of three sample tapes insulated with Polyurethane Resin-ER2220, Kapton tape, and heat shrink tubing respectively after a significant time. It can be found that tape with epoxy insulation showed further critical current degradation, however the critical current of other two tapes remained unchanged. Additionally, Figure 2.4 shows the result obtained by optical microscopy of cross sections of tape insulated with Polyurethane Resin-ER2220, which allows for inspection of the transition zone between the electrical insulation material and superconductor material, and the image reveals significant delamination between the superconductive material and the insulation. Therefore, a conclusion can be drawn that non-epoxy insulation either by Kapton tape or heat shrink tubing is a better selection as insulation material for the HTS coils applied as stator armature windings. In this dissertation, the following investigations will thus only focus on using these two materials for insulating the sample coils.

Table 2. 4: I_c degradation over significant time

Tape I_c (A)	**Polyurethane Resin-ER2220**	**Kapton tape**	**Heat shrink tubing**
Original tape	136	136	136
Insulation after 3 days	133	136	136
Insulation after 6 months	131	136	136

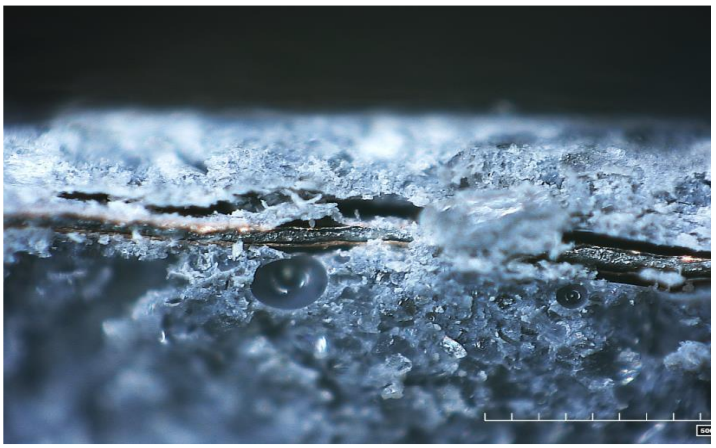

Figure 2. 4. *Optical microscopy of cross sections of superconducting tape insulated with Polyurethane Resin-ER2220*

To sum up, in this section, the 2G HTS tapes were insulated by different epoxy resins, Kapton tape, and heat shrink tubing. The DC characteristics of all the insulated tapes were tested in a self-field and compared with those of bare tape to find the proper insulating material to coat a long length of wire for a superconducting rotating machine. Based on the experimental results, non-epoxy insulation method by employing either Kapton tape or heat shrink tubing is more suitable in terms of critical current degradation and thermal cycling test. And it will be adopted to insulate our experimental 2G HTS coils for further AC loss measurements.

2.2.2 Coil manufacturing

The experimental 4 mm 2G HTS tapes are from SuNAM and Fujikura, respectively. Since 2G HTS tape is a ceramic material and very fragile during manufacturing, too much bending or mechanical stress will cause unrecoverable damage. To reduce the risk of mechanical damage, the winding process of the HTS coil is required to be as simple as possible. Double pancake coils are more suitable for machine purposes as both current leads are located on the outer layer. It requires the tape to be separated

into two spools, and the coil preparation should begin with the middle of the length. Firstly, half-lengths of the tape are separated into two spools, then one spool is fixed with the coil holder, and the first layer of the double pancake coil is wound using tape from another spool while the second spool rotates on its coil holder, so that no twisting or bending occurs to avoid the risk of any mechanical stress. After finishing the first layer of processing, the second spool is removed and the second layer of processing begins. Finally, two 4 mm sample coils were successfully prepared for the AC loss measurements. Coil 1, shown in Figure 2.5.a, is wound with 4 mm wide Fujikura HTS tape and Kapton insulation. Coil 2, shown in Figure 2.5.b, is wound with 4 mm wide HTS tape from SuNAM insulated with Kapton tape. Table 2.5 shows the specifications of Coil 1 and Coil 2.

Table 2. 5: Coil 1-2 specifications

Parameter	Coil 1	Coil 2
Used HTS wire	4 mm Fujikura	4 mm SuNAM
Insulation	Kapton tape	Kapton tape
Coil length	5 m	15.5 m
Coil type	Double pancake	Double pancake
Total turns	16	50
Inner diameter	95 mm	98 mm
Outer diameter	98 mm	103 mm
Inductance	44.2 μH	440 μH
Tape I_c @77 K	204 A	250 A
Coil I_c (Self-field) @77 K	130 A	102 A
Coil I_c (In-field), peak 0.45 T, @77K (magnetic field profile is presented in Figure 2.12)	72 A	59 A

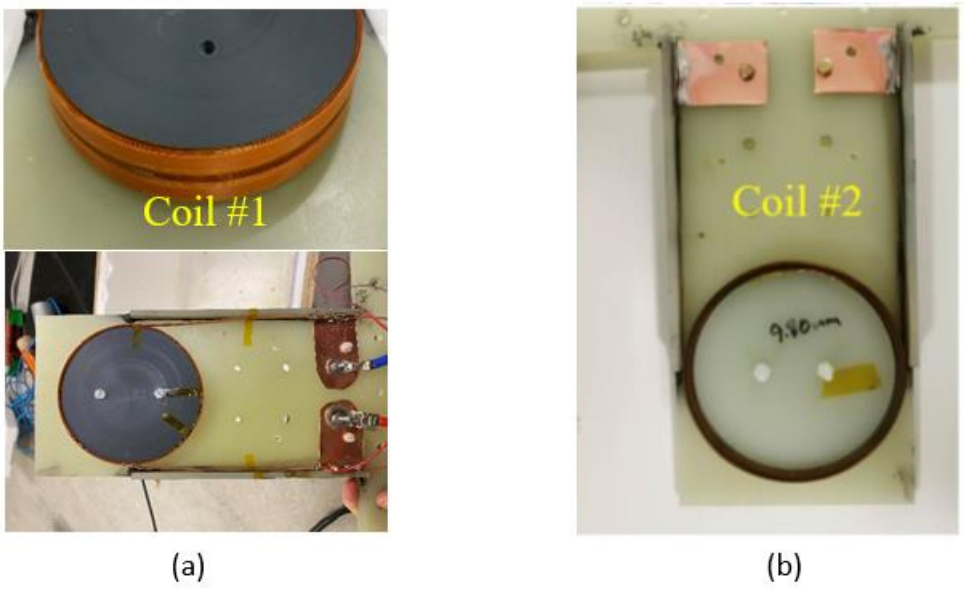

Figure 2. 5. *Prepared samples for experiment: (a) Coil 1 (b) Coil 2*

2.2.3 Critical current measurement

The most general method for measuring the critical current density J_c, an important parameter of superconductors, is the four-terminal method [112], in which the voltage drop V between the terminals is measured as a function of the transport current I. This is also called the resistive method. The critical current I_c is defined as the transport current at which the flow voltage clearly appears. The critical current density is given by I_c divided by the cross-sectional area S of the superconducting region: $J_c = \frac{I_c}{S}$. In multi-filamentary superconductors, the cross-sectional area may include a metallic stabilizer and reinforcing materials.

In practice, the current-voltage curves of superconducting wires are not straight lines. Instead, voltage gradually rises due to various causes. The measurement is also subject to sensitivity limits. Hence, there is no clear point at which the flow voltage appears. To define the critical current, the following criteria are used [113]. (1) Electric field criterion: This is the simplest method. The critical current is defined by the current at

which the electric field reaches a certain value. A value of 1 μV/cm or 0.1 μV/cm is commonly used [114]. (2) Resistivity criterion: The critical current is defined by the current at which the resistivity of the superconducting wire reaches a certain value. For composite superconductors with stabilizer, 10^{-13} Ω·m or 10^{-14} Ω·m is commonly used. (3) Off-set method: The critical current is determined by the current at which a tangential line from part of the current-voltage curve crosses the zero voltage line. In the following section, the four-terminal method to measure the critical current of different HTS coils will be presented.

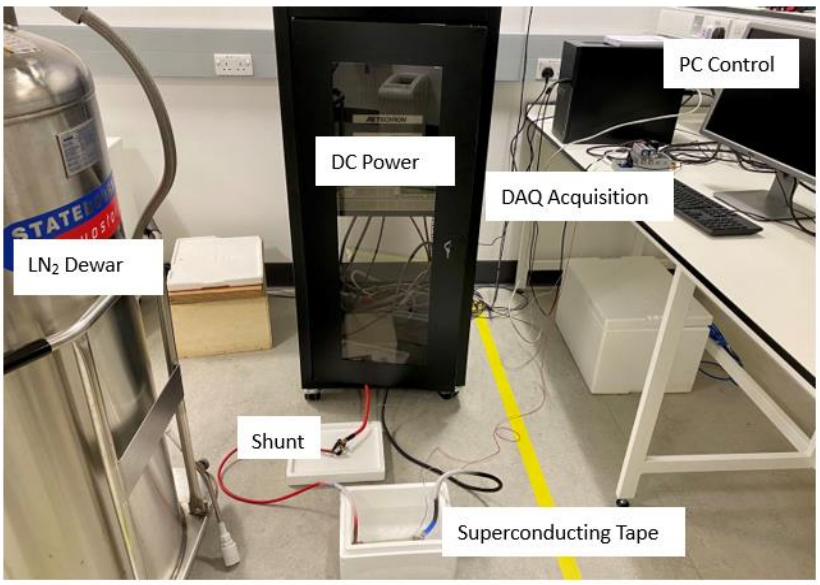

Figure 2. 6. *Critical current measurement platform*

A standard four-terminal method, based on a 1 μV/cm voltage criterion at 77 K, was employed for critical current measurements [112]. The ramp rate of the applied current was 1 A/s and controlled with LabVIEW and the NI data acquisition module. A LabVIEW interface panel was used to control the DC power supply. The critical current measurement system mainly consists of a sample holder, a liquid nitrogen tank, a shunt, a data acquisition system, and a DC power supply, as shown in Figure 2.6. The critical current measurement results for HTS coils are shown in Figure 2.7. The measured critical currents for Coil 1 and Coil 2 are 130 A and 102 A, respectively.

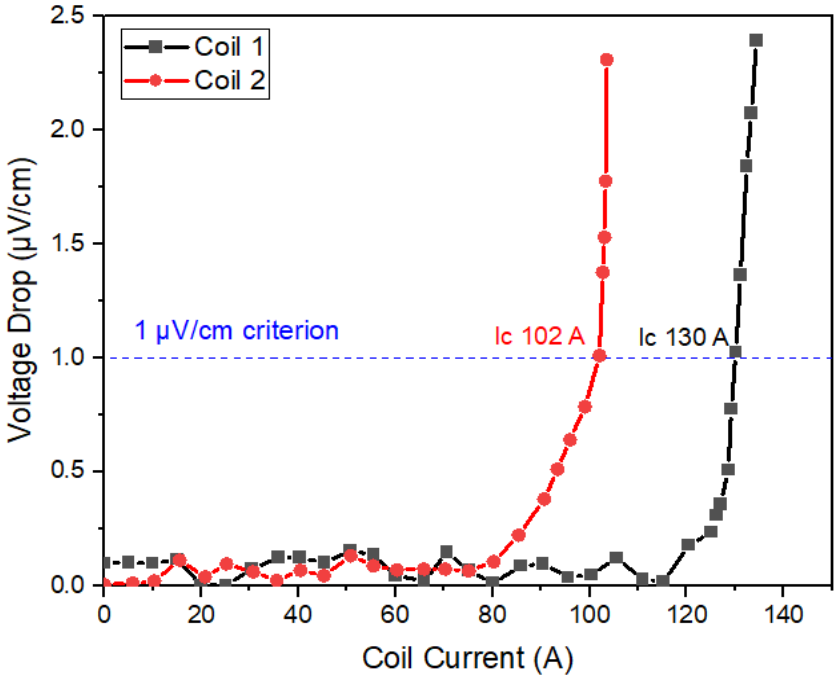

Figure 2. 7. *Critical current of Coil 1 and Coil 2*

2.3 AC loss measurements for sample coil

Transport loss due to the alternating transport current and magnetization loss due to the alternating magnetic field can both contribute to AC loss. As mentioned before, the electrical method and the calorimetric method can both be employed to measure AC loss. This section introduces in detail the experimental setups and results obtained using both methods to measure AC loss for HTS coils.

2.3.1 Electrical method for transport AC loss measurement

The electric method is extensively used because of its fast measurement speed and high sensitivity. Typically, the electrical method for transport AC loss measurement is the procedure of putting voltage taps on both ends of the coil conductor and measuring

the coil voltage during loading current [115];[116];[117].

A schematic diagram of transport AC loss testing circuit based on the electrical method is shown in Figure 2.8, and Figure 2.9 shows the transport AC loss testing platform which includes an AC power supplier, a power amplifier, an NI data acquisition, a LabVIEW interface panel, an LN_2 tank, a shunt, an HTS coil, and compensation coils. The experimental setup is built out of the lock-in amplifier technique [78], in which combines a modified existing experimental setup used for measuring the transport AC loss of superconducting tapes [118] with a compensation coil to cancel the large amount of voltage from the inductance component.

Since the HTS coil can generate a large inductive voltage, which can be orders of magnitude higher than the in-phase AC loss component [119], a compensation coil capable of providing compensating inductive voltage was added to the circuit [116];[120], in order to measure the transport loss of the HTS coil. The compensation coil consists of two coupled coils, which can be used to compensate for the coil voltage. The primary coil is wound by a few turns of the current cable, and the secondary coil is wound by thin copper wire with a large number of turns. Both the primary and secondary coils use wire as thin as possible to reduce the effect of any induced eddy currents in the windings due to time-varying fields. For the same reason, no magnetic material coils are used in the construction of the coils. By adjusting the relative positions of the primary and secondary windings, the inductance signal from the compensating coil's secondary winding can compensate for the inductive component of the HTS coil's voltage.

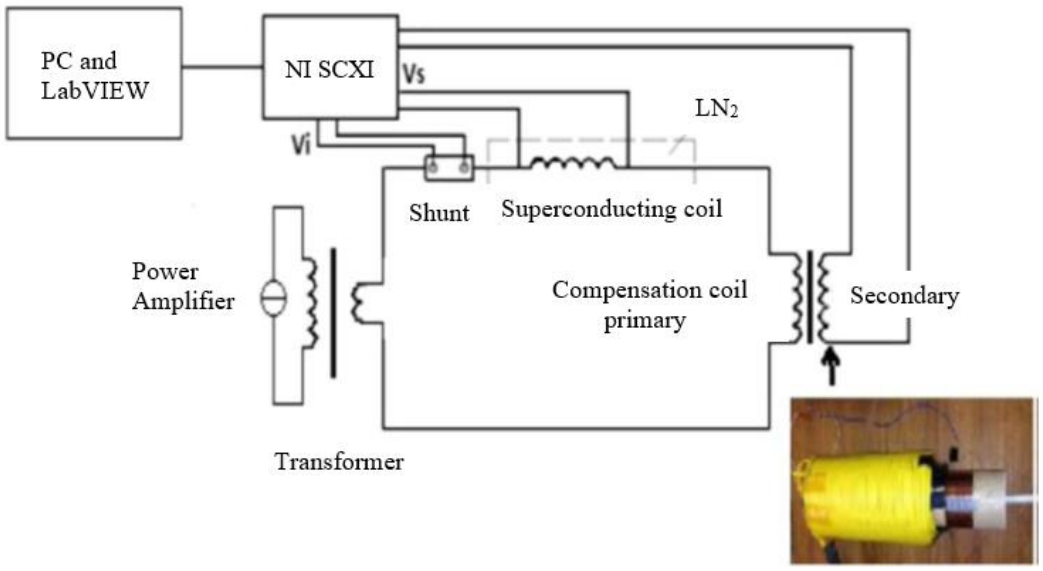

Figure 2. 8. *Circuit diagram of transport AC loss measurement [121]*

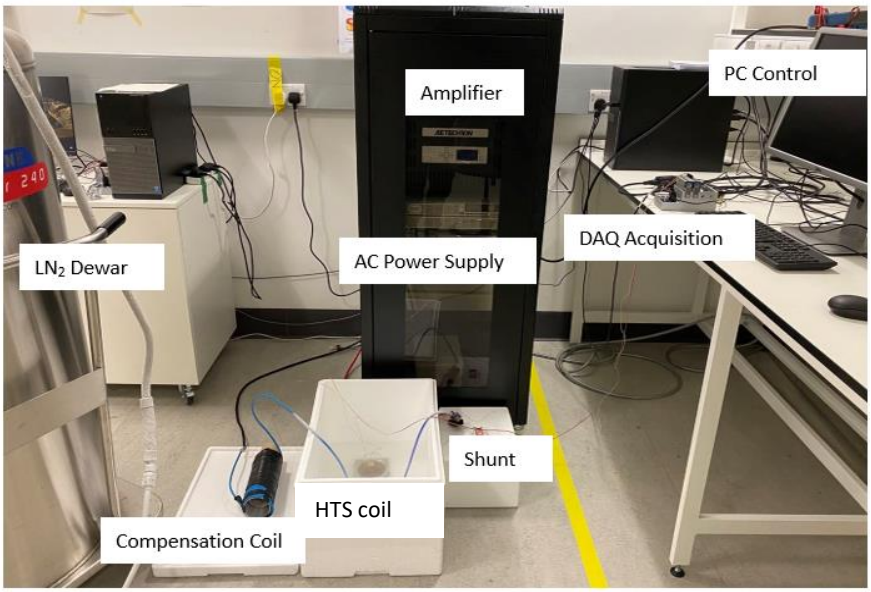

Figure 2. 9. *Transport AC loss testing platform*

As shown in Equation 2.1, the measured transport AC loss in J/cycle/m is calculated as following:

$$Q_{exp} = \frac{V_{rms} \cdot I_{rms}}{f} \frac{1}{L} \quad (2.1)$$

where f is the frequency of the applied current, L the total length of the HTS coil, I_{rms} is the root mean square value of the transport current flowing through the coil, and V_{rms} is the root mean square value of the in-phase voltage component from the voltage taps. In this dissertation, all AC losses results will be given in J/cycle/m which is commonly used and will allow us to compare the results of HTS coils despite their different constitutions.

Although the electrical method is simple in principle, it is still necessary to carefully consider any sources of error to obtain accurate results. One important source of error comes from the compensating coil. In theory, the compensating signal must be purely inductive in order to avoid adding any resistive signal to the measurement circuit. However, due to the eddy currents existing in conductors near the compensation circuit, an undesired resistive signal can be created [122]. The compensating coil must therefore be placed away from any conductors, in order to avoid introducing any in-phase signals, which would lead to overestimating the AC loss.

To be more specific, in order to accurately measure the AC losses, the voltage measurement loop should link the magnetic flux from the centre of the tape to an enough large distance, at least three times greater than the tape half-width [123];[124]. Unfortunately, in addition to the resistive voltage, such a large voltage measurement loop would pick up an inductive voltage, which could be several orders of magnitude larger [125]. At higher frequencies, this undesirable component is even more significant and thereby dominating the resistive component, since the inductive voltage is a linear function of the frequency. Due to this difficulty, few work have carrying out accurate high-frequency AC loss measurements. And our tests were hence only performed at relatively low frequencies, in which three different frequencies at 50 Hz, 75 Hz, and 100 Hz were chosen for both Coil 1 and Coil 2. Moreover, owing to the restrictions of the laboratory equipment, the applied peak transport current to the HTS coil was limited to 90 A. By using the Equation 2.1, the transport AC losses in J/cycle /m can be calculated and the normalized transport losses

versus normalized transport currents for both coils were shown in Figure 2.10. The experimental results indicate that the measured transport AC loss for both coils is independent of the operating frequency over this range of variation, suggesting that it was predominantly hysteretic in nature.

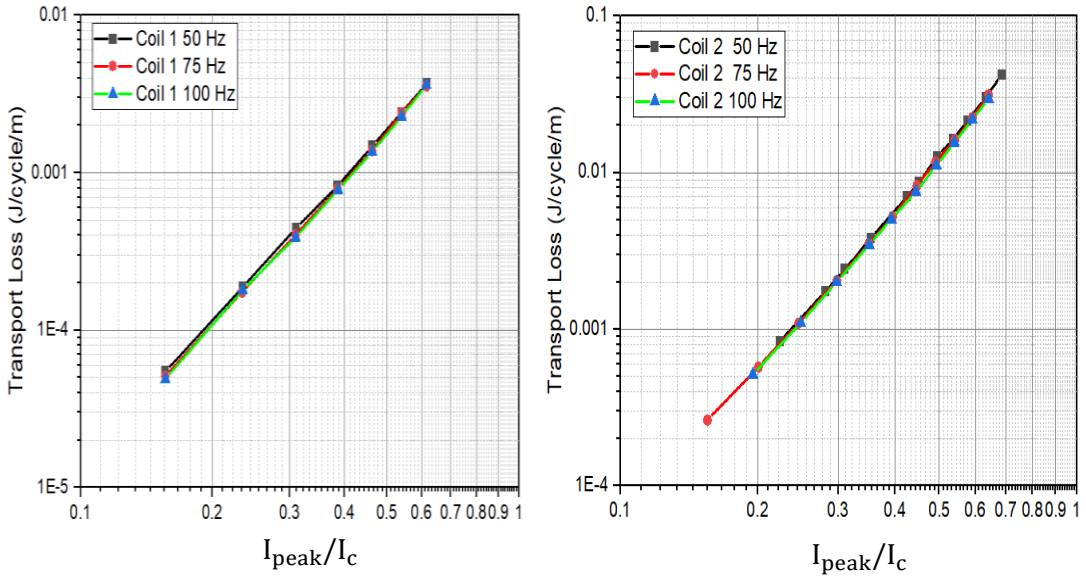

Figure 2. 10. *Normalized transport loss versus normalized transport current measured by the electrical method*

2.3.2 Calorimetric method for AC loss measurement

The calorimetric method (or boil-off method) has been demonstrated in many papers [126];[127];[128] as a means to measure AC losses of superconducting tapes. The same principle can be applied to measure AC losses in HTS coils. Figure 2.11 illustrate the structure of the boil-off method. The specimen is powered by the AC power supply and can produces heat in the cryostat, thus causing the evaporation of liquid nitrogen. So, by measuring the flow rate of liquid nitrogen using the gas flow meter attached to the vent tubes, the AC loss can be calculated. The accepted value of the latent heat for liquid nitrogen is 199 Joule/gram [129], which is equal to 0.25 standard litres per minute for every Watt of power (SLPM/W). Thus, the flow rate of

liquid nitrogen is 0.25 SLPM/W. However, due to temperature and pressure variations, different measuring systems experience flow rates in different conditions. Therefore, before the AC loss measurement can be taken, a calibration process should be carried out according to different system designs [130]. The following steps should be adopted: (1) A heater with known power is installed into a cryostat. A DC power supply is then applied to the heater, and the amount of evaporation gas is measured by flow rate meter. (2) The relationship between heat power and the flow rate of evaporation is obtained by repeating step (1). (3) When the specimen carries AC current or is exposed to an AC magnetic field, the flow rate of evaporation gas due to the created AC loss can be obtained by the calibration curve in step (2).

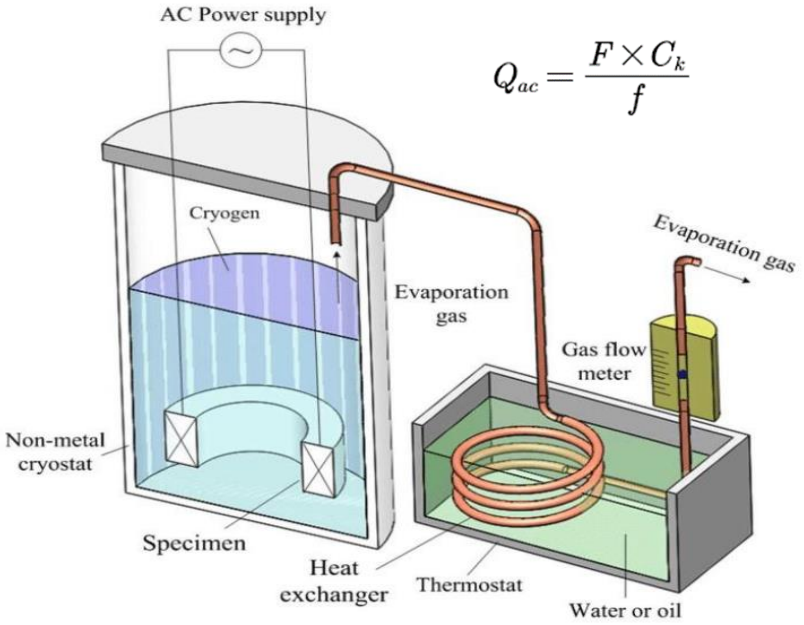

Figure 2. 11. *Diagram of the boil-off method [131]*

The advantage of using the calorimetric method compared to the electrical method is that it can be used in any condition of the background AC magnetic field to measure the total loss and magnetization loss of HTS coils, regardless of the phase difference between the AC and background field [132]. However, the sensitivity and accuracy of the calorimetric method are not as high as those of the electrical method. In our HTS

machine testing platform, a fluctuation of 0.08 SLPM and an unavoidable background flow rate around 1 SLPM were observed, indicating that the calorimetric method is not as sensitive as the electrical method. Moreover, the calorimetric method also has other shortcomings. Since the changes of heat and temperature are much slower than the electromagnetic propagation on which the electric method is based, the measurement process usually takes longer. For LTS superconductors, liquid helium is normally used as the coolant. Because its latent heat is very low, liquid helium is prone to evaporate easily, making the thermal measurement method relatively straightforward to measure the AC loss. However, HTS superconductors can use liquid nitrogen at 77 K, and the latent heat of liquid nitrogen is large, more than 60 times that of liquid helium. Therefore, the calorimetric method is not suitable for short samples or small coils.

To conclude, the electric method for transport AC loss measurement has faster speed and higher accuracy compared to the calorimetric method, and it is sensitive to electromagnetic disturbances, and is thereby suitable to measure short samples or small coils in relatively simple electromagnetic environments. On the other hand, due to the large latent heat of liquid nitrogen, the calorimetric method is more suitable for use in measuring the AC losses of larger samples and HTS coils. The calorimetric method also has a wide range of applications, and the setup does not require complex electronic circuits or high-precision instruments. It is also suitable for use with any AC magnetic field wave in any direction, regardless of the AC magnetic field and the AC current phase difference.

2.3.2.1 HTS machine platform setup and sample coils testing

In order to enable the measurement of LN_2 boil off inside a rotational machine, we have chosen the axial-flux machine design, so as to accommodate a measurement chamber for an HTS stator winding. As shown in Figure 2.12, this machine contains two four-pole permanent magnet rotor discs, two silicon steel back irons and a three-phase HTS stator, with a peak magnetic flux density of 0.45 T in the centre. Each

rotor disc consists of four large NdFeB permanent magnets, each with a diameter of 100 mm, sitting on a laminated silicon steel plate. The HTS stator disc is sandwiched between two rotor discs and consists of six stator coils. Only two coils of phase A are constructed of HTS materials; phase B and phase C are constructed of copper coils with the same diameter. The measurement HTS coil is placed in a separate measurement chamber with liquid nitrogen.

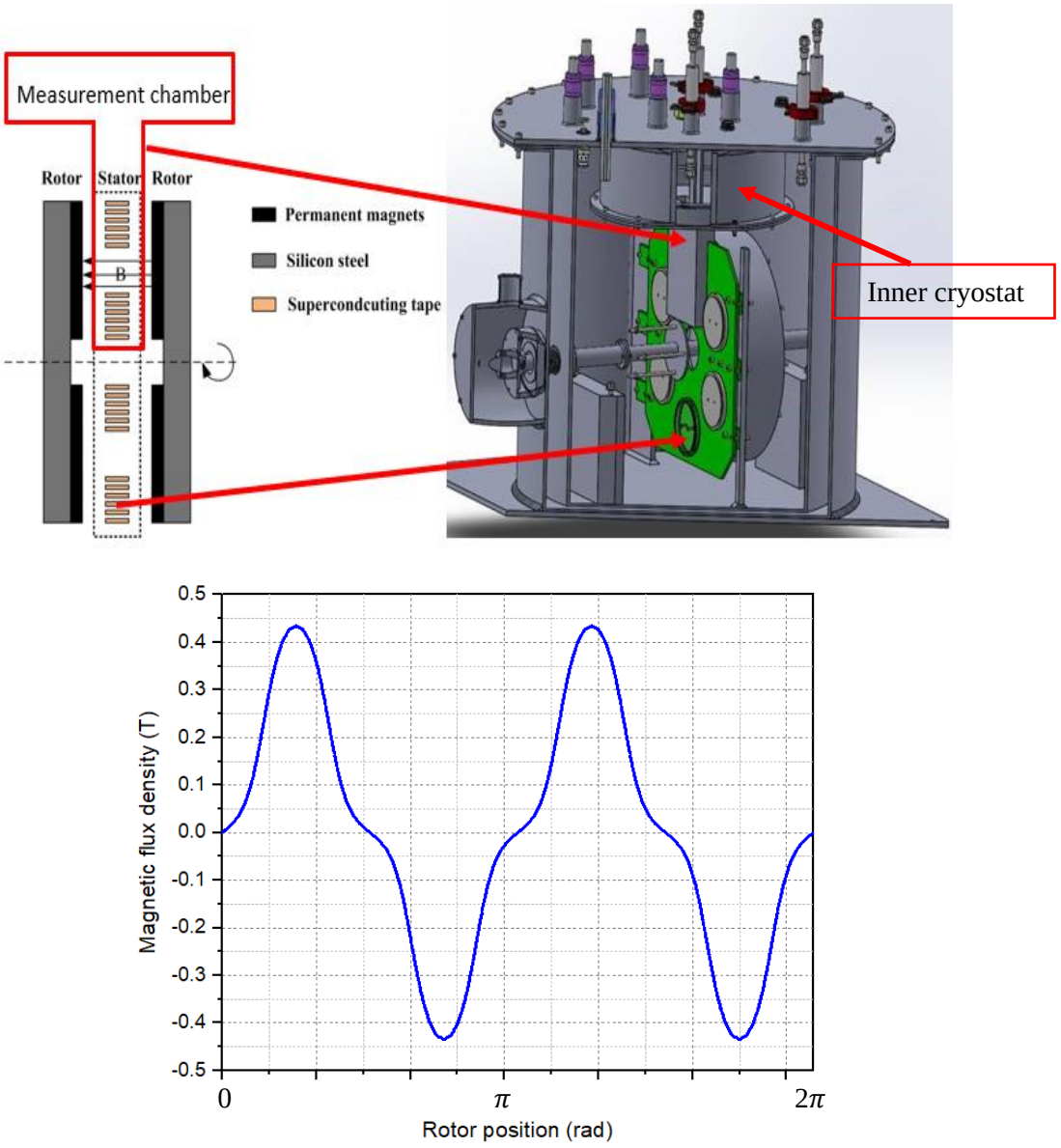

Figure 2. 12. *Measurement chamber structure and rotational magnetic field profile [133]*

The machine is housed in a LN_2 cryostat with a rotational seal and is designed to operate at a speed of 300 RPM, generating a 10 Hz three-phase voltage output. The phase A voltage is generated by two HTS coils, while the voltages of phase B and C are generated by copper coils. Figure 2.13 shows the configuration of the designed measurement chamber with the specific position for coils to be tested. The specification of tested sample coils is shown in Table 2.4 previously. Only one HTS stator coil is placed in the measurement chamber, and is connected to a flow meter to measure the flow rate of the nitrogen gas. Under ideal conditions, there should be no heat transfer inside, since the measurement chamber is vacuum insulated and fully immersed in LN_2 to minimize heat transfer with outer cryostat; both rotor and stator are fully immersed in liquid nitrogen during operation. The only conducting component inside the measurement chamber is the HTS stator coil, which ensures that the boil-off of liquid nitrogen is due only to the total AC loss of the HTS coil.

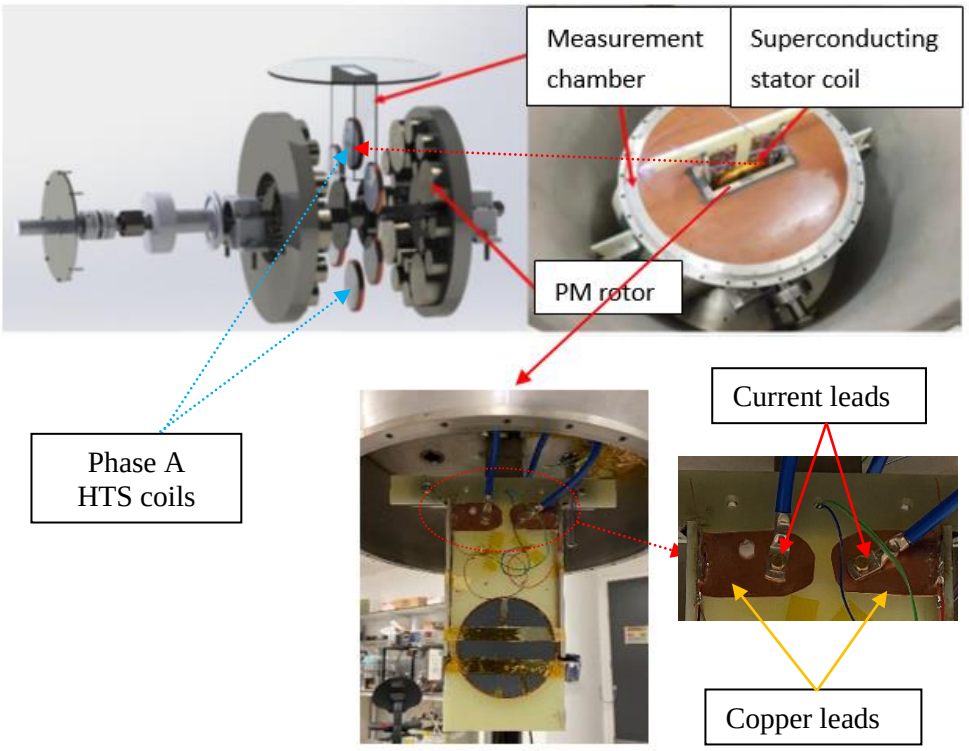

Figure 2. 13. *Measurement chamber configuration of HTS machine platform*

The nitrogen gas flow rate is measured by a flow meter (Omega FMA 2710). The total AC loss in J/cycle/m over a period of T in the measurement chamber can be calculated using Equation 2.2 [126] as the following:

$$Q = \frac{\int_T \frac{F(t)}{K} dt}{f} \cdot \frac{1}{L} \tag{2.2}$$

where $F(t)$ is the flow rate of nitrogen gas boiled off in the measurement chamber measured by a flow meter, L the total length of the HTS coil, and f is the operating frequency of HTS machine, and $K = 0.256$ ($1\ min^{-1}W^{-1}$) is the flow rate constant. When the HTS machine operates in a steady state with a fixed frequency f, $F(t)$ in the Equation 2.2 is simply a constant value with a very small fluctuation. After calibration procedures, by measuring the nitrogen gas flow rate, and calibrating the value of the AC loss element, the coil AC loss can then be calculated.

According to the platform setup, the total heat input to the measurement chamber (Q_{total}) includes the following components: the heat caused by the HTS coil (Q_{HTS}); the unavoidable heat leakage in the system ($Q_{background}$); the thermal balance condition change when liquid nitrogen was stirred by the rotor ($Q_{rotation}$); and the Joule heat caused by copper terminals and soldering joint resistance between HTS and copper current leads ($Q_{terminal}$). Hence, a dedicated calibration process for the whole system must be carried out before the AC loss measurement can be performed. The detailed information can be found at paper [133]. Then a resistive heater was placed inside the measurement chamber and heated using a DC current to calibrate the measurement chamber, in order to validate the system and demonstrate that there was no gas leakage between the measurement chamber and outer cryostat.

The entire system setup is illustrated in Figure 2.14. The separately excited DC motor is driven by two DC power supplies; during the measurement procedure, the rotation of the HTS rotors is driven by a DC machine. Three-phase power is generated by two HTS coils (phase A) and four copper coils (phase B and C), in which the measured single HTS stator coil is connected to a load bank. The LN_2 level in the cryostat is observed by 4 PT100 temperature sensors, LN_2 boil-off flow rate is recorded by a

flow meter, and all data were recorded by a NI DAQ system. An overview of the HTS machine performance, including coil voltages, coil currents, motor speed, flow meter data, and LN_2 level, is recorded by a status monitor.

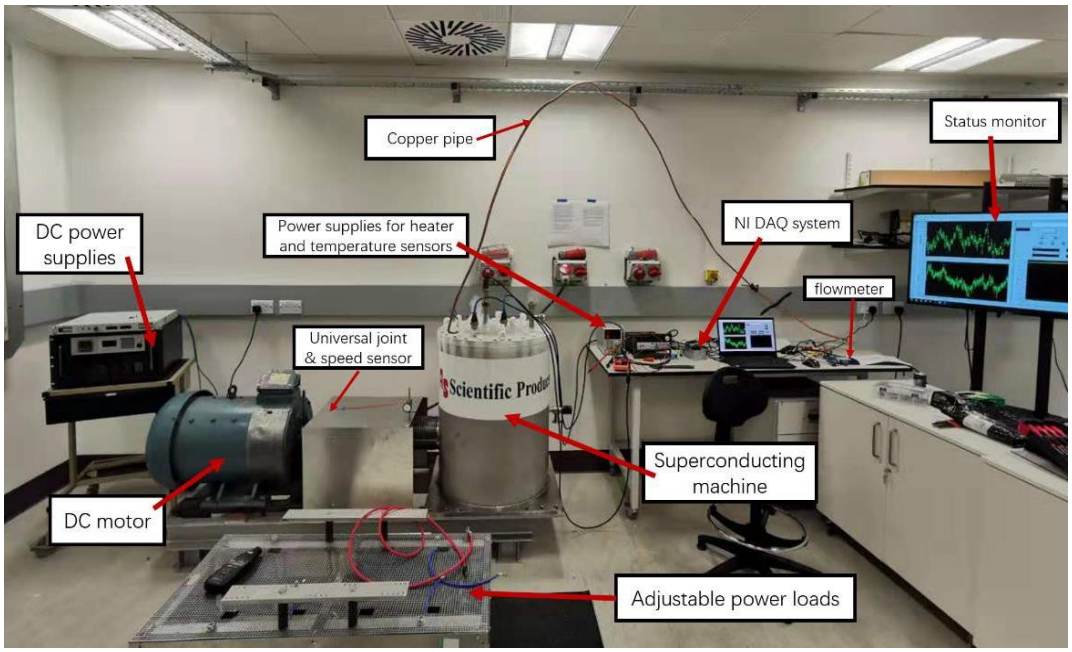

Figure 2. 14. *Total HTS machine system configuration [133]*

2.3.2.2 AC loss of HTS stator

(a) Magnetization loss

The magnetization loss of the coil can be measured by keeping the HTS coil open circuited, so that there is no transport current in the HTS coil, and only the magnetization loss is measured. We measured five different frequencies (2 Hz, 4 Hz, 6 Hz, 8 Hz, and 10 Hz) for both coils; as this is a two-pole-pair rotor, these frequencies correspond to rotor speeds of 60, 120, 180, 240, and 300 RPM, respectively. An integral operation was applied to calculate the total nitrogen gas volume for a period of time. After calibrating out flow-rate errors, the magnetization loss of the coil versus frequency can be calculated by Equation 2.2, as shown in Figure 2.15.

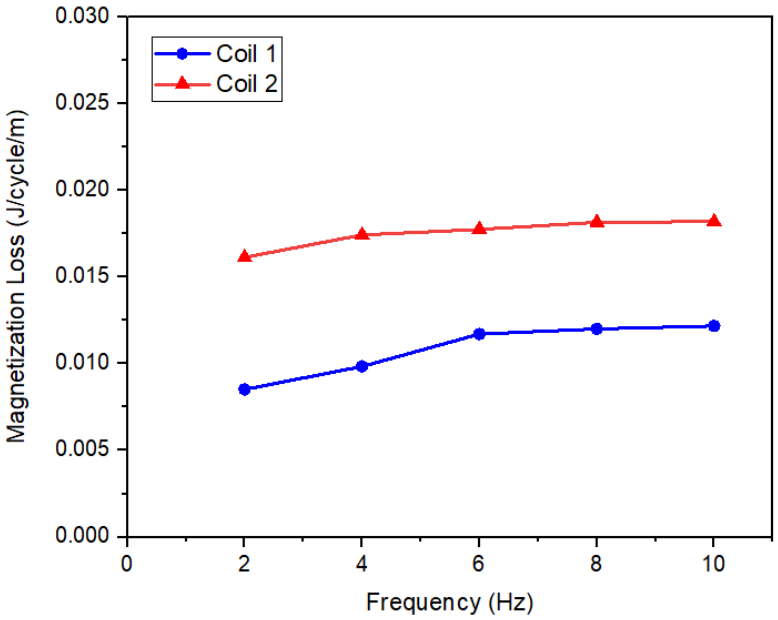

Figure 2. 15. *Magnetization loss versus frequency*

(b) Total AC loss

Using this platform, the total AC loss of a single HTS coil was measured by connecting the three-phase stator windings to adjustable power resistors [133];[134], when it was carrying a transport current and subjected to a peak 0.45 T rotational magnetic field. To measure the total AC losses at various currents generated by the HTS coil, the resistor values were changed accordingly. For this work, we measured several different peak transport currents between 10 A and 65 A for different frequencies corresponding to different rotor speeds up to 300 RPM and 10 Hz. An example of the current waveforms at various resistances for Coil 1 at 10 Hz is shown in Figure 2.6. It should be noted that the AC loss is a small value when a small transport current is applied and also at low frequencies. Therefore, if the level of fluctuation falls below 0.08 SLPM for more than 1 min, an integral operation may be used to calculate the flow rate data for the previous 10 seconds to improve accuracy. After calibration of the calorimetric measurement, the total AC loss in J/cycle/m versus normalized peak transport current is shown in Figure 2.17.

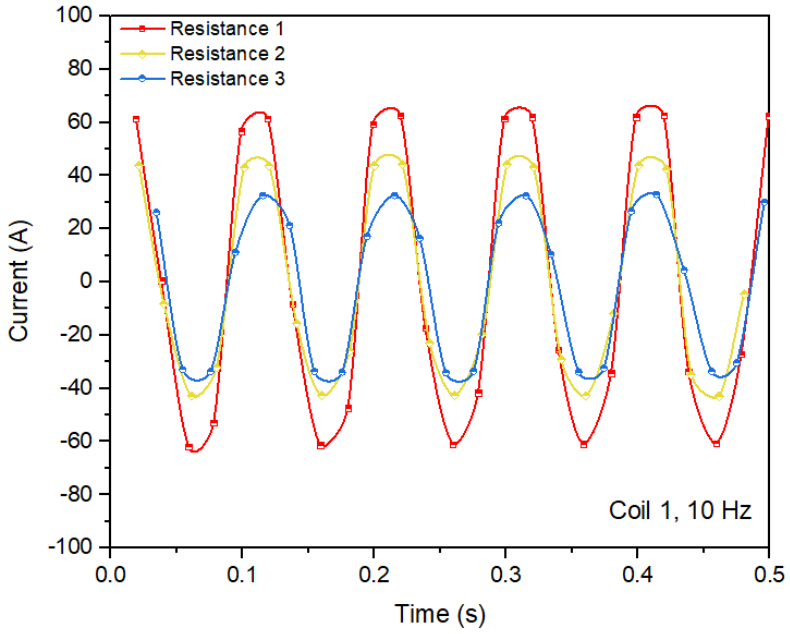

Figure 2. 16. *The current waveforms at various resistances for Coil 1 at 10 Hz*

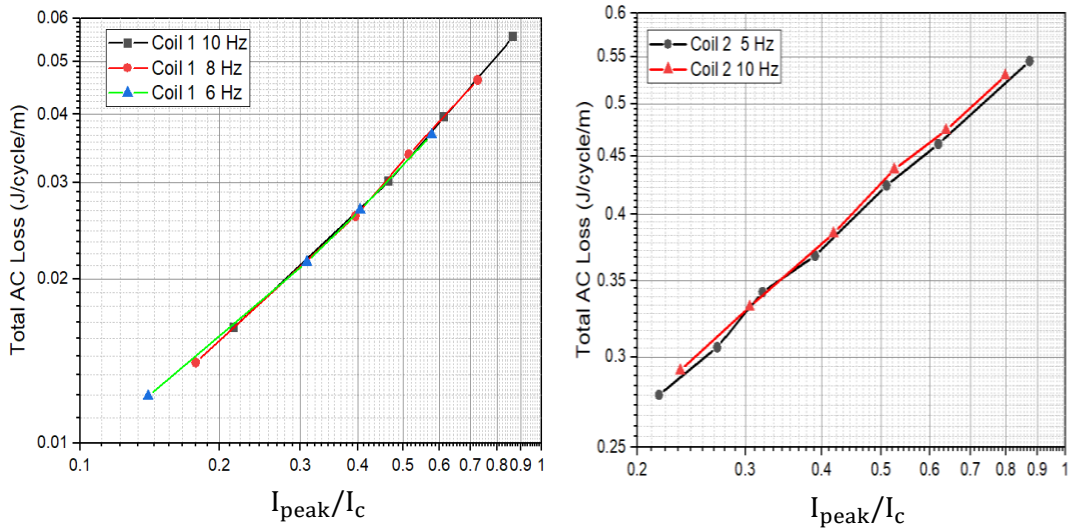

Figure 2. 17. *Total AC loss measured in a 0.45 T rotational magnetic field for Coil 1 and Coil 2*

To conclude, this section developed a platform for HTS coils in rotational magnetic machine environments. Two 4 mm HTS coils were tested using this platform. We have studied the tape characteristics in the machine environment, and good

characteristics of the tape can enhance the AC loss performance in the machine environment. We measured the magnetization loss and total loss of these two coils in the machine environment and were prepared for more HTS coils to be tested in order to find an effective way to achieve high efficiency of the HTS machine.

2.4 Conclusion

In this chapter, the AC loss measurements are well presented by experimental methods. To begin with, the insulation material selection for 2G HTS tape insulation was illustrated in detail. Kapton tape and heat shrink tubing were chosen for insulating all the experimental 2G HTS tapes. Then the manufacturing procedure of 2G HTS coils was introduced. Two double pancake 4 mm standard HTS coils were prepared for measurement. For the critical current test, using the 1 μV/cm criterion, the critical currents for the coils were determined. The transport loss, magnetization loss and total loss for the coils were measured using both the electrical and calorimetric methods. The transport loss measurements from the electrical and calorimetric methods were both frequency independent. The HTS machine platform illustrated in this chapter focuses on calorimetrically quantifying the HTS stator and provides valuable insights into the AC losses of the HTS stator in a rotational machine environment. Later, this platform can be used to identify AC loss reduction technologies, contributing to the development of a highly efficient fully HTS propulsion machine.

Chapter 3

AC loss reduction strategies

Fully HTS machines provide a high power density to meet the requirement of future electrical aircraft propulsion. However, the AC loss of HTS armature windings, as the technology stands, is hindering the improvement of overall machine efficiency. It has been an established understanding that the AC loss of 2G HTS windings must be reduced for fully HTS machine applications, which can lower the constraint on the cryogenic cooling demand. In this chapter, several ways to develop multi-filament HTS cables have been reported, focusing on the different approaches to make filamentized coils, on the effectiveness of the AC loss reduction, and on the applicability of those techniques to long lengths. Both transport losses in a self-field and total AC losses in a rotational magnetic field are measured to quantify the AC loss reduction for different multi-filament HTS coils. By comparing different proposed reduction strategies to lower AC loss, we can seek ways to improve the coil performance and optimize motor armature winding design, thereby contributing to future aircraft propulsion applications.

3.1 Introduction to AC loss reduction mechanism

3.1.1 Importance of AC loss reduction

2G HTS tapes have become a promising material for high current applications over recent decades, owing to their extremely high critical current density, in-field behaviour, and mechanical strength [98];[135];[136]. The current 2G HTS tapes normally have extremely large width-to-thickness ratio [137]. Their major drawback appears when used in AC conditions where the time-varying magnetic field/current will increase the hysteresis current loop, leading to increased AC losses and increased overall size of associated cooling systems. As a result, a lot of 2G HTS applications mainly focus on DC applications. However, there are certain applications that involve the use of 2G HTS in AC conditions, e.g., fully HTS machines for high power density aviation propulsions [42];[52];[138], and HTS cables, transformers and fault current limiters for AC power system applications [139]. In these applications, the increasing demand and widespread adoption of electrical drives in aircraft, automobiles and machines have intensified efforts and cost in the design and development of high-performance electrical machines combined with high power density, light-weight and high efficiency. Therefore, it is of paramount importance to reduce the AC loss of 2G HTS in order to minimize the cooling requirements.

In a fully HTS machine, the HTS stator is subjected to a rotational AC magnetic field, as well as an AC transport current. This generates AC losses, which potentially increases the size and weight of the machine cooling system. With the majority of the power loss within high power density electrical machines often being generated in the stator winding [140], it is necessary to reduce the copper losses and improve the heat transfer mechanisms for such losses. As a result, the key challenge of developing a fully HTS machine is to minimize the HTS winding AC losses. So far, most of the research in the area of HTS tapes and coils has focused on transport AC loss or magnetisation loss in a uniform magnetic field [141];[142]. Few studies have dealt

with the issue of the AC loss of HTS in a rotational magnetic field [100]. Therefore, for 2G HTS involved in AC applications, it is of critical importance to seek ways to accurately estimate the AC loss of HTS windings for maximizing machine efficiency.

3.1.2 Theory of AC loss reduction

To reduce the AC loss, ideally the HTS cable needs to be twisted into narrow filaments. Brandt et al [143] and Zeldov et al [144] indicate in their theory about thin HTS filaments placed in an external dynamic magnetic field that the magnetization loss is proportional to the square of the strip's width, which means that if a superconductor is striated into N filaments, its AC losses are expected to decrease by a factor of N. In order for the striation to be effective at reducing the AC losses, however, the filaments need to behave as separate objects, i.e., to be electromagnetically uncoupled. If the currents induced by the varying magnetic field couple the filaments together, the striation is practically ineffective. In order for the filaments to be uncoupled, conductive materials acting as an electrical path should not be contained between the space.

The magnetization AC loss per unit length of a thin superconducting strip of width 2a, thickness 2b, and sheet critical current density J_{cs} subjected to an AC perpendicular field $H_a \sin(wt)$ is given by Equation 3.1 in [143]:

$$Q_{strip} = 4u_0\, a^2\, J_{cs} H_a g(H_a/H_c) \tag{3.1}$$

where u_0 is the magnetic permeability of vacuum, $g(x) = (2/x)\ln\cos(x) - \tan h(x)$ and $H_{cs} = J_{cs}/\pi$. The expressions above show that the AC loss is proportional to the square of the width of the tape. Hence, dividing a tape into N filaments leads to an AC loss reduction of a factor N. Actually, this is true only if the magnetic field is large enough to fully penetrate the superconductor. If this is not the case, the sum of the AC losses in the individual filaments can be larger than the losses of the original unstriated tape at the end. Usually for HTS machine applications, the background

magnetic field is large enough to fully penetrate the HTS tape, so the magnetisation loss is proportional to the square of tape width according to this equation. Therefore, ideally, by narrowing the HTS tape width, the AC loss can be reduced accordingly.

3.1.3 Proposed AC loss reduction strategies

Many studies for narrowing HTS filaments to reduce AC loss have been reported previously. However, due to their flat geometry, this is difficult to achieve using HTS coated conductors. Four different technologies, as illustrated in Figure 3.1, have been documented so far to reduce AC losses in HTS windings. Figure 3.1.a shows a Roebel cable structure as a twisted HTS cable with laser striation [145]. Creating Roebel cables involves a large amount of wasted HTS materials and construction complexities, so they are not ideal for large-scale applications. Figure 3.1.b shows the CORC cable as a twisted HTS cable [146] which involves multiple HTS tapes helically wound along a copper former. CORC cables are mainly designed for high DC currents in high-field applications. The copper former of CORC cables is not ideal in a rotational machine environment because once the magnetic field penetrates the HTS layer, the eddy losses are huge. Figure 3.1.c shows a laser striated HTS: the magnetization losses of a striated HTS under an external AC field can be reduced, but there is no effective twisting solution to reduce the coupling effects via the copper stabilisers [137];[147];[148]. Figure 3.1.d shows a new soldered-stacked-square (3S) HTS wire taken by a novel structure of square cross section based on 2G narrow tapes with 1 mm width, suggested and successfully developed by Li et al [149].

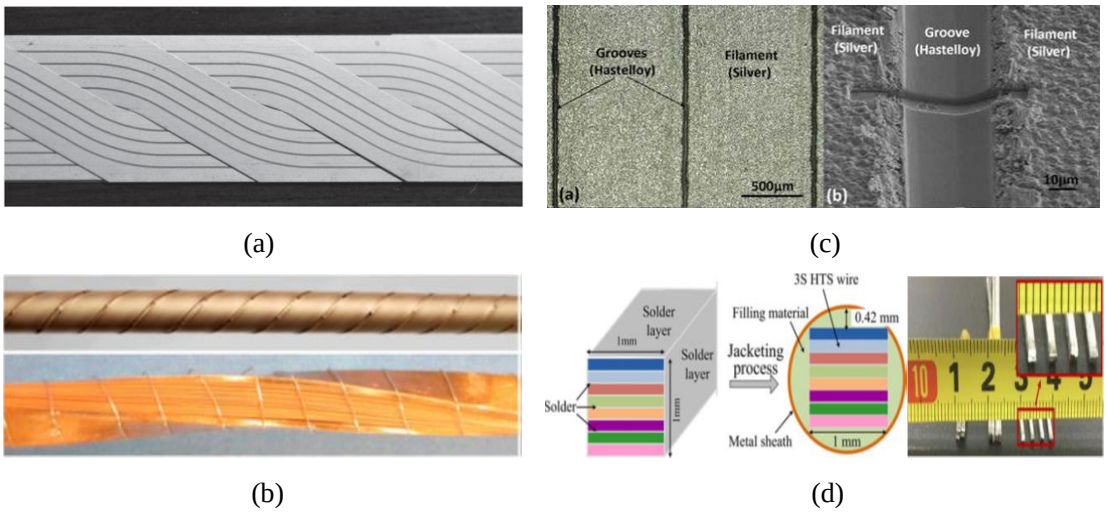

Figure 3. 1. *HTS technologies developed so far for AC loss reduction. (a) a Roebel cable with striation; (b) CORC cable; (c) Optical microscope and SEM micrographs after striation of HTS; (d) Soldering-stacking HTS cable.*

In order to effectively reduce the AC loss of 2G HTS cables, in this chapter, three different strategies are raised and evaluated for comparison and optimization of the motor armature windings design. To begin with, a new multi-filament HTS wire, called soldered-stacked-square (3S) wire, is proposed to reduce AC loss. The fundamental idea is to mechanically cut the normal 4 mm HTS tape into 1 mm wide and stack them into a wire and soldering simultaneously. This idea was first suggested and successfully validated by Li et al [149]. A follow-on study conducted by Wang et al [150] showed that the AC loss of this kind of multi-filament HTS cable can be effectively reduced, and the reduction depends on the width of the HTS strips, but the soldering stack will increase the coupling losses and eddy losses under an AC magnetic field. Hence, we need to further investigate its AC loss performance under a rotational magnetic field, and study ways to improve the cable design and further reduce AC loss for it to be used in the armature windings of fully HTS machines.

Secondly, striation techniques of 2G HTS superconductors as a way to reduce their magnetization AC losses have been the subject of intense worldwide research over decades. While the principle of this approach is well established, due to manufacturing

and technological constraints, its practical application on commercial materials to be used in power applications is still yet to be implemented. Moreover, due to coupling current flow between the copper stabilizer layers in AC magnetic fields, the overall AC losses may be increased at the end. Therefore, as the second strategy proposed in this chapter, we will evaluate the feasibility of this method through experiments by making a sample coil using the new striation technique of the Fujikura company, and further investigate how copper layers will affect the overall AC loss using the numerical modelling method.

The third strategy is to employ heat shrink tubing as insulation to increase the contact resistivity between filaments for developing a new HTS multi-filament cable. To remove the eddy losses and coupling losses introduced by the soldering stack [150], the new multi-filament HTS cable will be constructed without soldering stacking: narrow HTS strips will be directly stacked and insulated in heat shrink tube insulation, with the cabling tension provided by shrinkage of the insulation tube [100]. It is possible to further eliminate coupling losses by using insulated HTS filaments in the cable. However, the current sharing between filaments in thermal-run-away events will be prohibited, leading to low thermal stability. Ideally, we want to encourage current sharing between filaments when there is a quench while limiting coupling current in AC operations. Herein, this strategy studies the technology of stacking non-insulated HTS filaments into a cable and focuses on investigating the loss reduction achieved by using narrow HTS filaments.

For these three strategies, in this chapter, the transport AC loss for all prepared sample coils will be measured by the electric method and the total loss measurement in a peak 0.45 T rotational magnetic field will be characterized based on the calorimetric boiling-off of liquid nitrogen [151];[152];[153]. Finally, we can compare all results and quantify the reduction rate, thus achieving the purpose of further reducing AC loss for fully HTS machines.

3.2 AC loss reduction achieved by 3S coil

An effective way to reduce the AC loss of 2G HTS tape is to reduce the width of the tape [137]. Therefore, a filamentary structure has been proposed by many researchers. The multi-filament method may use either mechanical scribing, etching, or ink-jet printing to divide the HTS layer, or mechanical cutting or fast laser cutting to divide the HTS tape. The challenge is that the narrower tape width of the multi-filament 2G HTS tape can be easier to damage when manufacturing and operating in a complex electromagnetic environment. The overall losses could also increase due to a coupling current flowing between copper stabiliser layers in AC magnetic fields. Thus, in this section, we proposed 3S HTS wire concept [149] to reduce AC loss. The previous results have shown good critical current distribution and effectively reduce transport AC loss. It is reported that the 3S concept could help to reduce the transport AC loss by 80% compared with the original 4 mm tapes [150]. However, this wire has not yet been studied in a magnetic field. To push forward this wire in the HTS armature winding application and confirm the effectiveness of AC loss reduction of the new multi-filament wires in the machine environment, we studied the total loss and magnetisation loss of two double pancake coils made of the new multi-filament wire and normal 4 mm tape in a 0.45 T rotational background magnetic field, to prove that the new multi-filament wire can effectively reduce total AC loss in a machine environment.

3.2.1 Sample coil preparation

The used experimental 2G HTS tapes are from SuNAM. As shown in Figure 3.2, a 3S wire is fabricated through narrowing, soldering, and stacking processes. 4 mm commercial 2G HTS conductors are cut into 1 mm ones by the manufacturer. Then soldering and stacking of the 1 mm HTS conductors is undergone simultaneously. The average critical current of the 1 mm strips used in 3S wire fabrication is about 50 A

measured by the manufacturer. We employed heat shrink tubing as insulation to insulate the 3S wires and then winded them into coils. In order to reduce the effect on AC loss comparison caused by the critical current difference, the testing 3S coil is appropriately chosen to be close to a standard 4 mm coil, which is Coil 2 measured in the experiments presented in the previous chapter. Figure 3.2 shows the picture of two coils, the parameters for which are shown in Table 3.1.

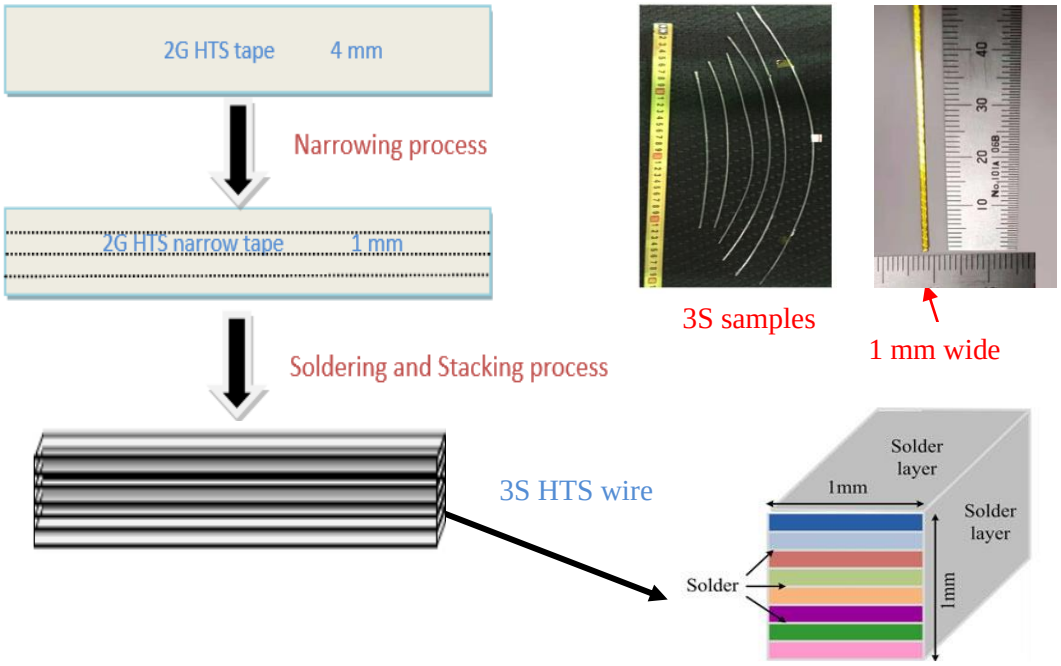

Figure 3. 2. *The fabrication process of solder-stacked-square (3S) HTS wire*

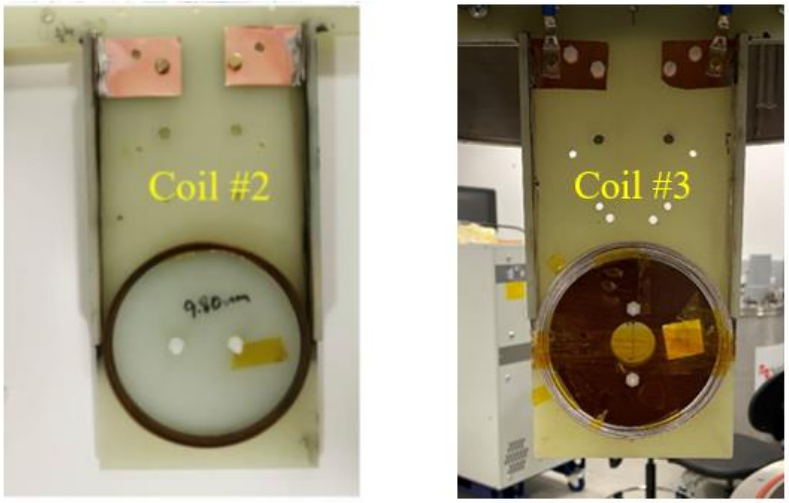

Figure 3. 3. *Photos of standard 4 mm coil (Coil 2) and 3S coil (Coil 3)*

Table 3. 1: Specifications of Coil 2-3

Parameter	Coil 2	Coil 3
Used HTS wire	4 mm SuNAM	4*1 mm SuNAM
Insulation	Kapton tape	Heat shrink tubing
Coil length	15.5 m	15.5 m
Total turns	50	52
Inner diameter	98 mm	90 mm
Outer diameter	103 mm	100 mm
Inductance	440 μH	449 μH
Tape I_c @77 K	250 A	200 A (50 A per filament)
Coil I_c (Self-field) @77 K	102 A	95 A
Coil I_c (In-field), peak 0.45 T, @77 K	59 A	49 A

The critical currents of the coil samples are measured by a standard four-probe method under self-field conditions in liquid nitrogen at 77 K operating temperature, as shown in Figure 3.4.

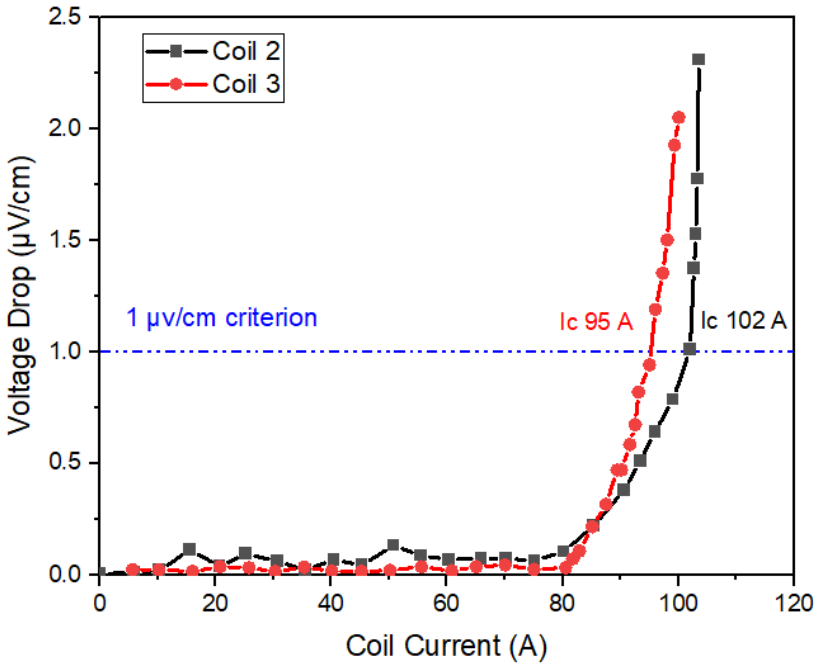

Figure 3. 4. *Critical current of Coil 2 and Coil 3*

3.2.2 AC loss measurements

In order to evaluate the effect of the 3S wire on AC loss reduction, the experimental value of AC loss was measured by both the electric and calorimetric methods. For transport AC loss measurement, the same testing platform as presented in Figure 2.9 was used, and a cancellation coil was used to compensate the inductive component of loss voltage, so that only the resistive component was picked up. The value of AC losses can be calculated by applying Equation 2.1. To remain consistent with the previous experiment, the same frequencies were chosen: 50 Hz, 75 Hz, and 100 Hz, respectively. Figure 3.5 shows the experimental measured results of transport AC loss and comparison between two coil samples. Our results indicate that the transport

losses of both Coil 2 and Coil 3 are frequency independent. This phenomenon means that the soldering layers added in the 3S wire to enhance the mechanical strength do not significantly affect the transport AC loss under different frequencies. According to the normalized transport AC loss results in Figure 3.5, our 3S wire reduced the AC losses of Coil 3 to about 84% of those of Coil 2 at the normalized current close to 70% of the critical current. We can see that the reduction rate we obtained is very close to the previous 3S coil test conducted by Wang et al [150], so it further demonstrates that 3S coil has great potential in minimizing the AC losses.

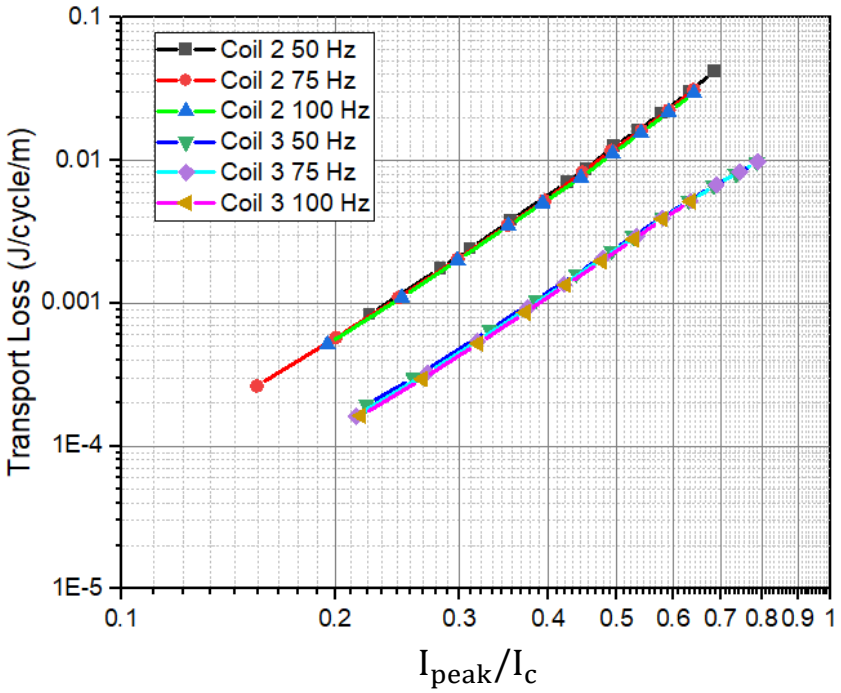

Figure 3. 5. *Transport AC loss comparison between Coil 2 and Coil 3*

The AC loss performance of 3S coil in a rotational magnetic field was then investigated, in order to prove that the multi-filament wire can reduce AC loss in a real machine environment and is more suitable to use in armature windings in a fully superconducting machine. As illustrated in Figure 2.14, both magnetization and total AC loss measurements for the 3S coil were performed using this testing platform.

The magnetization loss of Coil 3 in a 0.45 T rotational magnetic field is shown in Figure 3.6. Compared with the previous results, at 10 Hz, the magnetization loss of

Coil 3 is 0.0208 J/cycle/m, while that of Coil 2 is 0.0182 J/cycle/m. Due to soldering stack used in the process of 3S coil manufacturing, it increases the coupling losses and eddy losses under an AC magnetic field. As a result, the magnetization loss is 0.0026-J/cycle/m higher than standard 4 mm coil at 10 Hz. Further investigations are deemed necessary to study how the soldering stack added in the multi-filament coil will affect the AC losses.

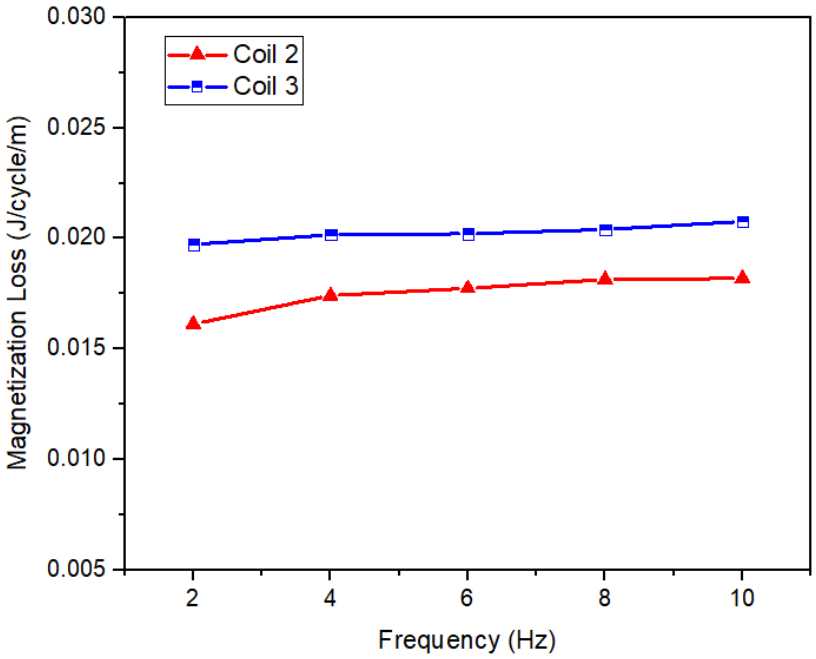

Figure 3. 6. *Magnetization loss comparison between Coil 2 and Coil 3 in a 0.45 T rotational magnetic field*

The total AC losses versus normalized currents were measured by the calorimetric method, as shown in Figure 3.7. The maximum rotational speed at 77 K is 300 RPM due to the limitation of the bearing, which means a maximum 10 Hz output. We set the frequencies at 5 Hz and 10 Hz, and the transport currents were chosen from 10 A to 50 A. According to the normalized total AC loss results, the total AC losses of both coils are frequency independent, and unlike magnetization loss, the total loss of Coil 3 is lower than that of Coil 2. This indicates approximate 26% AC loss reduction for 3S coil compared to standard 4 mm coil when applying the same normalized current subjected to a rotational magnetic field.

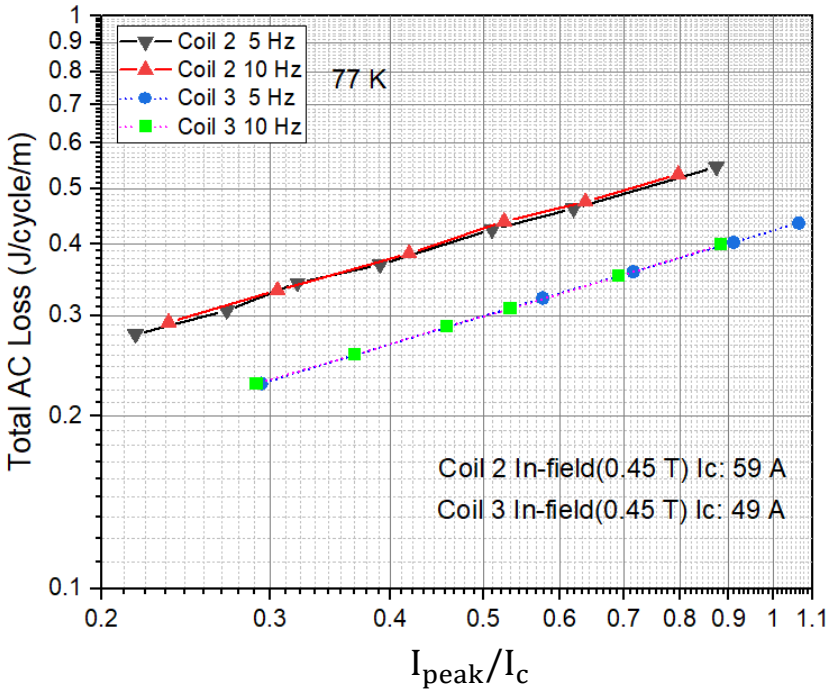

Figure 3. 7. *Total AC loss comparison between Coil 2 and Coil 3 in a 0.45 T rotational magnetic field*

3.2.3 Conclusion

To sum up, in comparison with a standard 4 mm coil wound by commercial 2G HTS tape, greater than 80% reduction of transport AC loss has been found in a 4-filament coil wound by the 3S wire. However, when placed under a 0.45 T rotational magnetic field, the total loss is reduced by only 26%, owing to the magnetization loss increased by the soldering layers used during the wire manufacturing process. Nevertheless, the 3S coil is still capable of reducing overall transport loss and total loss in the HTS stator. With development of the manufacturing technique for tape cutting, the critical current degradation and magnetization loss can be reduced further. So 3S wire has the potential to reduce total loss by more than 26% and has great advantages in minimizing AC losses. Further investigation regarding to AC loss affected by different soldering resistivities will be carried out in the next chapter by the numerical modelling method.

3.3 AC loss reduction achieved by laser striation

3.3.1 Laser striation technologies

Dividing the YBCO film into multiple thin filaments has been shown to be an effective method for reducing magnetization AC loss of 2G HTS coated conductors and several techniques have been investigated such as mechanical scribing [154], inkjet printing [155];[156], and laser ablation [157];[158]. Some of these methods have been shown to be scalable for the production of long-length multi-filamentary tapes [159]. Although there are many potential methods to fabricate the filamentary architectures described above, few have demonstrated a reliable method that is applicable to the low-cost manufacturing of practical conductor architectures. Whilst striation reduces the hysteretic loss in comparison with a single tape, it introduces a new loss in the form of a coupling loss due to the coupling of separate filaments [160];[161], and this loss can be significantly greater than the self-field loss for an uncoupled tape carrying the same current [162]. Therefore, coupling losses need to be suppressed by transposing the filaments in order for this technique to be effective over long lengths [137];[163]. Some solutions based on tape cabling techniques [164] have been proposed to solve the coupling issue where the tape is bend or twisted to achieve the transposed configuration. Other solutions based on a zig-zag pattern [165] have been proposed but this configuration imposes a reduction of the critical current just by geometrical considerations.

In this study, a new laser striation technique is developed by Fujikura company and followed by electroplating with copper to fabricate fully stabilized multi-filamentary tapes with the desired number of filaments. Laser cutting is a common manufacturing process employed to cut many types of materials, including ferrous metal, non-ferrous metal, stone, plastic, rubber, and ceramic [157];[158]. It also works perfectly with superconducting tapes by directing a high-power pulsed laser at a specific location on the surface to be cut. The advantage of laser cutting over mechanical cutting is, since

the cut is performed by the laser beam, there is no physical contact with the material therefore contaminants cannot enter or become embedded into the material.

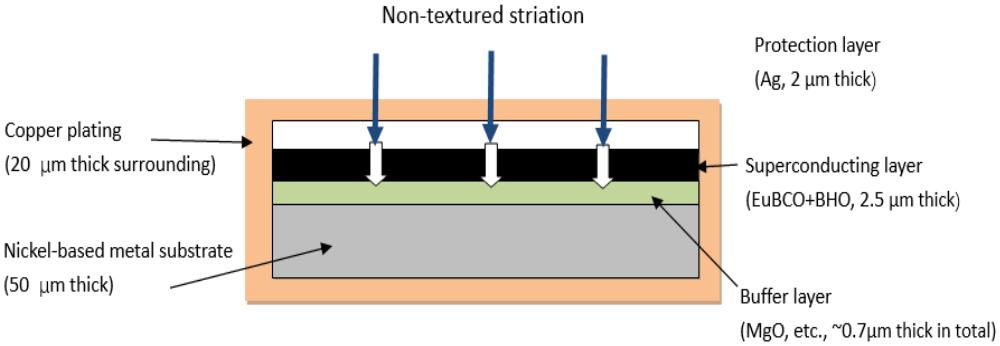

Figure 3. 8. *Striation structure*

For this work, non-textured striation is formed by slightly damaging the textured buffer layer (IBAD-MgO), and the textured superconducting layer is fabricated epitaxially with the striation non-textured, as Figure 3.8 shows, thus being able to significantly reduce the AC losses without any mechanical twisting. Herein, in this section, we report results on the AC loss investigation of prepared HTS coil wound by this novel 4 mm striated HTS tape. This new striation technique can be evaluated by both the electric method in a self-field and the boil-off method under a rotational magnetic field, and the reduction rate achieved by it can also be quantified.

3.3.2 Coil preparation and experiment results

The 2G HTS tapes used in this study were taken from a 5.5 m length of 4 mm strip wide manufactured by Fujikura company. As shown in Figure 3.8, the sample architecture consisted of a 50 μm thick nickel-based metal substrate with 0.7 μm buffer layers of MgO, and a 2.5 μm thick HTS layer, artificially pinned with striation into 4 filaments. A 20 μm copper plating layer was deposited on both sides of the tape. The critical current test of an entire short sample picked up from one side of the original HTS tape was performed by Fujikura company, and it had 120 A at 77 K in a

self-field condition. In general, the striation technique as a common approach is able to reduce the ac magnetization losses, however, it also causes the filamentized tapes having lower I_c [166]. In this work, compared to 4 mm non-striated HTS tapes, there exists large I_c reduction for our 4 mm striated tapes, which is possibly due to the following causes: the loss of superconducting material, the inhomogeneity of the superconducting material, and the possible damage caused by laser striation [167]. Also, the electroplating of the copper plate can potentially influence I_c.

After being insulated by Kapton tape, the 4 mm striated sample coil (Coil 4), as shown in Figure 3.9, was successfully prepared for the loss measurements. The non-striated standard 4 mm coil (Coil 1) is also presented for reference. Table 3.2 shows the specifications of Coil 1 and Coil 4. Figure 3.10 shows the self-field critical current measurement I–V curves for Coil 1 and Coil 4.

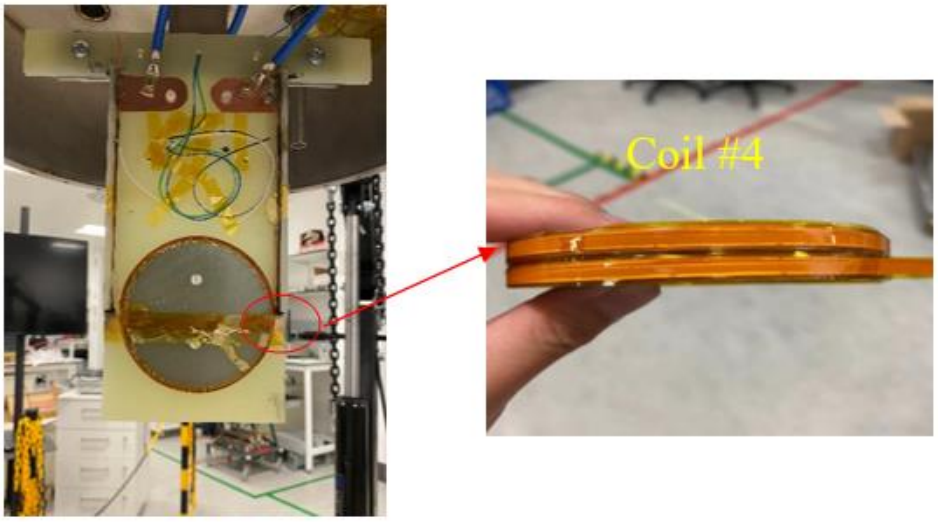

Figure 3. 9. *Prepared sample (Coil 4) for the experiment*

Table 3. 2: Coil 1 and Coil 4 specifications

Parameter	Coil 1	Coil 4
Used HTS wire	4 mm Fujikura (FYSC-SCH04)	4 mm striated Fujikura (FESC-SCH04/striated)
Insulation	Kapton tape	Kapton tape
Coil length	5 m	5.5 m
Coil type	Double pancake	Double pancake
Total turns	16	18
Inner diameter	95 mm	95 mm
Outer diameter	98 mm	98 mm
Inductance	44.2 μH	48 μH
Tape I_c @77 K	204 A	120 A
Coil I_c (Self-field) @77 K	130 A	97 A
Coil I_c (In-field), peak 0.45 T, @77K	72 A	58 A

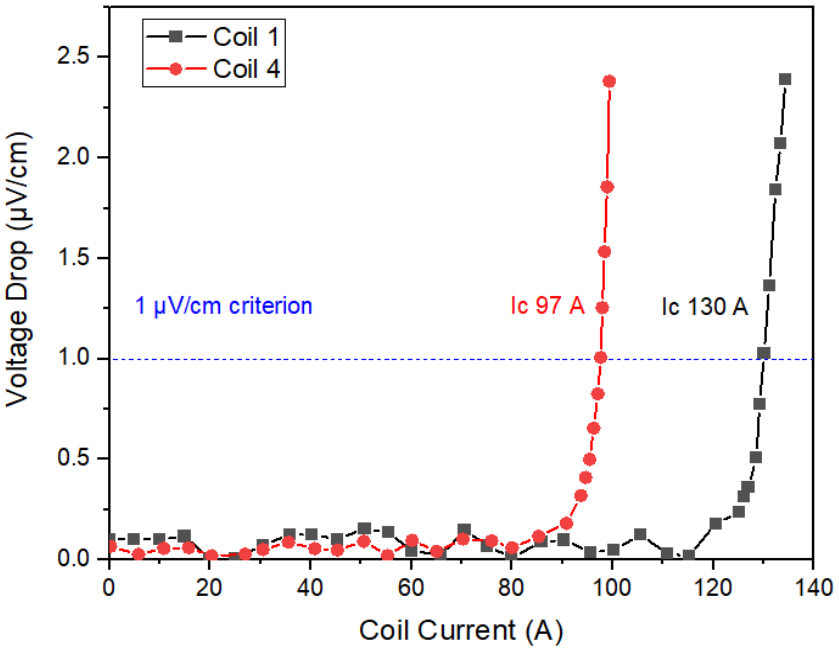

Figure 3. 10. *Critical current of Coil 1 and Coil 4*

Transport AC losses were measured at 77 K in a liquid nitrogen bath using the platform illustrated in Figure 2.9, and the experimental results are shown in Figure 3.11 for comparison between Coil 1 and Coil 4. It can be observed from this figure that the 4 mm striated coil shows 42% reduction in transport loss compared with the standard 4 mm coil.

Total loss measurements were carried out in the fully HTS machine platform and the results are shown in Figure 3.12, compared with the previous experimental results of Coil 1. Our measurements show that the total loss can be reduced by about 28% at the normalized current close to 70% of the in-field critical current.

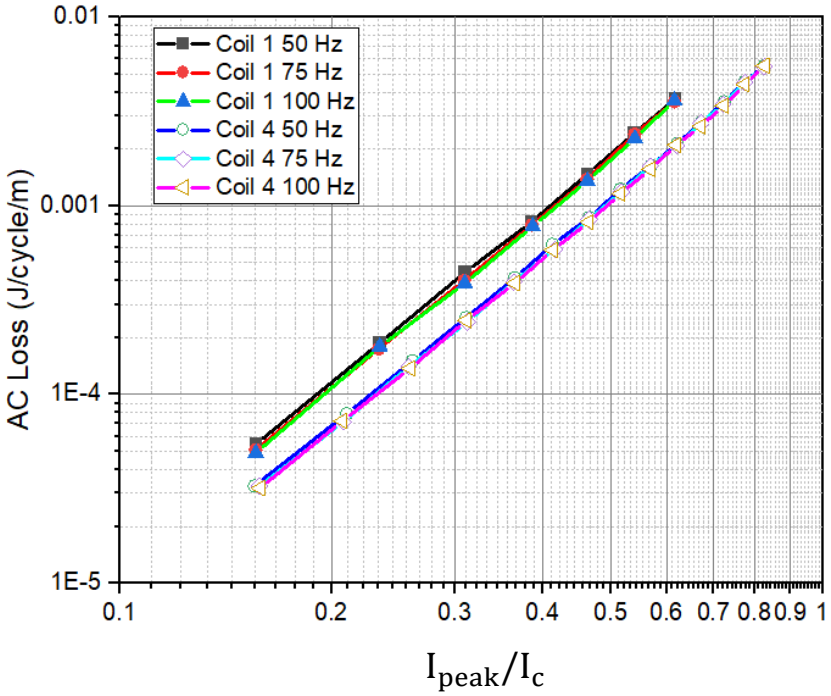

Figure 3. 11*. Transport loss comparison between Coil 1 and Coil 4 measured by the electric method*

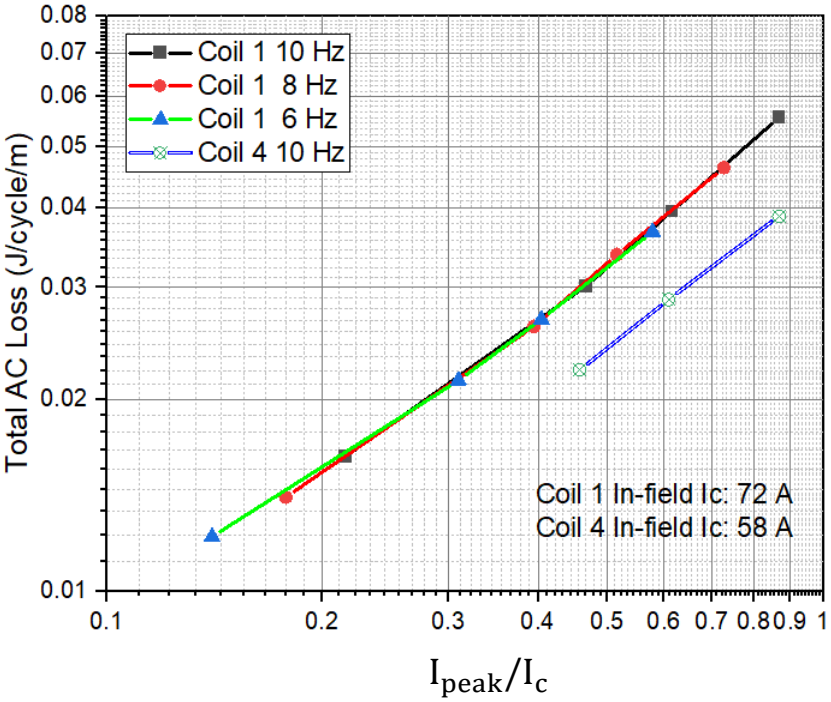

Figure 3. 12. *Total AC loss of Coil 1 and Coil 4 measured in a 0.45 T rotational magnetic field*

To conclude, we proposed another strategy in this section in order to further achieve greater AC loss reduction by using a laser striated coil. However, the results are not as expected compared with the 3S wire we presented before. The striated HTS coil can reduce the transport loss only by 42%, while the 3S coil reduced it by more than 80%. When subjected to a rotational magnetic field, the total loss for the striated coil can be reduced by 28%, very close to the 3S coil's 26%. This means that in a real HTS machine environment where the magnetic field of HTS AC windings has both perpendicular and parallel components, how to effectively suppress the coupling losses to further reduce total AC losses still remain a significant challenge, and more effective strategies should be addressed and developed.

Moreover, in addition to the winding procedure as a factor to cause the critical current reduction of the HTS wire, due to larger number of turns existed in the 3S coil (56 turns), which leads to greater local magnetic field inside the coil, the critical current is reduced from 200 A to 95 A for 3S coil. On the other hand, with a smaller number of turns (18 turns), the 4 mm striated HTS coil shows critical current reduction only from 120 A to 97 A, due to relatively less affected by local magnetic field. Therefore, two HTS coils with more similar number of turns should be investigated in the future, in order to provide more useful information on the HTS machine stator design.

3.4 AC loss reduction achieved by multi-filament HTS coils

3.4.1 Introduction

Previous study has reported the manufacturing of multi-filament HTS cables made from several narrow HTS filaments and confirmed a greater than 80% reduction in the transport AC loss in a pancake coil [150]. The HTS cable technology allows for the stacking of narrow HTS filaments, e.g., 2 mm and 1 mm, into a cable structure, thereby reducing the AC loss. However, large coupling losses were identified in magnetisation losses due to the existence of soldering layers. Therefore, in this section,

we report an improved way to develop multi-filament HTS cables using narrow HTS strips, mainly focusing on suppressing the coupling losses to further reduce total AC losses. Heat shrink tubes are used to directly insulate narrow HTS filaments into a cable structure. Sample coils were made with 4 mm, 2 mm and 1 mm wide HTS strips. Both transport losses and total AC losses in a rotational magnetic field were measured to quantify the AC loss reduction for the narrow HTS strips.

3.4.2 Sample coil preparation

The experimental 2G HTS tapes were from Fujikura. The insulation materials used were heat shrink tubing and Kapton tape, and their specifications are shown in Table 2.2. Figure 3.13 illustrates the process for a short piece of two 2 mm HTS tapes insulated with the heat shrink tubing before winding into coils, in order to validate the feasibility of employing this insulation method. Two 2 mm thin HTS strips were stacked together in parallel, then inserted into the heat shrink tubing, and evenly heated up to 422 K for a few seconds, until the tube shrank and became firmly attached to the HTS tapes. At the same time, the two thin strips were tightly folded together. The heat shrink tubing insulation provides a smooth surface for the HTS tapes, and it forms no gap between the insulation and HTS wire. Moreover, the tubing material works perfectly at the temperature of liquid nitrogen, and no degradation of the insulation itself has been observed during or after the cooling down [100];[168]. Finally, two sample coils were successfully prepared for the AC loss measurements. Coil 5, shown in Figure 3.14.a, is wound with two 2 mm wide HTS cable insulated with heat shrink tubing. Coil 6, shown in Figure 3.14.b, is wound with four 1 mm HTS strips and is also insulated by heat shrink tubing into a cable structure. In order to compare AC loss results between the multi-filament coil and a standard 4 mm coil, Coil 1 wound with a 4 mm wide HTS tape and Kapton insulation will be used to quantify the reduction rate for prepared multi-filament coils. Critical current measurements of the prepared coils showed that Coil 5 was healthy, while Coil 6 was

damaged during the stacking and winding process. So, in this study below, only the experimental results of Coil 1 and Coil 5 are investigated. Table 3.3 shows the specifications of Coil 1 and Coil 5. Figure 3.14 shows the critical current measurement results for Coil 1 and Coil 5. Respectively, the measured critical currents are 130 A and 94.5 A.

Table 3. 3: Coil 1 and Coil 5 specifications

Parameter	Coil 1	Coil 5
Used HTS wire	4 mm Fujikura (FYSC-SCH04)	2*2 mm Fujikura (FESC-SCH02)
Insulation	Kapton tape	Heat shrink tubing
Coil length	5 m	3.2 m
Coil type	Double pancake	Double pancake
Total turns	16	10
Inner diameter	95 mm	95 mm
Outer diameter	98 mm	102 mm
Inductance	44.2 μH	21.5 μH
Tape I_c @77 K	204 A	77 A per tape
Coil I_c (Self-field) @77 K	130 A	94.5 A (2 tapes)
Coil I_c (In-field), peak 0.45 T, @77K	72 A	54 A

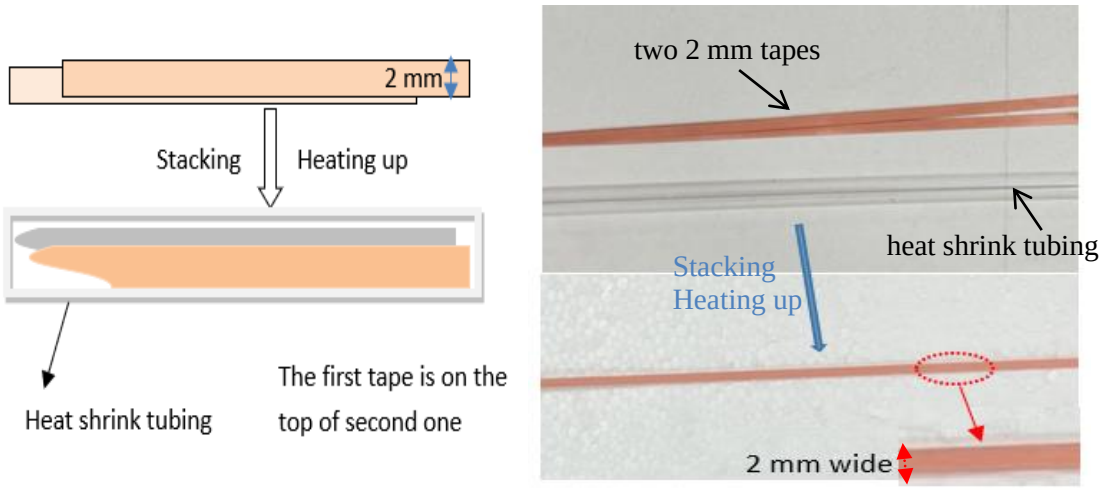

Figure 3. 13. *Insulation process for two 2 mm HTS tapes*

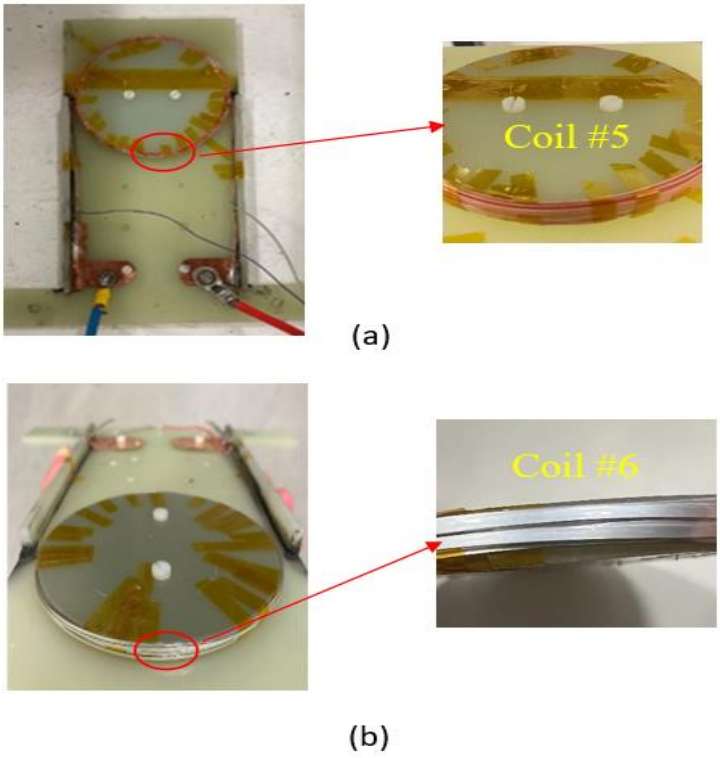

Figure 3. 14*. Prepared samples for experiment. (a) Coil 5 (2*2 mm multi-filament coil) (b) Coil 6 (4*1 mm multi-filament coil, damaged)*

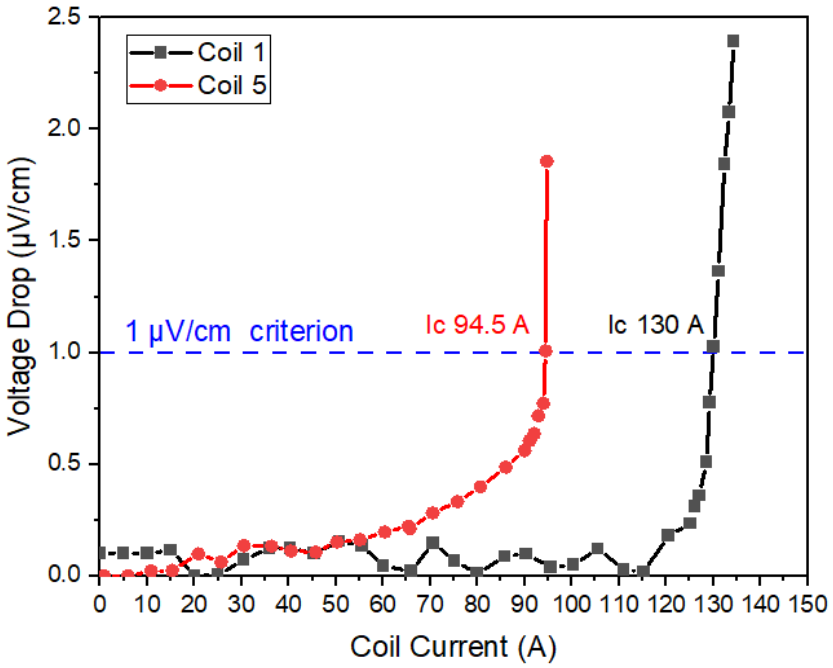

Figure 3. 15. *Critical current of Coil 1 and Coil 5*

3.4.3 Experiment results comparison

Figure 3.16 shows a comparison between the two measured coils in terms of the transport AC loss measurement results. Due to the effect of experimental errors and harmonics, the measured transport losses are too small to collect accurately for a small HTS coil like Coil 5 with a smaller magnetic field, leading to the results not overlapping completely under different frequencies. However, we can still obviously see the differences between the two sample coils from the figure. The reduction for the multi-filament coil is approximately 78% at the same normalized current, which is a very promising feature for distributed armature windings for future applications. Meanwhile, we can see that the reduction rate we obtained is very close to the 3S coil test, which is around 84%. It should be noted that there are only two filaments rather than four in one tape for this tested multi-filament coil. Therefore, the eddy losses and coupling losses originating from the soldering stack connections can be mostly

eliminated, leading to lower AC losses, by employing heat shrink tubing.

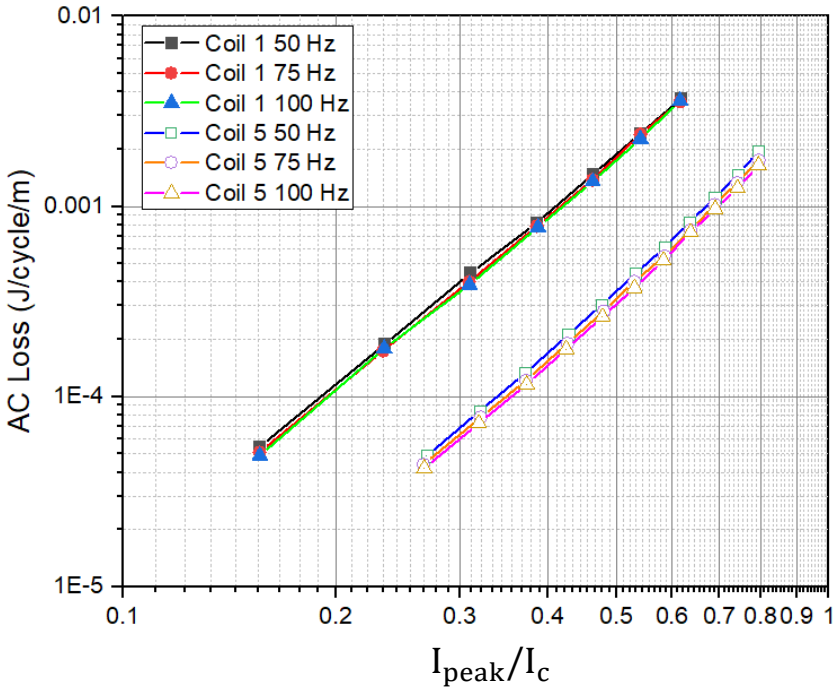

***Figure 3. 16**. Normalized transport AC loss comparison between Coil 1 and Coil 5 measured by the electric method*

For total AC loss measurements, we measured several different peak transport currents between 10 A and 65 A for different frequencies corresponding to different rotor speeds up to 300 RPM and 10 Hz. After calibration of the calorimetric measurements, the total AC loss versus normalized peak transport current is shown in Figure 3.17. From our previous study [133], the results are more accurate with the application of higher currents and at higher frequencies, since HTS machine applications are normally required to carry a high current. For the multi-filament HTS coil use under low frequencies, the boiling-off of liquid nitrogen from the measurement chamber was not big enough to offset the minimum error that the platform can tolerate. So, for Coil 5, only the result of 10 Hz corresponding to the maximum rotor speed was collected in the figure. Our results show that with a ratio of the operating current over the critical current of 69% and a peak rotational field of

0.45 T, the total AC loss for Coil 5 is 0.0218 J/cycle/m at 10 Hz and 37.2 A, while Coil 1 is 0.044 J/cycle/m at the same frequency and peak current of 69% in-field I_c (49.7 A). This indicates that the total AC loss of multi-filament cable can be effectively reduced by approximately 50% for the same normalized current in a rotational magnetic field, suggesting that using it for the armature windings of a fully HTS machine can be highly competitive to potentially satisfy future electric aircraft applications in the future.

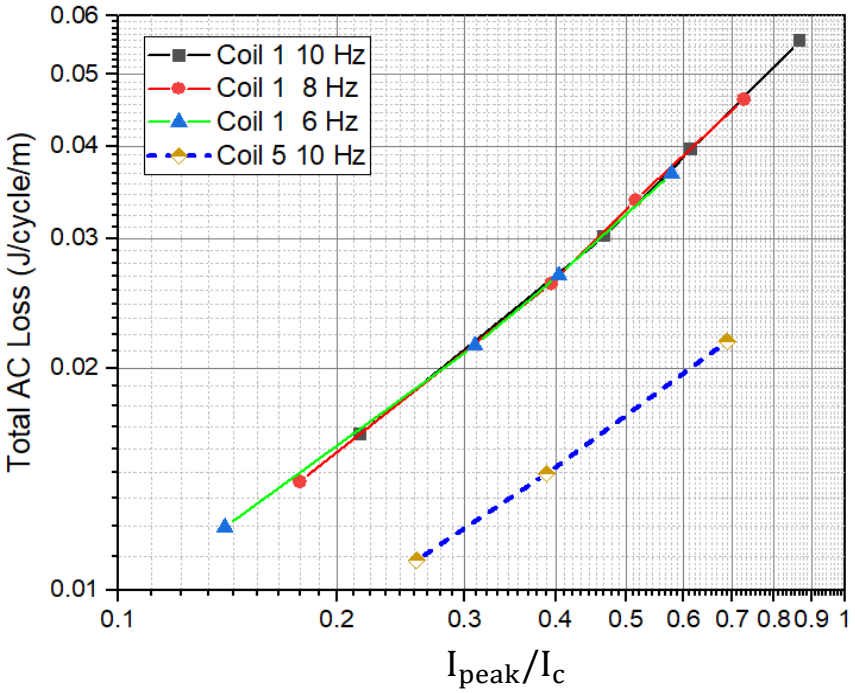

Figure 3. 17. *Total AC loss of Coil 1 and Coil 5 measured in a 0.45 T rotational magnetic field*

To further study the impact of a rotational magnetic field and quantify the loss reduction, we compared the transport loss of the HTS coils with the total AC loss, as shown in Figure 3.18. Similar to the transport loss results, the measured total loss of the HTS coil was dominated by hysteresis loss. The AC loss measurements from both electrical and calorimetric methods confirmed different levels of reduction for the multi-filament coil. Finally, we can see in Figure 3.18 the significant impact of a rotating magnetic field on the AC losses.

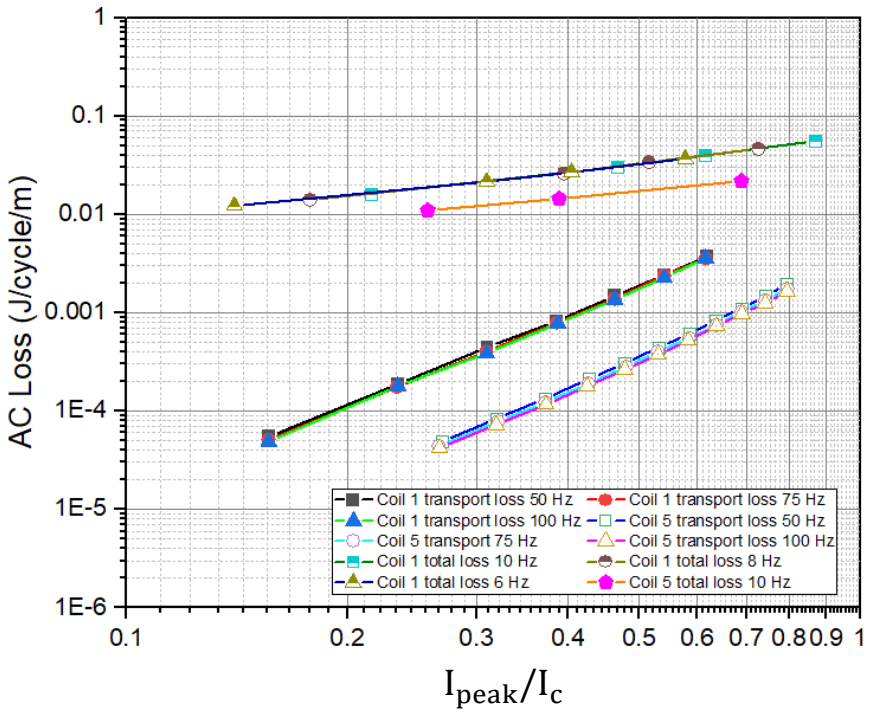

Figure 3. 18. *Comparison between transport loss and total loss for Coil 1 and Coil 5*

In conclusion, after performing loss measurements, comparing with a standard 4 mm coil wound by Fujikura 2G HTS tape, 78% reduction of transport AC loss has been found in a 2*2 mm multi-filament HTS coil through the experiment. Further study was carried out by inserting the coil into a novel HTS machine testing platform. The total AC losses of the HTS stator windings with multi-filament coil showed greater loss reduction up to around 50%. Compared with previous experimental results, the 3S coil achieved a 26% reduction rate and the striated coil can reduce the total loss by 28%, therefore, an important conclusion can be drawn here; by employing the strategy proposed in this section, the total AC loss can be further greatly reduced, making it highly competitive for future aircraft prolusion applications.

3.5 Discussion

3.5.1 Conclusion

In this chapter, we proposed three different AC loss reduction strategies and successfully performed AC loss measurements to characterize the AC loss reduction of different multi-filament cables in transport AC loss as well as total loss in a rotational magnetic field. All prepared multi-filament cables show an obvious loss reduction in regard to both a self-field and a real machine environment to different levels. Based on the experimental results, here is a summary of our findings for different strategies in reducing AC loss:

For different strategies, the 3S coil achieved 84% reduction in transport loss and 26% in total AC loss; the striated coil showed it can reduce the transport loss by 42% and total loss by 28%; the 2*2 mm multi-filament coil is capable of reducing the transport loss by 78% and total loss by up to around 50%. All the results are listed in Table 3.4 for comparison.

Table 3. 4: Reduction rate comparison between three strategies

Reduction rate	3S coil	Striated coil	2*2 mm multi-filament coil
Transport loss	84%	42%	78%
Total loss	26%	28%	50%

For the first and second strategy, soldering layers and copper plating exist in the 3S coil and striated coil, respectively. When placed under a rotational magnetic field, the induced coupling losses originating from the soldering stack connections or via the copper plating stabilizer cannot be effectively suppressed, leading to the reduction rate we achieved by these two strategies being not as expected. Therefore, we proposed a new method to make multi-filament HTS cable with increased contact resistivity

between filaments by using heat shrink tubing as insulation. To minimize the eddy losses and coupling losses, narrow HTS strips were directly stacked and insulated in heat shrink tube insulation without soldering. Perfect uncoupling between the filaments is desirable to further reduce or eliminate the coupling loss, as demonstrated in our experiments.

Last, when considering the optimization of HTS tape narrowing technology, it is essential to choose an appropriate number of filaments (or the width of the filaments) for specific applications. As performed in our work, producing filaments that are too narrow, e.g., 1 mm in long conductors is extremely risky, not only referring to the increasing probability of the presence of defects blocking the current path between different filaments, but to the potential appearance of imperfections of different types that occur during the manufacturing process of very thin strips.

3.5.2 Challenges of multi-filament HTS coils used for future electric aircraft propulsion

A particular developing component for the next generation commercial aviation fleet is the propulsion system. Three electric propulsion architectures including all-electric aircraft, turbo-electric aircraft, and hybrid-electric aircraft are therefore proposed, in order to design an electrical propulsion system with lower noise, reduced fuel consumption and high reliability. As addressed in previous section, the power-to-weight ratio associated cryocooler system remains one of the major challenges of scaling up electric propulsion to larger aircraft, since today's electrical systems cannot meet the necessary power requirements without adding extra weight to the aircraft. With the development of HTS technologies as a promising solution to this technical challenge, it can increase the power density in the propulsion chain while significantly lowering the mass of the distribution system.

Our experiment results indicate successful reduction on the AC losses of the multi-filament HTS coils used for the HTS machine stator windings, and thus being

considered as a promising candidate for the future propulsion system of an electric aircraft. However, some concerns must be taken into account, e.g., for a practical propulsion system of an electric aircraft, there could be higher harmonics in the current due to the switching frequency of the current power source, and the induced harmonic currents in generators and motors, as well as AC/DC converters, are hence unavoidable [169], which might have a significant impact on the total AC losses of the coil. Moreover, the loss induced by these undesired higher harmonic currents in contribution to the total loss increases substantially at higher frequencies, which must be evaluated when considering the design of practical propulsion system. Therefore, further investigations regarding to the coil testing at frequencies of up to few hundreds of Hz or few kHz should be conducted in the future.

Moreover, our prepared multi-filament HTS coils only consist of small number of turns, and it is necessary to expand further studies in consideration of multi-filament coils with larger size. It is because according to our measurement results, the larger the multi-filament HTS coil, the larger local magnetic field existed inside, thereby causing greater critical current degradation. Due to the lowering of the critical current, it might have an increase in AC losses caused by external rotational magnetic field. However, this issue probably can be addressed with HTS materials cooled down to lower temperatures, in this case the critical current of the HTS superconductor can be increased. More details regarding to this will be discussed in Chapter 5 when we introduce the AC loss measurement at temperatures lower than 77 K.

Last, although our experiments have proven that the coils are capable of maintaining good stability by using heat shrink tubing and Kapton tape as insulations in a 0.45 T rotational magnetic field environment, and meanwhile the insulations can withstand high voltage test up to 3 kV, but provided the magnetic field strength in the air gap being larger than that investigated here, the mechanical stability characteristics and AC loss estimation of the multi-filament coils under this circumstance need to be re-evaluated before applied for electric aircraft propulsion system.

Chapter 4

AC loss modelling and validation

In this chapter, the modelling of superconducting coils using the finite element method is described in detail, including validation of the experimental transport loss results for the tested coils and further extended exploration based on empirical data to evaluate the AC loss reduction strategies we have proposed as the research in this dissertation has progressed. Firstly, the FEM models based on experimental coils were built to numerically calculate the transport AC loss, followed by solving a set of Maxwell's equations in 2D implementing the H-formulation using the commercial software package COMSOL Multiphysics. The effectiveness of the simulation was first validated through comparison with experimental results of coils tested in previous chapters. Then, the simulation offered the possibility to extend the results to more profound fields that were not involved in the experiments.

Different scenarios to investigate how soldering stack or copper plating increases coupling losses and eddy losses in HTS coils were also discussed. Then the models were developed to further modify contact resistivities via soldering stack according to the different scenarios present in the experimental coils. This investigation raised some interesting points for further analysis, and a detailed discussion on the AC loss reduction affected by soldering stacks with different contact resistivities existing in HTS coils was carried out at the end. The first part of this chapter introduces the modelling method. The second part validates the experimental transport AC loss measurements. The final part discusses the influence of the soldering layer or copper plating on AC losses.

4.1 Review of numerical modelling

In a conventional electromagnetic problem, it is commonly accepted that Maxwell's equations can be used to determine the current and magnetic field distribution. By modifying the material properties, superconducting problems can be also solved using the same equations. This section starts with solving a conventional electromagnetic problem, and then extends the concept to a superconducting problem. To begin with, Ampere's Law describes the relationship between field and current:

$$\nabla \times \mathbf{H} = \mathbf{J} \tag{4.1}$$

If the distribution information of magnetic field H is obtained, Equation 4.1 can be used to find the solution for current density **J**. Usually, the material to be solved has certain electrical and magnetic properties written as:

$$\mathbf{E} = \rho\mathbf{J} \tag{4.2}$$

$$\mathbf{B} = \mu_0\mu_r\mathbf{H} \tag{4.3}$$

where ρ is the resistivity of the material and μ_r is the relative permeability. Once the distribution of **J** is determined, the electric field **E** can be determined. Faraday's Law is written as:

$$\nabla \times \mathbf{E} = -\frac{\partial \boldsymbol{B}}{\partial t} \tag{4.4}$$

If the **E** distribution is known, the increment of **H** can be solved. By adding to the existing **H** distribution, the new **H** distribution is available for the next time step.

Although Maxwell's equations can be used for solving a superconducting problem, in this situation, change must be made to account for the material properties. Ignoring the Meissner Effect, $\mathbf{B} = \mu_0\mathbf{H}$ can be used for superconductivity in the mixed state. The E-J power law for Type II superconductors has been given in Equation 1.1 previously, which now is the common way to describe the electrical properties of superconductors. By solving Equation 1.1 together with Equation 4.1 and Equation 4.4, the current and magnetic field distribution of a superconductor can be obtained.

This method depends on solving equations using H as variables and is therefore called the H-formulation [170].

To analyse the use of superconductors for practical applications as well as optimize the systematic design, in most circumstances the finite element method (FEM) is used to determine the current and field distributions inside superconductors under complex geometry conditions. There are three main numerical methods, each named after the variables used in the partial differential equations: the A-V-formulation [171];[172] based on the magnetic vector potential, the T-Ω-formulation [173];[174] based on the current vector potential, and the H-formulation [170];[175] based on the magnetic field. Comparisons between the formulations have been drawn in many studies [176];[177]. In this chapter, we only use H-formulation as the basis for our 2D models because methods based on the H formulation can converge more easily than other methods, and it is easy to impose boundary conditions related to the current flowing in the superconductor and externally applied magnetic fields. In many circumstances, a transport current and a background field must be considered together in the model. The H-formulation has proven to be the most practical model for integrating boundary conditions. Background fields can be applied directly by setting boundary values of H, while transport currents can be incorporated into the model according to Ampere's Law. Moreover, there is no need to differentiate the vector potentials, which might otherwise introduce some inaccuracy in the calculation.

Using the finite element software COMSOL Multiphysics, the 2D H-formulation has been successfully implemented and carried out in many studies for validation. In this chapter, three aspects will be carefully considered throughout numerical modelling. The first part is to validate the experimental results and confirm the effectiveness of empirical data by means of numerical AC loss calculations. Secondly, the current distribution and current sharing between HTS filaments are numerically studied, taking into account that the soldering stack added between HTS filaments affects the AC loss. Last, the simulation offers the possibility to predict AC loss reduction for the 1 mm wide HTS cable insulated with heat shrink tubing that was damaged during the

manufacturing process, to validate our AC loss reduction strategies as well as achieving further loss reduction theoretically.

4.2 FEM model for 4 mm standard coils

The FEM models introduced in this section were based on Coil 1 and Coil 2. They were built by the H formulation for numerical calculations of transport AC losses. In order to validate the effectiveness of the simulation, the outputs will be compared with the experimental results of Coil 1 and Coil 2. The coils were made from 4 mm Fujikura and SuNAM tapes, consisting of 16 and 50 turns, respectively. Details of the coils are given in Table 2.5. A 2D axial symmetrical model ([r; φ; z]) was applied to the double pancake coils, hence a cross section of the coil could be modelled (as shown in Figure 4.4). The model contains two variables, defined as $\mathbf{H} = [H_r; H_z]$. In a 2D axial symmetrical geometry, the induced or applied current J_φ in the superconductor flows in the φ direction, as shown in Figure 4.1, so the electric field $\mathrm{E} = \rho J_\varphi$, where ρ is the resistivity of the material.

Ampere's law is written as:

$$J_\varphi = \frac{\partial \mathrm{Hr}}{\partial \mathrm{z}} - \frac{\partial \mathrm{Hz}}{\partial \mathrm{r}} \tag{4.5}$$

Substitute $\mathbf{H} = [H_r; H_z]$ and $\mathbf{E} = E_\varphi$ into the Faraday's law for cylindrical coordinates:

$$\begin{bmatrix} -\frac{\partial E_\varphi}{\partial \mathrm{z}} \\ \frac{1}{r}\frac{\partial (\mathrm{r}E_\varphi)}{\partial \mathrm{r}} \end{bmatrix} = -\mu_0\mu_r \begin{bmatrix} \frac{\partial \mathrm{Hr}}{\partial \mathrm{z}} \\ \frac{\partial \mathrm{Hr}}{\partial \mathrm{z}} \end{bmatrix} \tag{4.6}$$

The E − J power law can be written as:

$$E_\varphi = E_0 \left(\frac{J_\varphi}{J_c(B,\theta)}\right)^n \tag{4.7}$$

where $n = 27$, $E_0 = 1\ \mu V/cm$, and $B = \mu_0\sqrt{{H_x}^2 + {H_y}^2}$. θ defines the angle between the tape surface and the local magnetic field. $J_c(B,\theta)$ is the magnetic field dependence of the critical current of 2G HTS tapes as introduced in the following section.

Substituting Equation 4.7 and Equation 4.5 into Equation 4.6, for Coil 1 and Coil 2, it is $\mu_r = 1$ everywhere, so the equations of H_x, H_y for the models can be formed as:

$$\mu_0 \frac{\partial \mathbf{H}}{\partial t} + \nabla \times (\rho \nabla \times \mathbf{H}) = 0 \tag{4.8}$$

In these models, the space is divided into two subdomains: the superconducting region and air. The resistance of the air is set as 1 Ω·m. For YBCO, the E-J power law is used to simulate its superconductivity, so the resistance of YBCO is:

$$\rho = \frac{E_0}{J_c(B,\theta)} \left(\frac{J_\varphi}{J_c(B,\theta)}\right)^{n-1} \tag{4.9}$$

where $n = 27$, $E_0 = 1\ \mu V/cm$, and $J_c(B,\theta)$ is the anisotropic characteristic of the 2G HTS tape. The n-value is identified from DC measurements of the superconductor's highly non-linear I-V characteristic. E_0 is the electric field when the superconductor carries its critical current I_c.

The $J_c(B,\theta)$ relationship must be considered carefully while modelling, because the J_c anisotropy of 2G HTS tapes under an external magnetic field will tremendously influence the current and magnetic field distribution inside HTS coils. Therefore, the modelling work will take into account the anisotropic magnetic field dependence of the critical current density. For the modelling of Fujikura tapes, the influence of the magnetic field on the critical current of 2G HTS tape is defined by interpolating data from the manufacturers, as shown in Figure 4.1. Generally speaking, the local critical current density is inversely proportional to the magnitude of the magnetic field, and in most case the perpendicular component of the magnetic field has a more obvious effect on J_c than the parallel component [10]. Figure 4.2.a shows the normalized critical current density used in the models and the angular dependence of the critical current is shown in Figure 4.2.b.

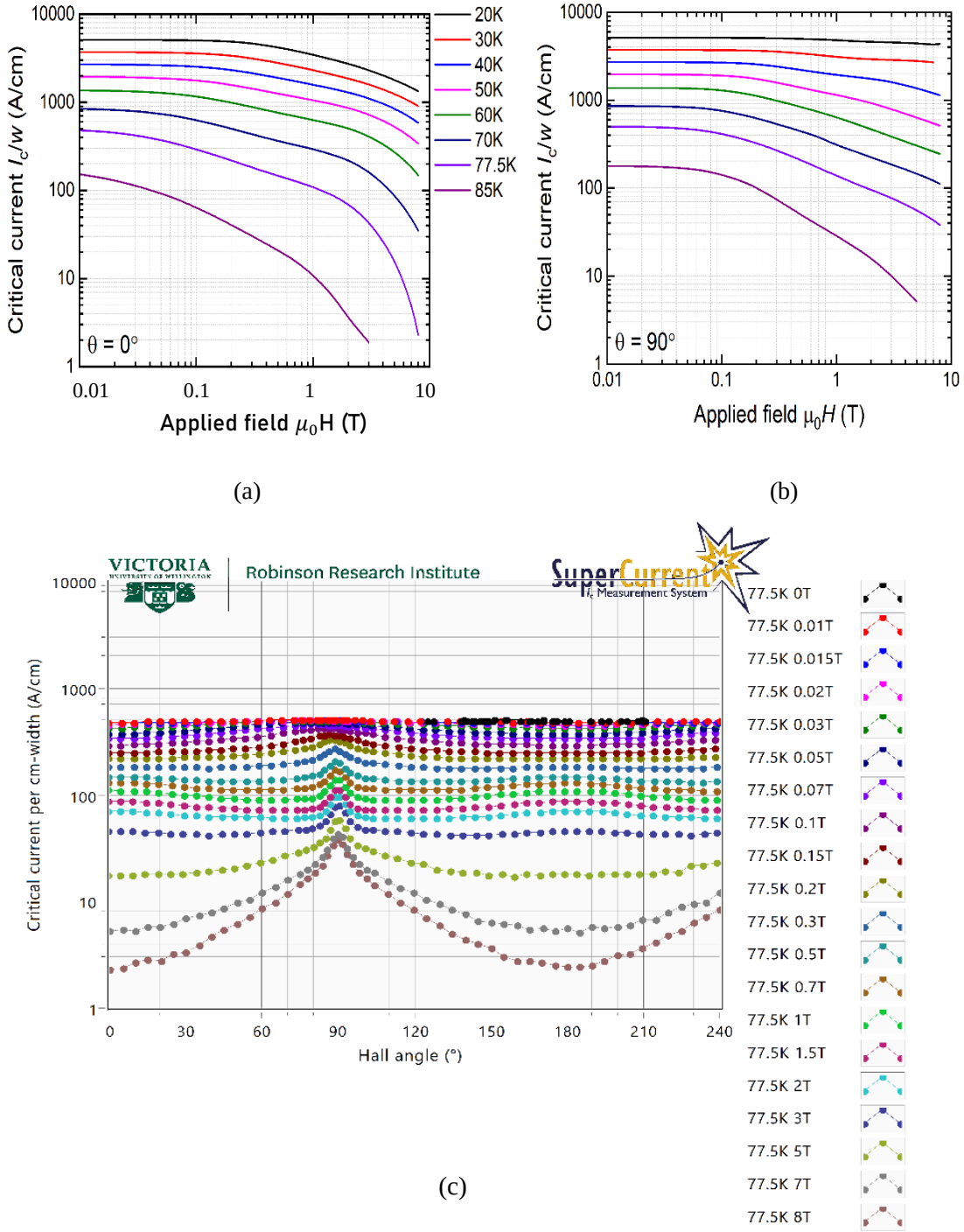

Figure 4. 1. *Critical current characterisation of Fujikura 2G HTS superconducting tape. Graphs showing the (a) perpendicular filed, (b) parallel field, and (c) angle dependence of the critical current of Fujikura wire sample under the specific conditions noted on the graphs, which is produced by the Robinson Research Institute of Victoria University of Wellington [178]*

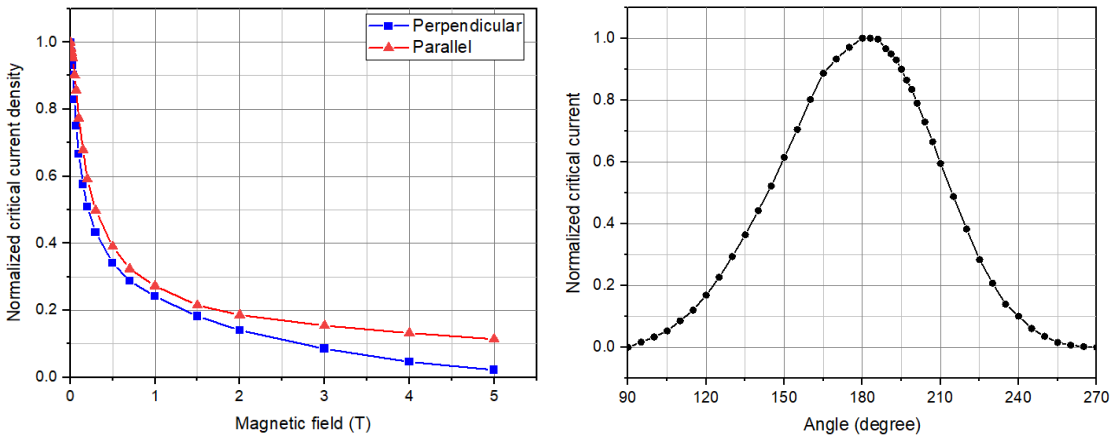

(a) (b)

Figure 4. 2. *(a) Magnetic field dependence of critical currents of Fujikura tapes at 77 K under the perpendicular and parallel field; (b) Normalized data of the angular dependence of tape critical current*

The perpendicular field in Figure 4.1.(a) is $\theta = 0^{\circ}$ and the parallel field in Figure 4.1.(b) is $\theta = 90^{\circ}$. Hence, the data in Figure 4.2.(b) is normalized so that the perpendicular magnetic field ($\theta = 0^{\circ}$ and 180°) corresponds to the value of 1 and the parallel field ($\theta = 90^{\circ}$ and 270°) corresponds to the value of 0. More detailed theory and equations about modelling anisotropic 2G tapes can be found in paper [10].

For SuNAM tapes, the interpolated data used in the FEM models is from the manufacturer-supplied data for the tape's in-field performance, which is shown in Figure 4.3, and the data was taken for a temperature of 77 K.

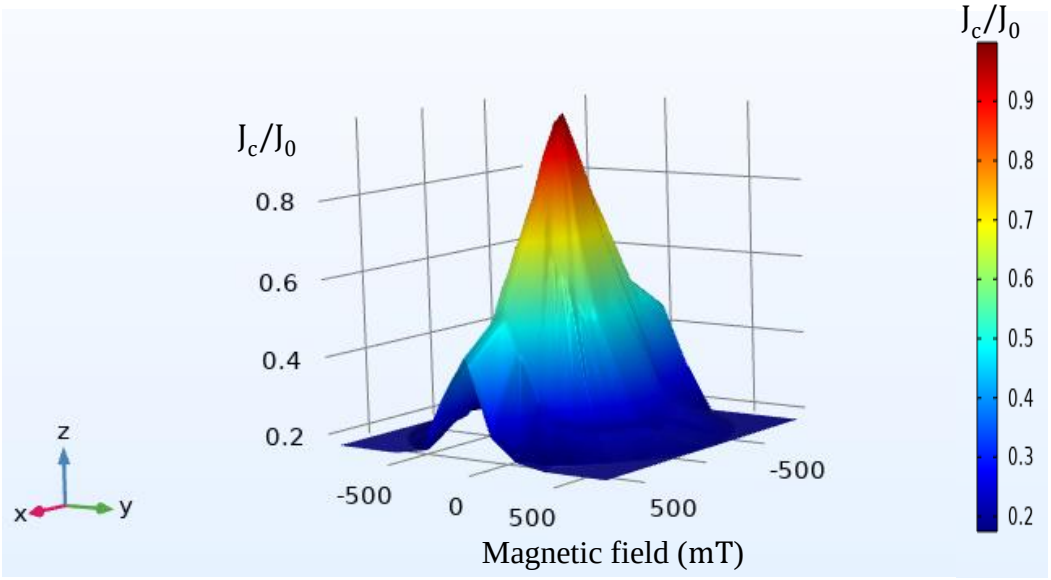

Figure 4. 3. *Critical Current profile interpolated in the COMSOL models. This was obtained by interpolation of experiment data of SuNAM tapes at 77 K [114]*

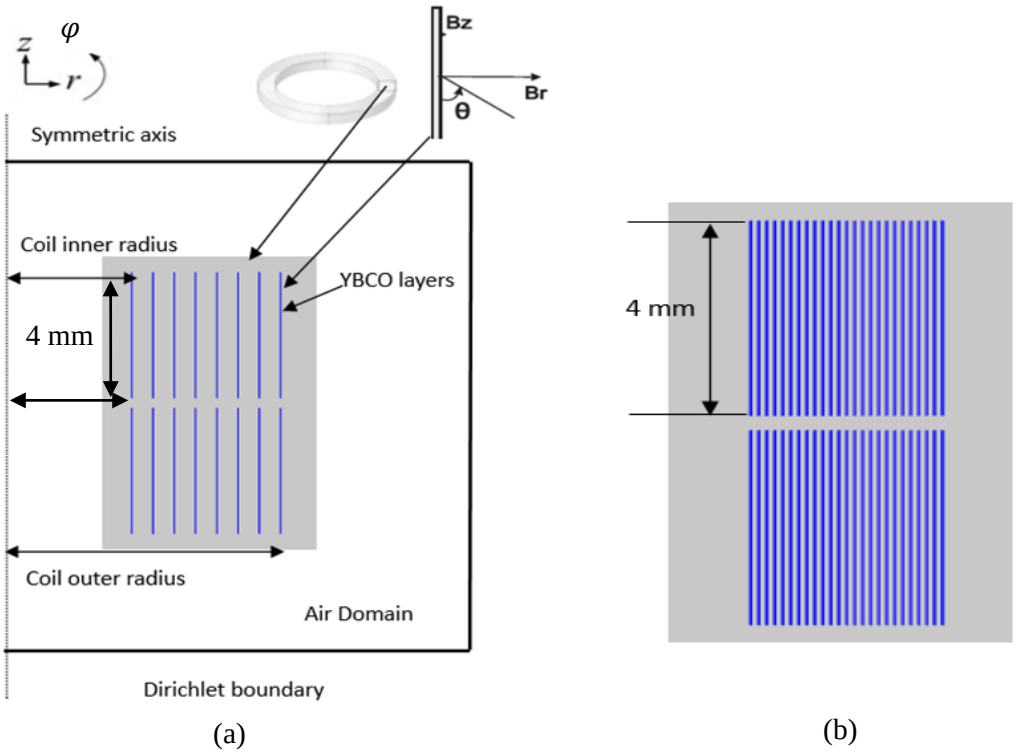

Figure 4. 4. *Geometry of the axial symmetric model [r; φ; z] shows the cross section of two double pancake coils. (a) Coil 1; (b) Coil 2*

Figure 4.4.(a) shows the model geometry of Coil 1, consisting of 8 turns in the radial direction and 2 columns in the axial direction. Figure 4.4.(b) shows the FEM model of Coil 2, which is made of 50 turns in total.

In these models, care was taken to ensure that the model has an air domain large enough to be calculated because of the assumption that the magnetic field generated by the YBCO domains decays to zero at the outer boundaries. So the Dirichlet boundary condition of the air domain can be written as $H_r = 0, H_z = 0$. With the presence of a background field, the boundary conditions become $H_r = H_{rapp}$ and $H_z = H_{zapp}$. Each HTS layer represents one turn of the pancake coil. Current was assigned to each YBCO layer using the Pointwise constraint of COMSOL. The integration of local J_φ in each HTS layer gives the total current of each turn. The Pointwise constraint equals the total current to the predefined applied current. A distributed mapped mesh with 50 elements was applied to the YBCO domains to control the total mesh size, and the free triangular mesh was applied to the air domain.

Another issue must be considered to accurately predict the AC losses for one cycle, which is that during the first half cycle of the calculation, the pre-magnetization condition is zero current inside the HTS, and the AC loss per cycle is lower than that when the pre-magnetization condition is nonzero. From the second half cycle onwards, the model returns a constant rate of loss [130]. In our experiment, the AC loss is always measured under pre-magnetization conditions, so that the results from the second half cycle and subsequent cycles are used in the calculation.

In the AC loss calculations, we only model the 1 μm thick YBCO layer of each turn. The AC loss in J/cycle/m is calculated using the following equation in our models:

$$Q_{sim} = \frac{2\int_{1/2f}^{1/f}\left[\sum_1^N \int_\Omega 2\pi r * E_\varphi * J_\varphi dr dz\right]dt}{L} \tag{4.10}$$

where $1/f$ denotes the period of the AC current of frequency f, N is the total number of turns, and L is the total length of the coil. J_φ and E_φ the critical current density and electric field in the direction of φ, respectively. We performed loss calculation for 50-Hz AC current of the models and summarize the results in Figure 4.5, which gives the

comparison between empirical data and modelling calculations. Solid lines are for experiment results and the dotted lines are for the simulation results.

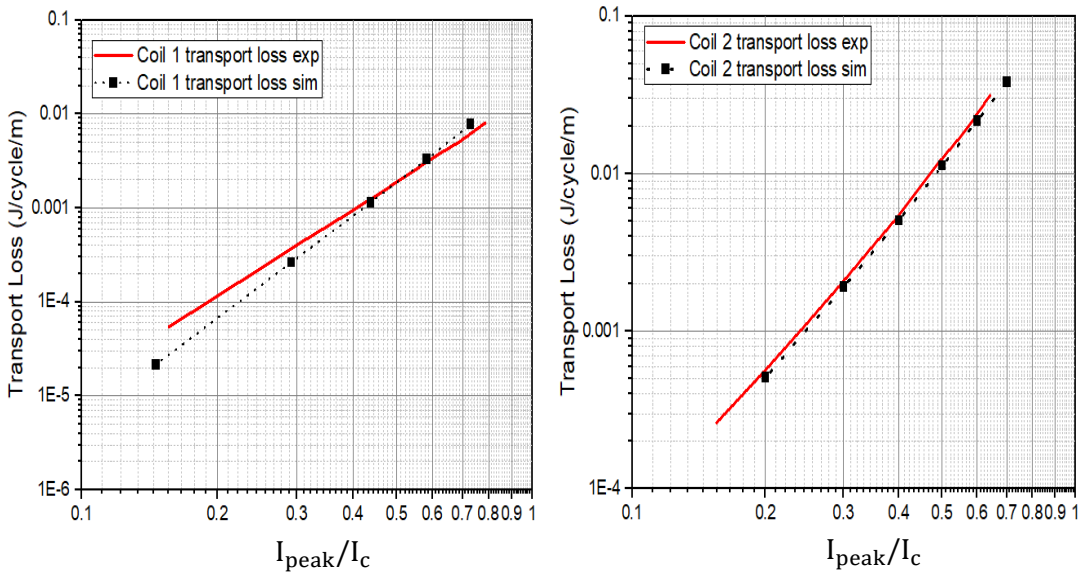

Figure 4. 5. *Comparison between experiment and simulation results of transport AC loss at 50 Hz for Coil 1 and Coil 2*

For Coil 1, we found a few discrepancies between the simulation and measurements. The modelling results are slightly lower than the experimental results for smaller currents, but become more consistent as the current increases towards the critical current. That is probably because the loss due to the magnetic substrate was not included in the model. For smaller currents, the magnetic substrate loss is significant and cannot be ignored in this case, thus dominating the superconductor loss [179]. Hence, further improvement could take this into account in the model and achieve more accuracy.

For Coil 2, the simulation results have good agreement with the measurement results. Generally speaking, the FEM models predict the AC loss accurately.

4.3 Modelling analysis of 3S coil

4.3.1 Experimental validation

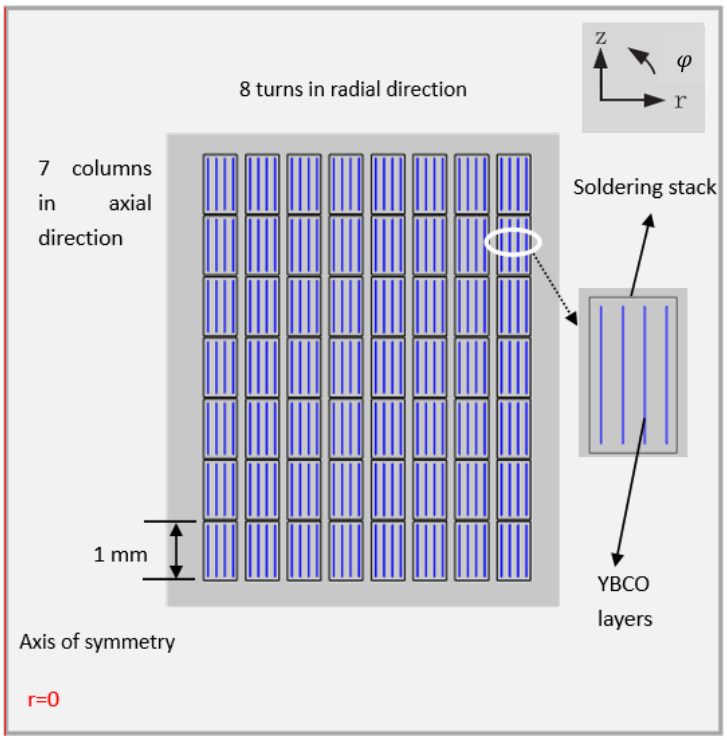

Figure 4. 6. *The model geometry of Coil 3 wound by 3S wire. It includes 8 turns in the radial direction and 7 columns in the axial direction, with a total of 56 turns.*

An FEM model based on the 3S coil (Coil 3) is introduced in this section. Figure 4.6 shows the cross section of the 3S coil, which is made of 4-filament 1 mm SuNAM tapes, consisting of 8 turns in the radial direction and 7 columns in the axial direction, with a total of 56 turns. Details of the specification about the 3S coil are given in Table 3.1. In this work, both the 1 μm HTS layer and soldering layers were modelled and neglects any substrate losses. The square side length of the 3S coil is set as 1 mm. The thickness of the HTS layer is 1 μm, and the other parts are set as soldering layers. The resistivity of the air domain is set to 1 Ω·m.

Since the resistivity of soldering materials data used in the 3S coil is not provided by

the manufacturer, we have to define resistivity for soldering layers in the model from references. During the manufacturing process, low melting temperature solders usually can provide more processing tolerance and build a wider temperature window, in consideration of a hierarchy of solders needed in the packaging technology [180]. Hence, in the modelling work the soldering resistivity is considered to be selected close to one of the low melting solders. Table 4.1 lists some low meting point solders. And we therefore set the soldering resistivity at 1×10^{-7} Ω·m.

Table 4.1: Specifications of some low melting point solders [181]

Solder	Composition	Melting point (K)	T_c (K)	H_c （T）	Resistivity at 77 K (Ω · m)
InBi	$In_{66}Bi_{33}$	345	5.65	< 0.01	1.5×10^{-7}
InSn	$In_{52}Sn_{48}$	391	5.4	0.066	9.0×10^{-8}
InAg	$In_{97}Ag_{3}$	416	2.4	0.028	1.6×10^{-8}
SnBi	$Sn_{42}Bi_{58}$	411	2.25	0.038	3.8×10^{-7}
SnPb	$Sn_{63}Pb_{37}$	456	7.05	0.083	2.5×10^{-8}

Another issue that need to considered is about the model geometry. Due to large amount of soldering material used in the wire manufacturing, both thickness and hardness of the 3S wire are tremendously boosted compared with normal HTS tape. Hence, the double pancake structure is not suitable for the winding process in this case, leading to relatively complex geometry for this coil. So, in the modelling work we have to simplify the coil geometry to a simple model, consisting of a total 56 turns in comparison to Coil 3 with 52 turns. Unfortunately, this might unavoidably cause the simulation results not that accurate due to the geometry discrepancies.

Equation 4.8 is applied as a governing equation for the model, as described in the previous section. The interpolated data of $J_c(B, \theta)$ relationship used in the model can be found in Figure 4.3. Finally, the AC losses for a 50 Hz AC current were calculated

using the model and compared to the experimentally measured AC losses, which is shown in Figure 4.7. The FEM results of total transport loss are slightly higher than the experimental results, which might be due to discrepancies in geometry (a coil model with larger turns is used) and the soldering resistivity used in Coil 3 not being that specified by the manufacturer. More precise model geometry and accurate soldering resistivity will improve the accuracy of simulation results in the future. However, generally speaking, the FEM model still predicts the AC loss accurately.

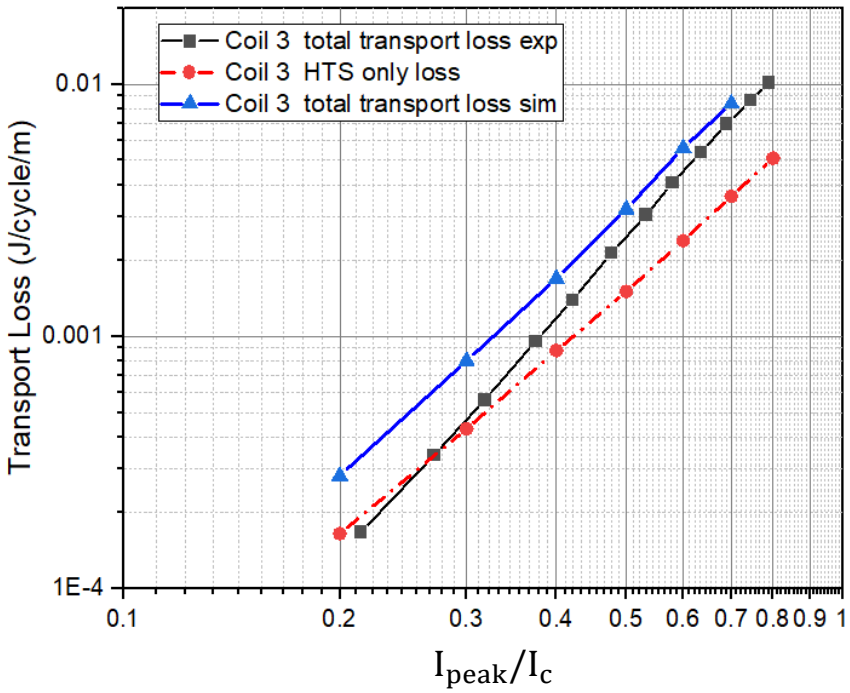

Figure 4. 7. *Transport loss of the 3S coil: comparison of measurements and model results*

4.3.2 Modelling of 3S coil without soldering layer

Theoretically, in the fabrication processes of the 3S wire, a narrow 2G tape with 1 mm width is applied, and the stacking and soldering processes are completed simultaneously. This technology allows the stacking of 1 mm narrow HTS filaments into a cable structure, thereby reducing the AC loss. However, our measurements (as shown in Figure 3.6) indicated that the magnetization loss of the 3S coil in a 0.45 T rotational magnetic field is larger than that of a standard 4 mm coil. Large coupling losses were identified in the magnetization losses due to the existence of soldering layers. It confirmed quantitatively that the use of soldering in the cabling process will lead to higher magnetization loss in the HTS coils. Therefore, to predict the AC loss as well as identify further AC loss reduction achieved under the assumption of there being no soldering stack in the 3S wire, this section develops for comparison another FEM model for a 3S coil without a soldering layer. The soldering layer presented in Figure 4.6 was removed and set as air domain, while the remaining parts were kept invariable. The total AC losses for a 50 Hz AC current were calculated using this model by Equation 4.10 and compared with the 3S coil with soldering layer. As Figure 4.8 shows, without soldering layers present in the 3S coil, thereby increasing the contact resistivity between HTS filaments, the total AC loss is tremendously reduced. Moreover, the soldering stack itself contributed a certain amount of coupling loss to the total transport loss, but the sole AC loss of HTS in the presence of a soldering stack proved to be still higher than the 3S coil without the soldering layer, which can be observed in Figure 4.8. Finally, we can see that the soldering stack added in HTS coil has a significant impact on the AC losses.

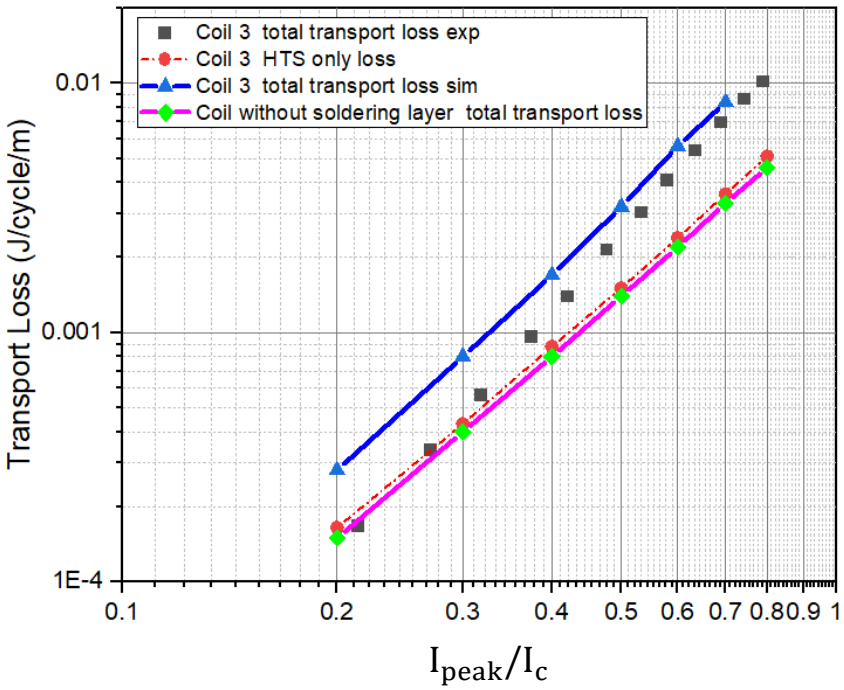

Figure 4. 8. *Transport AC loss comparison between 3S coils with and without soldering layer*

Besides, the existence of soldering layer also changes the current distribution inside the HTS coil. The current distributions of one filament at the inner extreme from layers 1, 2, 3, and 4 in row 4, 5, 6, and 7 for 3S coils with and without soldering layer are plotted in Figure 4.9. Due to geometrical symmetry, only the results for the lower left half of both coils are presented in this section for comparison. The value is normalized by the self-field current density, J_c. The green solid lines are for 3S coil with soldering layer, and the black dotted lines are for 3S coil without soldering layer.

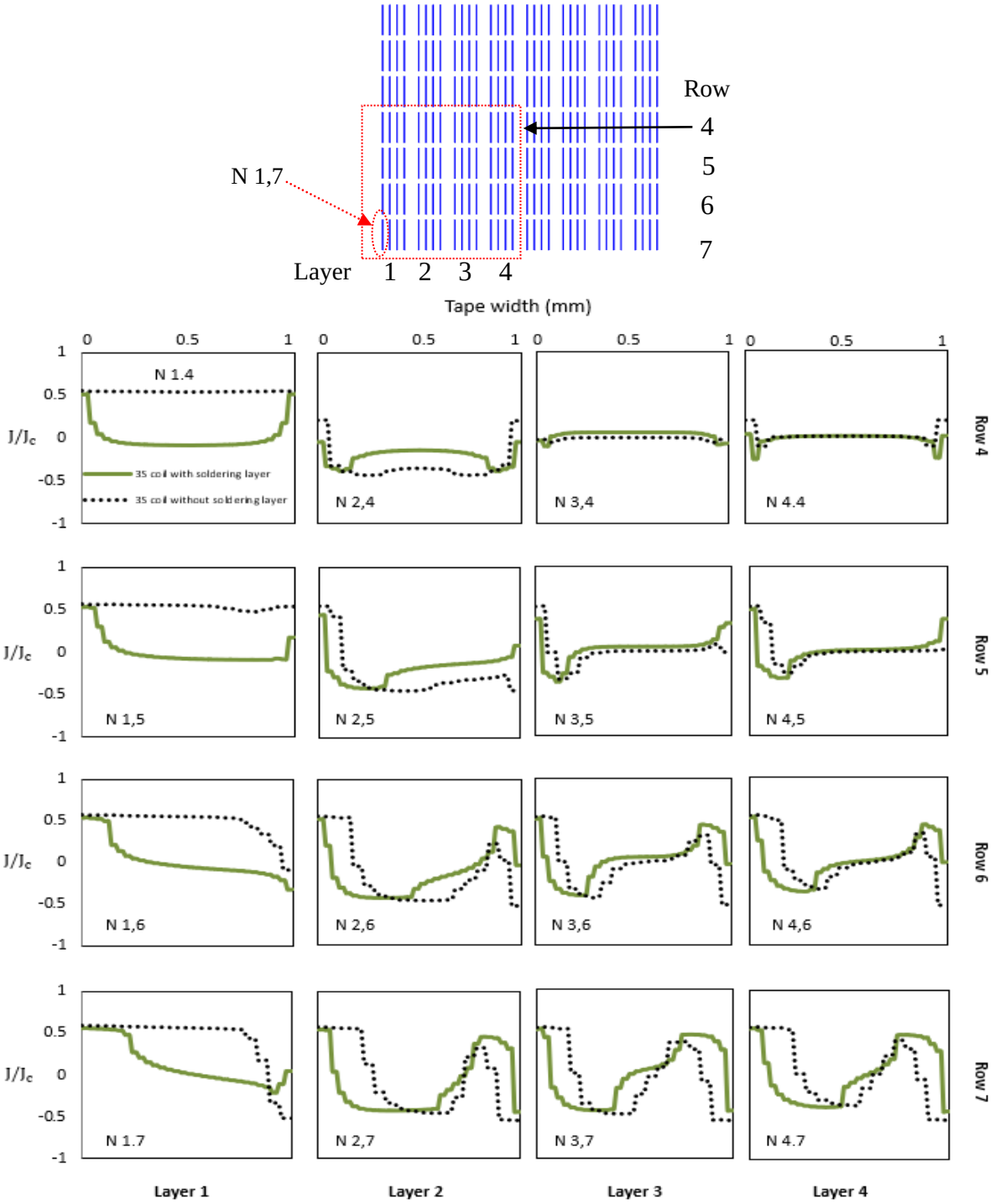

Figure 4. 9. *Simulated current distributions for both 3S coils with and without soldering layer with applied peak transport current of 15 A. The positions of the plotted turns in both coils are marked by the number N. The current distribution is calculated at the centre of each filament.* J_c *is the self-field current density calculated by* I_c *= 50 A for each single tape*

4.3.3 Influence of soldering resistivity

Although experiments on multi-filamentary HTS coils have confirmed AC loss reduction to a certain degree, in practice, additional contribution to AC loss appears to be due to several factors, notably by an electrical coupling caused by the conductivity of thick normal metal layers and the network of superconducting bridges between the HTS strips [137];[182]. As a result, the contact resistance becomes an essential factor in determining the coupling loss in the cable. In most applications of HTS superconductors, an additional layer of metallic stabilizer is necessary to give the tape sufficient thermal, mechanical and electrical protection [183]. Similarly, the addition of a soldering stack is inevitable in the manufacturing process of 3S wire, which significantly increases its total AC loss due to the large coupling losses identified under external magnetic field. Hence, exploring the influence of the resistance value of the soldering layers for multi-filamentary HTS conductors is deemed necessary to be investigated in this section, providing the possibility of improving the cable design during the manufacturing process.

The FEM model for the 3S coil without soldering layers was introduced in previous work. In this study, different resistivity values of the soldering stack were employed in the model for AC loss comparison. The critical current was set at a constant 50 A for single 1 mm tape, and the applied peak transport current was 15 A and 50 Hz. By comparing the instantaneous total transport AC loss in Watt in one cycle, from Figure 4.10, it was found that as the soldering resistivity increases, the total AC loss of the coil was accordingly reduced.

Meanwhile, we plotted the results of AC loss comparison for the 3S coil with different soldering resistivities at the normalized transport current, as Figure 4.11 shows. When the soldering layer resistance value was set at 1×10^{-7} Ω·m, the total AC loss of 3S coil was greatly reduced by approximately 90% compared with the same circumstance for a soldering layer resistivity of 2×10^{-9} Ω·m, due to the elimination of the large coupling losses in the HTS coil.

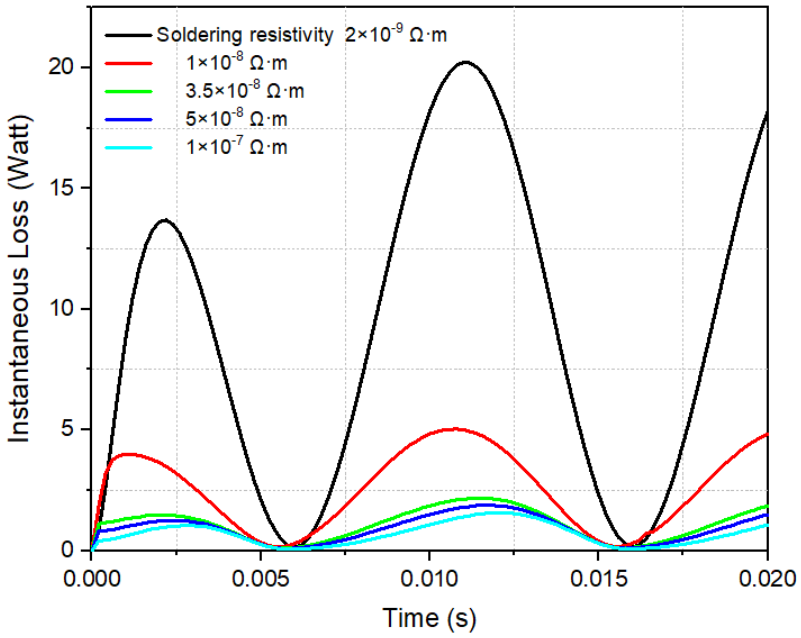

Figure 4. 10. *Instantaneous total transport AC loss comparison of 3S coil with different soldering resistivity at one cycle. Critical current for the single HTS tape is set at a constant 50 A, and the applied peak transport current is 15 A and 50 Hz.*

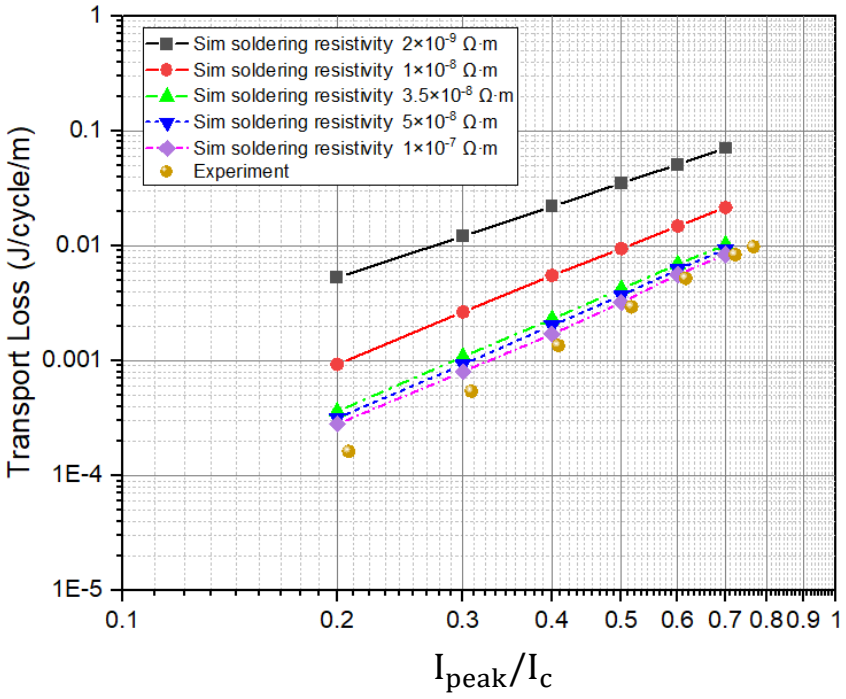

Figure 4. 11. *Comparison of the normalized transport AC loss of 3S coil with different soldering resistivity.*

4.3.4 Conclusion

To sum up, in this section, a FEM model based on the 3S coil was used to calculate transport AC losses, and the calculated loss are slightly higher than the experimental results due to discrepancies in geometry and soldering resistivity issue. The model was then extended to numerically evaluate the AC losses of the 3S coil without a soldering layer. The calculation results further demonstrated that this is a good strategy for the reduction of AC loss by using 3S wire. The influence of soldering layer resistivity on AC loss was also studied, and it was found that the existence of the soldering stack increases the AC loss of HTS, and also changes the current distribution inside an HTS coil. The lower the contact resistivity in the soldering stack, the larger the AC loss that will be induced in the HTS coil.

One shortcoming of this model is that the simulation does not account for the external rotational magnetic field, which is present in our fully HTS machine platform, so it is not able to accurately predict the AC loss reduction achieved by the coil without the presence of soldering layer when subjected to a 0.45 T rotational magnetic field. However, in general, the FEM model predicts the transport AC loss measurements well and lays a solid foundation for further investigations on other HTS cables, i.e., the 2*2 mm and 4*1 mm multi-filament cables.

4.4 Modelling of copper-based striated coil

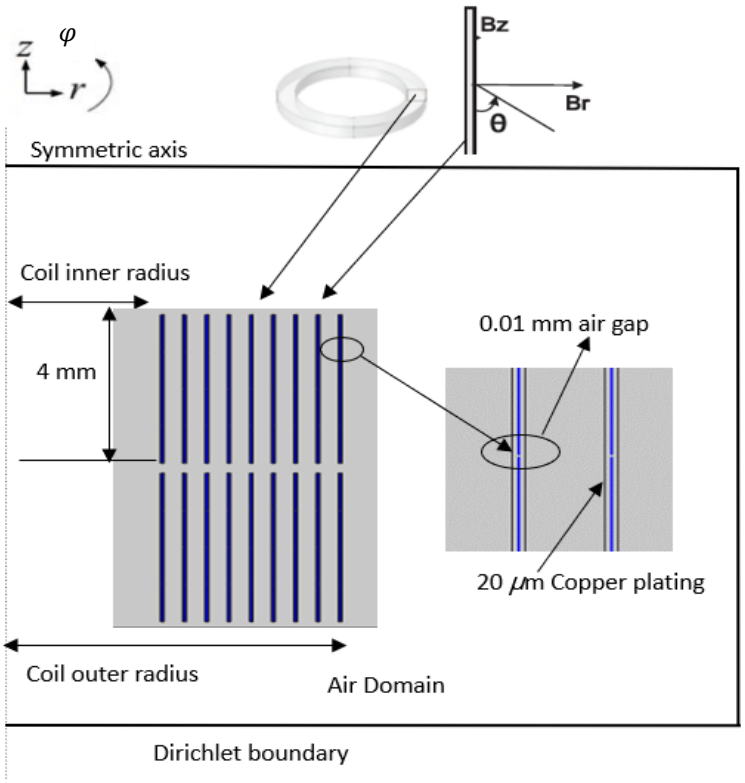

Figure 4. 12. *The model geometry of 4 mm striated HTS coil (Coil 4) consisting of 18 turns. Four 0.01 mm air gaps existed in each single HTS layer surrounded by a 20 μm copper plating*

The geometry of the model is shown in Figure 4.12 and the specification of the simulated coil is listed in Table 3.2. The model geometry is based on the material used in the 4 mm 2G HTS striated coil shown in Figure 3.8 and built using the H-formulation, consisting of 18 turns. In addition to the thin layer of silver on top of the superconducting film, a 20 μm copper stabilization is added on both sides of the tape. Hence, in this model, each single HTS layer is surrounded by a 20 μm copper plating and four 0.01 mm air gaps are added to indicate the striation technique. The resistivity of the air domain is set to 1 Ω·m, and the resistivity of copper plating at 77 K is set under the assumption 1×10^{-7} Ω·m, in order to compare with previous 3S coil model.

The 1 μm thick YBCO layer of each turn and copper plating were both modelled in this study. The $J_c(B,\theta)$ data used in this model is from Figure 4.2. After performing loss calculation at a 50 Hz AC current, calculated by Equation 4.10, the simulation results are shown in Figure 4.13 and compared with the experimental measurements to validate the model.

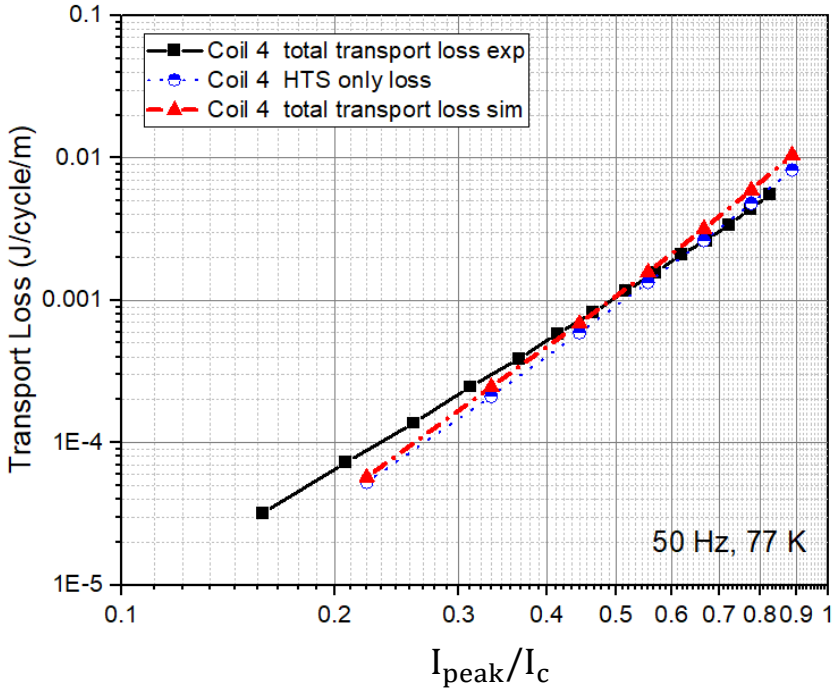

Figure 4. 13. *Transport AC loss of Coil 4: comparison of measurements and model results*

To conclude, the modelling results are slightly lower than the experimental results for smaller currents, while as the current increases towards the critical current, it becomes more consistent but a little deviated from the empirical data. Moreover, the sole AC loss of HTS in the presence of copper plating proved to be very close to the experimental results. Compared to our previous work of 3S coil modelling, the copper plating has less effect than the soldering stack on the AC losses. However, in this case , in order to compare the influence of them on AC losses with the same contact resistance value, we assume the resistivity of copper plating at 77 K is the same as that we used in the model of 3S coil. It is necessary to employ accurate copper plating

resistivity in the model to accurately predict the AC loss in the future. Last, this case study also raises some interesting points for further analysis. According to our experiment results, due to large coupling losses identified, the total loss reduction of striated sample coil is not proportional to the number of striations. Therefore, under the assumption if we increase the number of filaments achieved by the laser striation technique, the effect of copper plating existing in a striated coil with larger number of striations on AC losses should be carefully investigated in future work.

4.5 Numerical modelling of multi-filament coils

4.5.1 Validation for 2*2 mm multi-filament coil

In this section, an FEM model based on Coil 5 was built using the H-formulation for numerically calculating the transport AC losses. As illustrated in Figure 4.14.a, the model is based on the 2*2 mm multi-filament coil (Coil 5) with 10 turns in total and made of 2-filament 2 mm tape with 0.04 mm air gap between strips. In this study, we only modelled the 1 μm thick YBCO layer of each turn. The $J_c(B,\theta)$ data of the tape is obtained from Figure 4.2, and the AC loss in J/cycle/m is calculated using Equation 4.10 in our model. The completeness of the simulation was validated by comparing the output with the experimental results of Coil 5. We performed loss calculations for 50 Hz AC current of the model and summarized the results in Figure 4.15, which shows close agreement with the measurement results.

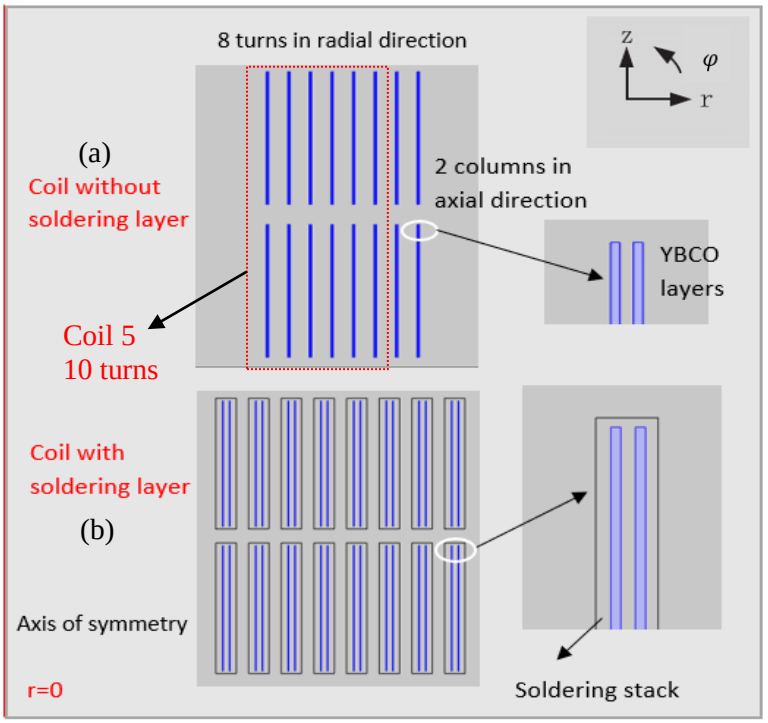

Figure 4. 14*. The model geometry of 2*2 mm multi-filament HTS coil. (a) Coil without soldering layer (b) Coil with soldering layer*

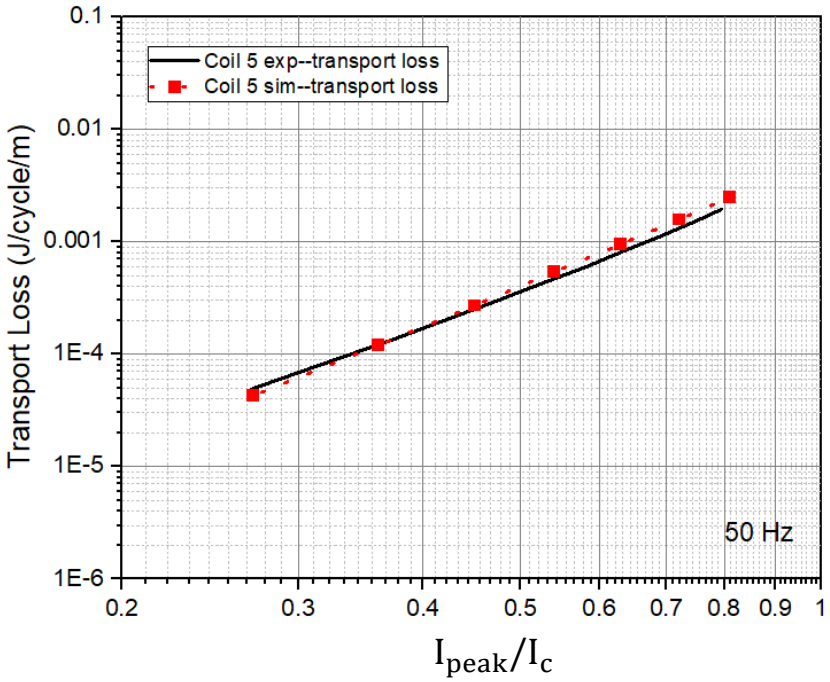

Figure 4. 15. *Transport AC loss of Coil 5: comparison of measurements and model results*

4.5.2 Coupling loss affected by soldering stack

To further explore the idea that heat shrink tubing as insulation can effectively eliminate eddy losses and coupling losses and to understand the influence of the soldering stack increasing the coupling loss in HTS cables, two FEM models regarding 2*2 mm coils with a total of 16 turns both with and without soldering layer, as illustrated in Figure 4.14 previously, were established for studying the current sharing between HTS filaments and transport loss comparison. The current distributions of two HTS filaments from layers 1, 2, 3, and 4 in column 1 for both coils are plotted in Figure 4.16. Due to geometrical symmetry, only the results for the upper left half of both coils are presented in this section for comparison. The value is normalized by the self-field current density, J_c.

According to Figure 4.16, we can see that with the soldering layer, the carrying current density between two filaments from the same turn of the coil have smaller differences, indicating it is more capable of sharing currents between HTS filaments compared to the coil without a soldering layer. The impact of current sharing is less notable in high magnetic regions but is more notable in the region where the magnetic field does not fully penetrate. When currents flow from one filament to another, they can couple the filaments together into a single large magnetic system, which encounters a resistance along the current path through the soldering stacks, thereby inducing coupling losses.

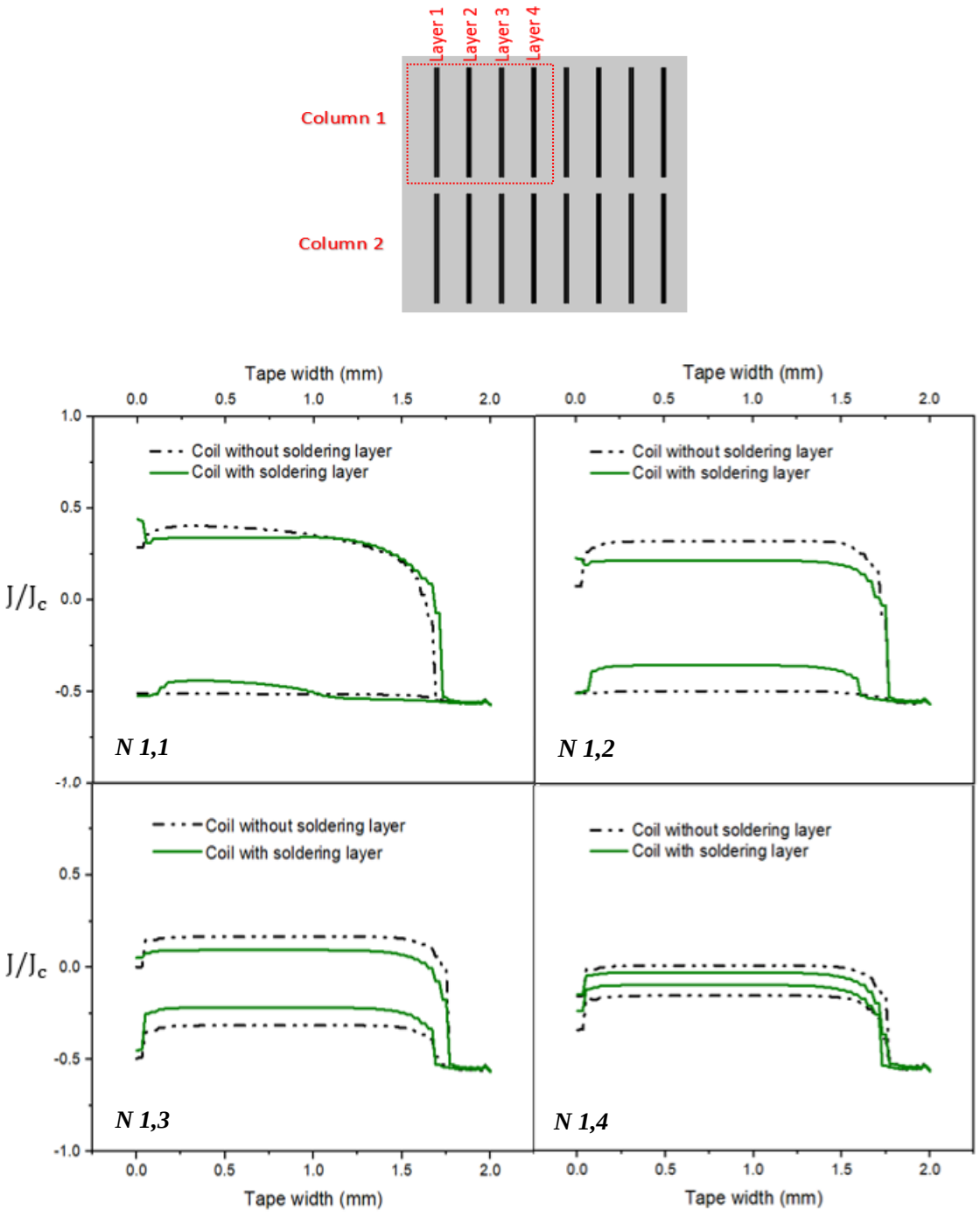

Figure 4. 16. *Simulated current distributions between two HTS filaments of a single turn for both coils with and without soldering layer at applied peak transport current of 40 A. The positions of the plotted turns in both coils are marked by N, where N 1,1 means the turn at Column 1 and Layer 1.* J_c *is the self-field current density calculated by* I_c *= 77.5 A for each single tape.*

We performed loss calculation for 50 Hz AC current using these two models and summarized the results in Figure 4.17. It can be observed that with the presence of the soldering layer, the total transport losses are greatly increased, however the HTS loss remains almost the same between two coils, and the increased AC losses come mainly from coupling losses induced through the soldering stacks. As a result, our experiment can confirm that employing heat shrink tubing as insulation can effectively reduce the eddy losses and coupling losses originating from the soldering stack connections.

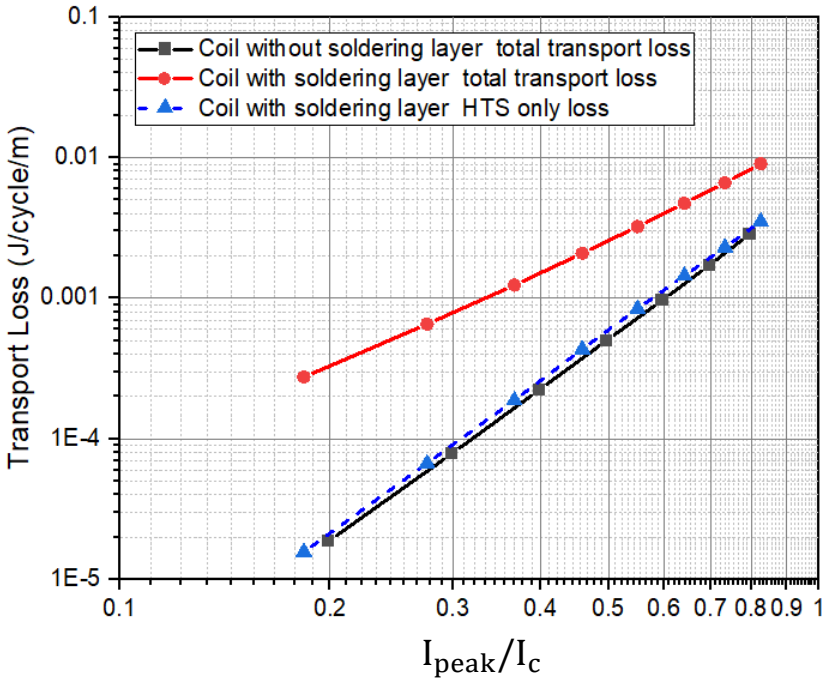

Figure 4. 17. *Transport AC loss comparison between coil with and without soldering layer at 50 Hz. The soldering resistivity is set as* 1×10^{-7} *Ω·m*

4.5.3 Modelling of 4*1 mm multi-filament coil

Considering the fact that the method of reducing the losses is to produce narrow filaments and the losses of the new filamented strip reduce proportionally with the number of filaments, it is necessary to further investigate the thinner multi-filament cables in reducing AC loss. As shown in Figure 4.18, another FEM model regarding

4*1 mm multi-filament coil (Coil 6) was built in this section, offering the possibility to numerically calculate the transport AC loss results of a coil wound with four 1 mm HTS strips and insulated by heat shrink tubes.

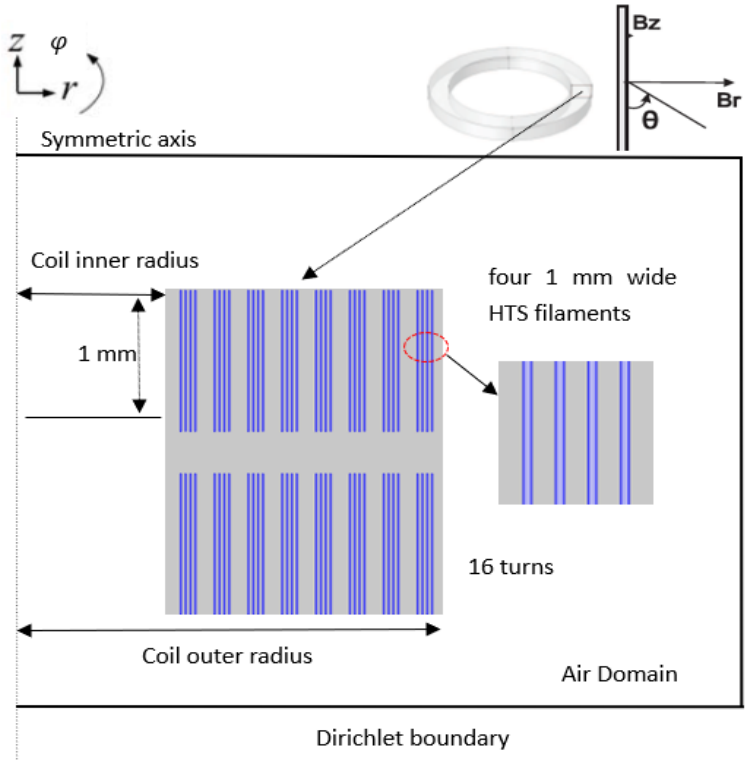

Figure 4. 18. *Model geometry of 4*1 mm multi-filament coil, containing of 4 filaments in each tape and a 0.04 mm air gap between filaments*

The model was constructed with a total of 16 turns of 1 mm coil, containing of 4 filaments in each tape and a 0.04 mm air gap between filaments. Loss calculations for 50 Hz AC current of the model were performed and all results are summarized in Figure 4.19 for comparison. It shows that the modelling calculations identified approximately 90% further loss reduction, which is close to 4 times expected lower transport loss compared with Coil 1 (standard 4 mm coil), and hence it validates the theory as we mentioned previously that the filamentized strip loss reduction is proportional to the number of filaments. However, as illustrated in Chapter 3, the stacking and winding process of this kind of coil is extremely complicated due to the

vulnerability of 1 mm thin HTS tape. Further investigation on the balance between selection of appropriate filaments and AC loss reduction for armature windings is deemed essential to be studied more carefully.

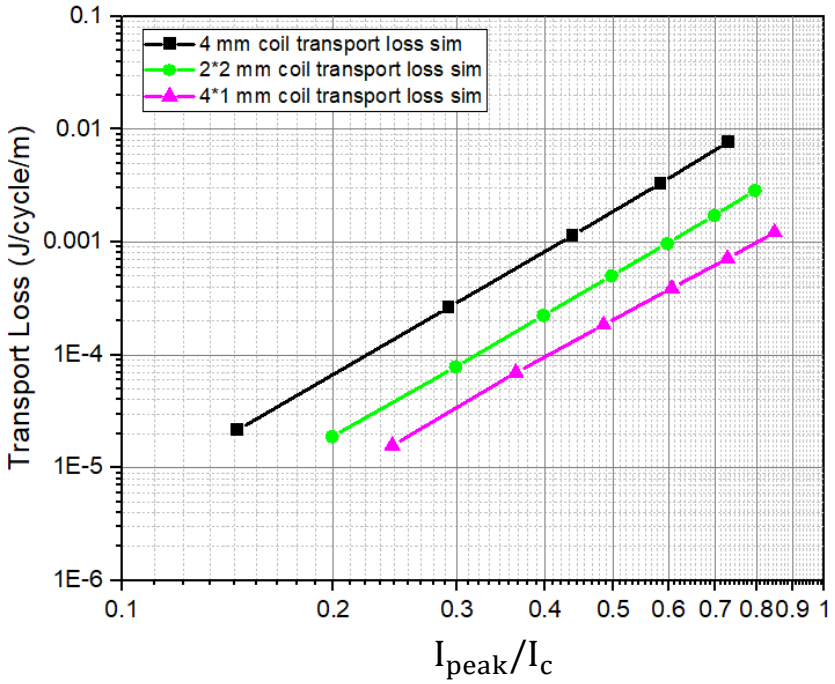

Figure 4. 19. *Simulation comparison of transport AC loss between 4 mm standard coil, 2*2 mm multi-filament coil and 4*1 mm multi-filament coil at 50 Hz. All coils have a total of 16 turns*

4.6 Discussion

4.6.1 Total AC loss modelling in a rotational magnetic field

In order to estimate the total AC loss of experimentally measured 2G HTS coils in a rotational magnetic field, FEM models are used for the total loss calculations. Previous studies have demonstrated that finite element modelling using H-formulation can estimate transport AC loss for the 2G HTS coils. In this section, we simplify the model via the application of a time-variant magnetic field using Figure 2.12. According to [136], the total AC loss of machine AC windings depends not only on

the magnitudes of the magnetic field and transport current, but also on the interaction between the magnetic field and the current. When the applied current and external magnetic field are in phase, the total AC loss is the highest; when the applied current and external magnetic field have a 90° or 270° degree phase shift, the total AC loss is the lowest. Therefore, we consider applying the transport AC currents with a phase shift α equal to 0°, 90° and 180° in the models, which is shown in Figure 4.20, and simulating all the cases.

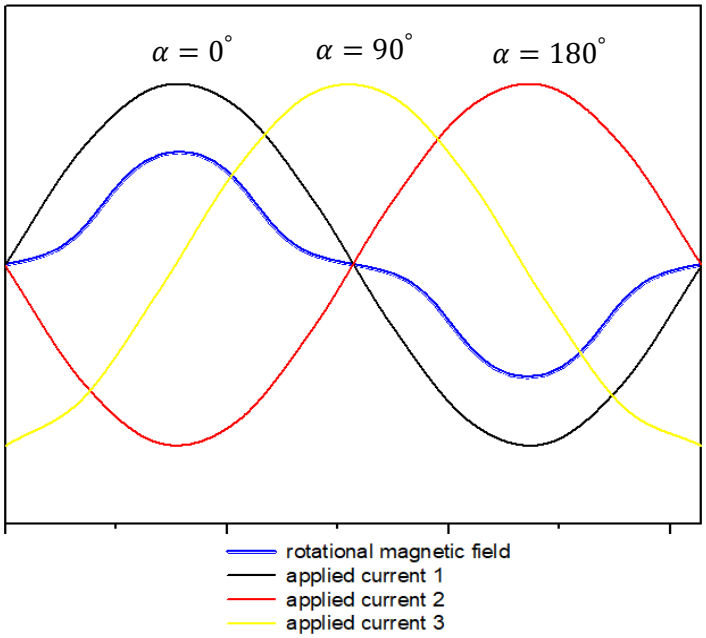

Figure 4. 20. *Current phase shift graphs for different α values (not to the scale)*

However, when we performed the loss calculations, our simulation results were not as expected, which have differences in order of magnitude compared with experimentally measured total AC loss results. Since the modelling work is calculated by means of a time variant magnetic field waveform with only perpendicular magnetic component; however, the magnetic environment we applied is not exactly the same as for the experiments, because in terms of a fully HTS machine, the HTS AC winding is subject to two magnetic fields with both parallel and perpendicular components to the HTS flat surface, which is quite complex. Hence, strategies must be proposed in order

to accurately estimate the total AC losses of HTS coils in such rotational magnetic field in the future.

4.6.2 Conclusion

This chapter presented several 2D models of 2G HTS coils using the H-formulation and the E-J power law, to validate the experimental measurements, as well as to quantify the AC losses of multi-filament cables affected by the use of the soldering stack or copper plating. The 2D model can easily be implemented using FEM software such as COMSOL, and the advantages of using the H-formulation were also listed. We performed several FEM models and studied the relationship between empirical data and simulation results in detail. The calculation of AC loss results has been used for validation of experimental measurements, on the other way being confirming the completeness of the model. The modelling results and the measurements have close agreement for our experimentally tested coils, except for a few deviation for Coil 3. Additionally, we performed loss calculations for the 4*1 multi-filament coil based on Coil 6 (which was damaged during the stacking and winding process), and the simulation results showed further loss reduction up to around 90% in the presence of thinner filament cable, compared with standard 4 mm coil.

The effect of the existence of soldering stack or copper plating in HTS coils on AC loss and current distribution were also investigated. According to our modelling results, for the 3S coil without a soldering stack, at the normalized current close to 70% of the critical current, the AC losses were reduced by approximately 68%; for 4 mm striated coil, the copper plating had little effect on the AC losses, since the sole AC loss of HTS in the presence of copper plating proved to be very close to the total losses. As for the 2*2 mm multi-filament coil without a soldering stack, the AC losses were reduced by around 66% at the normalized current close to 70% of the critical current. All results are concluded in Table 4.1.

Table 4. 1: AC loss reduction rate for multi-filament coils without soldering stack or copper plating (all resistivity were set the same at 1×10^{-7} Ω·m)

Reduction rate	3S coil	Striated coil	2*2 mm multi-filament coil
Total transport loss (at the normalized current close to 70% of the critical current)	68%	25%	66%

To sum up, the study from our modelling work regarding to transport AC loss further demonstrates the effectiveness of the AC loss reduction strategies we proposed of using 3S coil, striated coil, and multi-filament coil for design optimization, and offer suggestions for cable manufacture as well as the selection of stacking and insulation materials. However, the modelling of total AC loss in a rotational magnetic field encountered many problems and still remains unsolved, which will be addressed with further improvements in future work. The successful implementation of the 2D models in FEM software enables a systematic study of experimental coils and then extends it to some theoretical assumptions. It is an easy tool to use and represents a very powerful foundation for optimizing the superconducting system.

Through Chapters 2–3, we experimentally measured five coils, and further validated the transport loss results by numerical modelling in this chapter. These three AC loss reduction strategies we proposed will improve the overall efficiency of the fully HTS machine. In terms of the AC loss reduction rate, the multi-filament cable insulated by heat shrink tubing has more advantages, however, the stacking process is not easy and could lead to the coil becoming easily damaged. In the next chapter, the AC loss measurement at temperatures lower than 77 K will be discussed, providing the possibility to achieve the AC loss reduction by employing standard 4 mm HTS coils instead of multi-filament coils, for comparison with the previous proposed strategies.

Chapter 5

AC loss measurement at temperatures lower than 77 K

In fully HTS machine applications, the majority of devices under development are cooled by liquid nitrogen [184];[185], owing to its several advantages including low cost and ease of availability. However, the operating temperature of liquid nitrogen cooled power devices is limited to 77 K. It has been demonstrated that as HTS materials are cooled to lower temperatures, the critical current increases significantly, and for each degree the temperature lowers, the critical current of the HTS superconductor increases by approximately 10% [186]. Hence, with temperatures cooled down lower than 77 K, the HTS machines can operate at much higher currents, and become more compact and lightweight when operated at lower temperatures. Using a cryogenic helium circulation system that is able to cool the samples to 20 K, in this chapter, a novel HTS machine demonstrator which allows calorimetric AC loss measurements at temperatures lower than 77 K will be introduced.

5.1 Introduction

Gaseous helium circulation has been used as means of providing the required cryogenic environment for HTS applications [186];[187];[188]. The wide operating temperature range offers it great advantages for use as a cooling method. Compared to liquid nitrogen, helium provides the possibility of lower operating temperatures that will allow the cable designs to take advantage of the significantly higher critical currents of HTS tapes, making the cables smaller in size and weight. Lower operating temperatures are also essential for cables based on MgB_2 superconductors whose superconducting transition temperature is around 39 K, and typical cable operating temperatures are between 10 K and 20 K [189]. It has been envisioned that HTS power devices for naval and airborne applications be cooled by cryogenic gaseous helium. Fitzpatrick et al. [190] and Kephart et al. [191] have described a helium flow cryogen based HTS degaussing system for Navy ships. The optimum temperature for the degaussing system was reported to be 55 K, making it inevitable to use a gaseous cryogen. The two gases suitable for the temperature range are helium and neon. Helium was chosen for the degaussing system application because it is less expensive and has higher thermal conductivity compared to neon. Therefore, circulating gaseous helium will be the cryogen of choice for the applications.

Electric or hybrid aircrafts are thought to be one the most promising technologies to realize the net zero aviation. Superconducting machines with potential high power and low weight are agreed to meet the future demands for aircraft propulsion. In order to enable the design of future cryogenic systems and achieve further AC loss reduction for fully HTS machines, it is necessary to generate the data on AC losses at different operating temperatures. However, there is little data available on AC losses at temperatures between 15 and 35 K due to the lack of suitable experimental facilities. Furthermore, a wider operating temperature range is ideal for devices that require large variations in operating current density because devices can be operated at the temperature most appropriate for a given current density. In some military

applications, compact and lightweight power devices that offer a wide operating current density window are beneficial. Two gases might be considered suitable for offering wide range operating temperatures, which is helium and hydrogen. Helium takes advantage over hydrogen due to the safety concerns, since hydrogen is highly inflammable and incredibly dangerous, on the contrary, the non-flammable nature makes helium gas very safe. Therefore, the use of gaseous helium as a cryogen can offer the required operational flexibility for such HTS power applications. Another benefit of helium gas is that there is no phase change in the coolant, allowing for a much larger temperature gradient across the power device [192].

However, some drawbacks appear in using gaseous helium as the cooling medium such as lower heat capacity, inferior dielectric strength, higher cost, and lower efficiency of the commercial cryocoolers used for maintaining helium gas at cryogenic temperatures. One additional challenge in using gaseous helium as the cryogenic medium is the difficulty in achieving the required mass flow rates due to its low density. However, when operating temperature is not an issue, safety concerns in the event of a system break caused by a distributed liquid cryogen circulation system make liquid nitrogen an unfavourable choice as a cryogen [193];[194];[195]. In order to take advantage of the flexibility in operating temperatures, compact size, and lower weight, smart power system and cryogenic designs are required to mitigate some of the challenges posed by using gaseous helium as the cryogen.

Along with the cryogenic helium gas circulation system, a newly designed 200 kW fully HTS machine demonstrator was delivered to our laboratory in 2022. Using helium gas as the coolant, the temperature of the key positions of the HTS machine can achieve less than 30 K, which can further improve the performance and power density of the machine. However, it is a relatively new idea to use cryogenic gaseous helium circulation system for cooling HTS power devices, and requires some systematic investigations for system optimization and to understand the limitations of such systems. Therefore, this chapter provides a description about the testing of a versatile cryogenic helium gas circulation system for the purpose of understanding the

helium gas based cryogenic system operation issues and to understand the benefits and limitations of using gaseous helium circulation systems in providing the cryogenic environment for HTS power devices. The overall design concept of the new HTS machine platform is also introduced, and finally a calibration process as well as the AC measurement protocol for our entire machine system is proposed, laying the foundation for later investigations on 2G HTS coils to be inserted into it to accurately study the total AC loss at temperatures lower than 77 K. As a result, the cooling methodology through such a cryogenic gas circulation system is expected to further improve the performance and power density of the fully HTS machines, thus maximizing the overall machine efficiency.

The overall system was designed by Prof Min Zhang and there were two cryostat suppliers involved in manufacturing the components. In this chapter, the system and cryostat design is introduced in Section 5.2.1 as a background information. Then, Section 5.2.2 illustrates the work this dissertation involved in the design of the measurement chamber for machine cryostat. Last, the specific contributions of this PhD thesis on this project is to set up the testing and calibration procedures, as well as proposing an AC loss estimation methodology for our new system, which are described in detail in Section 5.3.

5.2 Background

5.2.1 Introduction to design concept

A fully HTS machine based on the calorimetric method for AC loss measurement of HTS at liquid nitrogen temperature 77 K has been reported in our previous work [133];[134], including a rotational background magnetic field. It can measure the total loss from an HTS coil regardless of the phase difference between the applied current and the background field.

In this section, based on our previous fully HTS machine setup, the Applied

Superconducting Group in University of Strathclyde proposed a novel HTS machine platform using a cryogenic helium circulation system that is capable of cooling the samples to 20 K, in order to measure the total AC loss of HTS coils at temperatures lower than 77 K by the calorimetric method. This newly designed cryostat was manufactured in cooperation with Shanghai Jiaotong University and delivered in 2022, as shown in Figure 5.1.a, to achieve the operating temperature of key positions lower than 77 K, cooling down by helium gas. The cryogenic helium gas circulation system was designed and produced by AS Scientific company, and the Figure 5.1.b shows the photograph of the manufactured cryostat.

(a) (b)

Figure 5. 1. *(a) Superconducting machine cryostat; (b) Helium circulation cryostat*

Theoretically, in the AC loss measurements, the heat in the HTS is generated due to the AC losses caused by the external AC magnetic field. The sample coil is cooled to the set temperature and the external magnetic field (B_{ext}) is applied. When the sample temperature and ΔT reach stable values, ΔT, B_{ext}, frequency f, and the helium flow parameters are recorded. The value of losses for the set B_{ext} is calculated in Watt unit using Equation 5.1 [196] as follow:

$$Q = \dot{m} C_p(T_{exp}) \Delta T \quad (5.1)$$

where $\dot{m}$ is the helium gas mass flow rate, C_p is the heat capacity of helium at constant pressure, T_{exp} is sample temperature, and ΔT is the temperature difference between inlet and outlet helium gas. The power losses Q were divided by the frequency f of the external magnetic field to estimate the AC losses per cycle. More details regarding to AC loss measurement principles will be illustrated in Section 5.3.3.

5.2.2 Design of measurement chamber

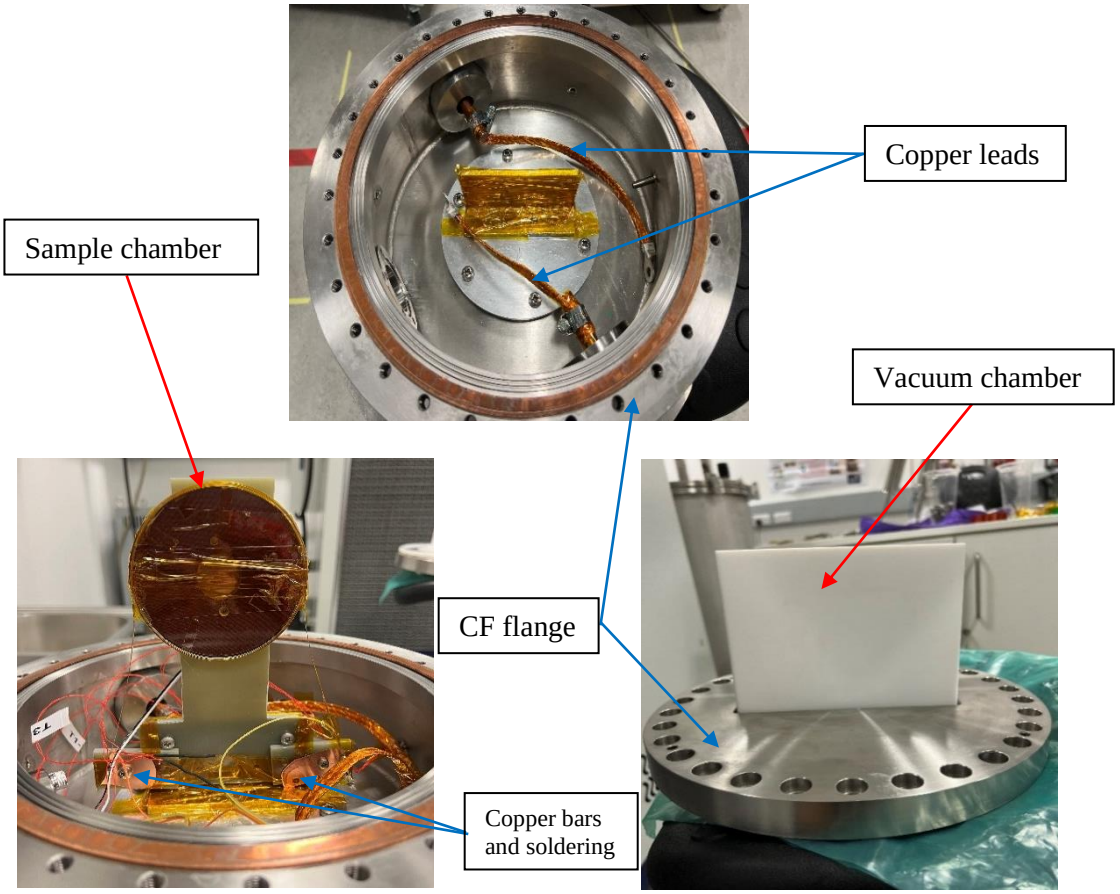

Figure 5. 2. *Photographs of the measurement chamber*

Based on previous work, for this design, we have chosen the idea to place the HTS coil in a sample chamber sandwiched between the PM rotors that provide an external magnetic field for the sample coil. The photographs of the measurement chamber are shown in Figure 5.2, in which two high-current withstood copper leads insulated by Kapton tape are used to run current into the sample chamber. The sample chamber is made with fibreglass reinforced epoxy with nonmagnetic characteristics to ensure obtaining reliable data in an AC magnetic field.

Three design aspects have the potential to affect the background flow, including the heat leak from the room temperature environment into the chamber through conduction, radiation and convection, potential eddy current losses in the isolation barrier, and leakage between the measurement chamber and outer cryostat [197]. While a perfect insulation system doesn't exist, properly designed cryostats can largely reduce the heat leak to a very low level. Moreover, the eddy current losses issue can be mitigated by employing a material for the barrier that is non-conductive. Whilst this seems like a trivial decision, in actuality, the specifically designed shape of the vacuum chamber and extremely low operating temperatures make it more challenging. Meanwhile, due to the cryogenic temperatures, the use of insulation materials for vacuum chamber are limited to those such as metals, reinforced plastics, resins, or specially treated glass, etc. Hence, care should be taken to ensure that the sample chamber is vacuum insulated and capable of withstanding extremely low cryogenic temperatures and high helium gas pressure, meaning that the material selection of the vacuum insulation need to be carefully considered, which is an important aspect of cryostat design.

In consideration of not lending to eddy current losses, cost, complexity, and safety concerns of manufacturing process, we decided to trial an assembly of Teflon, a synthetic polymer containing carbon and fluorine called polytetrafluoroethylene (PTFE), owing to this material being greatly heat-resistant, cold-resistant, chemical-resistant, and owning excellent dielectric properties, high thermal expansion coefficient and a low thermal conductivity. The top flange of the vacuum chamber is

equipped with a vacuum pumping port, thus being able to provide a vacuum shield for the sample chamber. As a result, the sample chamber for our design can be thermally shielded from the liquid nitrogen bath in which the measurement chamber and the permanent magnet reside. The sample chamber surrounded by the vacuum chamber is glued to a ConFlat (CF) flange and finished with a bottom cap. The top plate of the CF flange has ports for helium gas inlet and outlet, temperature sensor wiring, and the two HTS current leads. Besides, an indium seal is used on the CF flange to prevent liquid nitrogen and gas ingress.

5.3 Testing

5.3.1 Stator coil preparation

In order to further investigate the AC loss of 2G HTS coil at higher operating currents, in this section we prepared another 4 mm HTS coil as the stator winding of the new HTS machine demonstrator. The experimental 2G HTS tape was developed and supplied by SuperOx, which is based on Hastelloy C276 4 mm wide tape, consisting of two 4 mm tapes face-to face stacked together and soldered by PbSn.

The minimal critical current of the tape along overall length is 302.6 A at 77 K in a self-field condition according to the manufacturer's specification. As shown in Figure 5.3, after being insulated by Kapton tape, the sample coil (Coil 7) is successfully prepared, and its specifications are shown in Table 5.1.

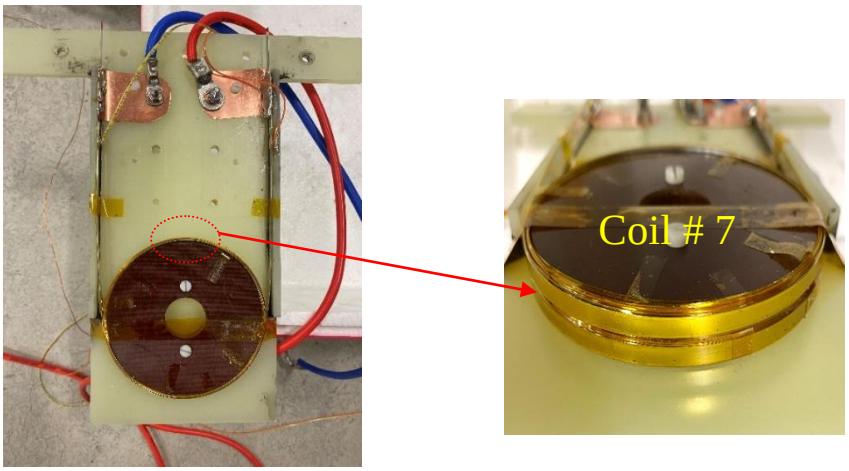

***Figure 5. 3**. Prepared sample coil (Coil 7) for HTS machine stator winding*

Table 5. 1: Coil 7 specifications

Parameter	Coil 7
Used HTS wire	4*4 mm SuperOx #1250C_stack(518-523)
Stack:	
Number of tapes in stack	2
Type	face-to-face
Solder	PbSn
Insulation	Kapton tape
Coil length	5 m
Total turns	16
Inner diameter	95 mm
Outer diameter	101 mm
Inductance	37.8 µH
Tape Min. I_c @77 K	302.6 A
Coil I_c (Self-field) @77 K	197 A

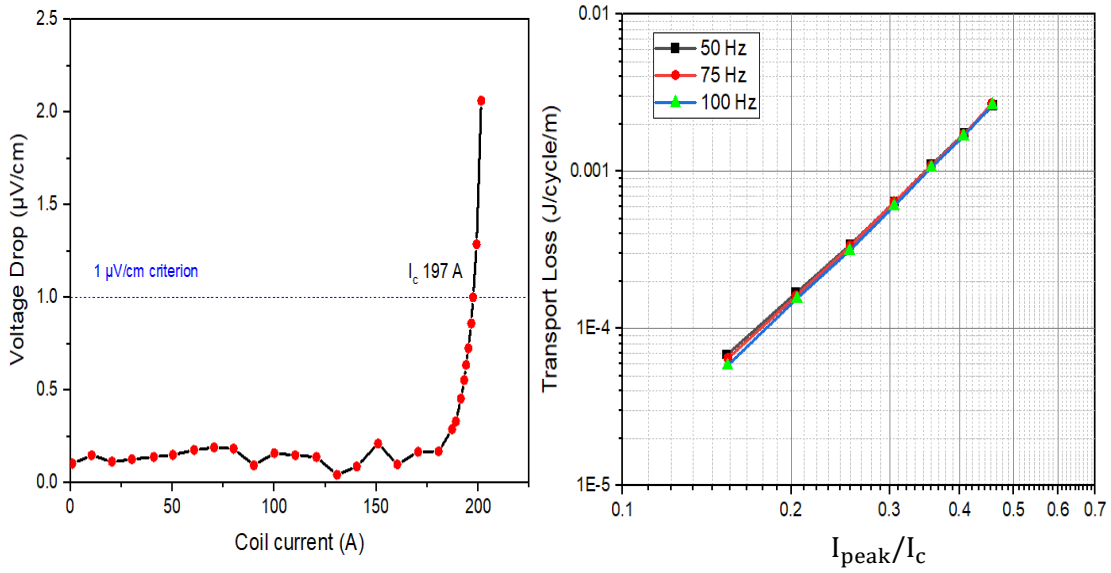

(a) (b)

Figure 5. 4. *Experimental measurements of Coil 7. (a) Critical current; (b) Transport AC loss*

The critical current of the coil sample was measured by a standard four-probe method under self-field conditions in liquid nitrogen at 77 K operating temperature, and the result is shown in Figure 5.4.a. The critical current of Coil 7 is 197 A at self-field, which is much higher than our previous experimental coils, and hence it can be used to study AC loss at higher operating currents.

Transport AC losses were then measured at 77 K in a liquid nitrogen bath using the platform illustrated in Figure 2.9, and the experimental results under different frequencies at 25 Hz, 50 Hz and 100 Hz respectively are shown in Figure 5.4.b, which indicates it is frequency independent over this range of variation. Finally, the prepared sample coil can be inserted into our new HTS machine platform for total AC loss measurement.

5.3.2 Testing procedure

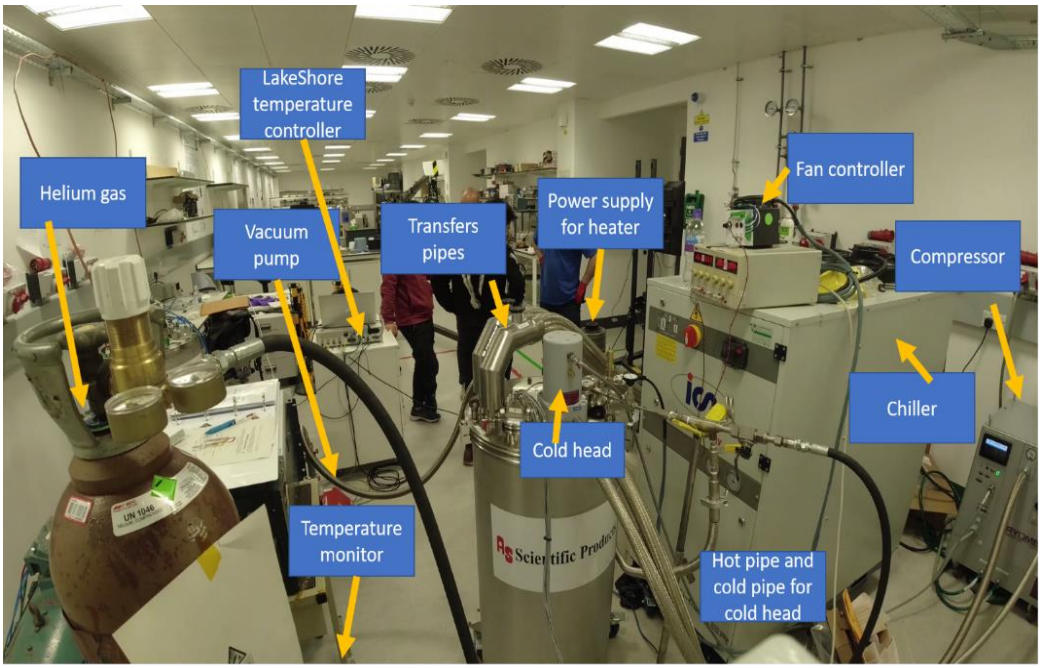

Figure 5. 5. *Helium circulation system configuration*

As shown in Figure 5.5, we have to test the whole helium gas circulation system before connecting it to a cryostat. The whole system setup includes a helium gas tank, a vacuum pump, a temperature monitor, a Lakeshore temperature controller, inner and outer helium gas pipes, a cryogenic fan, a power supply for the heater, a manifold, a cold head, a chiller, a water-cooled compressor, and a cryostat.

To begin with, in order to make the pressure reach the desired level, the cryostat should be fully vacuumed. The process starts with evacuating the vessel by turning on the black valve on the cryostat, then connecting the flexible pipes to the pump to evacuate the air inside until the desired pressure level is reached. Before adding helium gas into the system, we need to purge the manifold, which is used to connect between the hose of the helium bottle and the helium circulation system, and then turn on the vacuum valve and helium inlet valve. After infusing 1 bar helium gas to the pipes, the helium bottle valve should be closed and the pumping begun. The same

procedures are repeated by infusing 5 bar helium gas to the system, until the manifold is fully vacuumed.

After the evacuation work is finished, we can start to turn on the chiller, waiting for the temperature to decrease to around 283 K. Care should be taken to check the connections for any leakage, to properly connect the fan and to keep it closed. An input voltage at 24 V or 26.2 V from the DC power supply is applied, with the voltage level checked by the multi-meter connected with the fan. Then the temperature sensor at the end of transfer pipe is connected to the Lakeshore temperature controller and recorded on a computer.

Meanwhile, when the vacuum vessel pressure reaches the desired level, the compressor should be activated with the pressure level to be checked. Then the fan should be started with a low speed with the voltage for two leads at 0.5 V. During the process of the pipes cooling down, the helium gas pressure will drop with the decrease of temperature, so it is necessary for us to keep slowly filling the system with the gas from the helium inlet valve. When the temperature of the cold head on the cryostat reaches 100 K, the fan speed should be increased, and the voltage of the two leads should be changed to 2 V accordingly. Then when the temperature of cold head reaches 20 K, we can start to turn the fan with full speed at 4 V.

In order to arrange the helium gas temperatures, a heater with AC compensator is employed to increase the temperature. The heating power of the heater can be changed accordingly by modifying the input voltage. During the whole process, the pressure of helium gas must not exceed 12 bars to avoid the safety valve limit. It is important to keep watching the pressure gauge and, if it decreases, to add more helium gas slowly until reaching 5 bars.

Finally, the whole testing procedure for the helium circulation system is illustrated in Figure 5.6. We conducted the testing according to the whole procedures presented above. Under no load conditions, the test runs on the system took approximately 4 hours for the gas stream temperature to cool down to around 20 K from room temperature with pressure less than 10 bars. Then, this set-up can be installed in our

laboratory to be prepared for connecting with our new superconducting machine cryostat, to achieve the purpose of cooling down our sample coils in the HTS machine to less than 77 K temperatures.

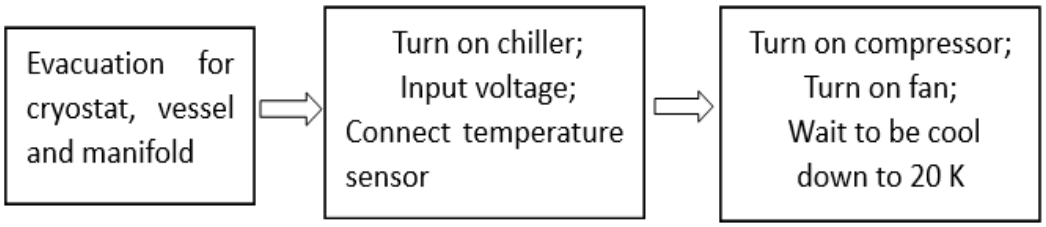

Figure 5. 6. *The whole working procedure for the helium gas circulation system*

5.3.3 AC loss measurement protocol

Before the AC loss measurement can be taken, a calibration process should be carried out based on system design. The calorimetric measurement system involves calculation of the heat load in the sample chamber due to the AC losses generated in the superconductor [196]. As the calculated AC losses involve many input helium flow parameters and potential static heat leaks through the vacuum jacket, the first step in the measurement process is to validate the measurement protocol, including obtaining the background value and terminal heat value, and then calibrating the system using a heater for the purpose of obtaining the relation between the heat load in the sample chamber and the corresponding temperature gradient of the helium stream across the sample chamber.

According to the platform setup, the total heat input to the measurement chamber consists of the following parts in Equation 5.2:

$$Q_{total} = Q_{HTS} + Q_{Background} + Q_{terminal} \tag{5.2}$$

Where Q_{total} refers to the total heat produced in the sample chamber, Q_{HTS} refers to the heat generated by the HTS coil AC losses, $Q_{Background}$ refers to the unavoidable

heat leakage in the system, and $Q_{terminal}$ refers to the Joule heat caused by copper terminal and soldering joint resistance between HTS and copper current leads. These losses in Equation 5.2 can be quantified by a set of calibration procedures.

To begin with, a background ΔT_B value needs to be obtained for reference, when there is no current through the system. Secondly, as shown in Figure 5.2, two terminals of the HTS coil are soldered to two copper current leads, and then connected to two copper bars to be fed through the top flange, so there exists resistance in copper bars and copper current leads and also a contact resistance in the soldering between the HTS and the copper current leads. When there is a transport current, there is a terminal heat loss. The impact of terminal resistance can be measured by shorting two copper terminals. Thus, a terminal ΔT_t value can be obtained and calibrated.

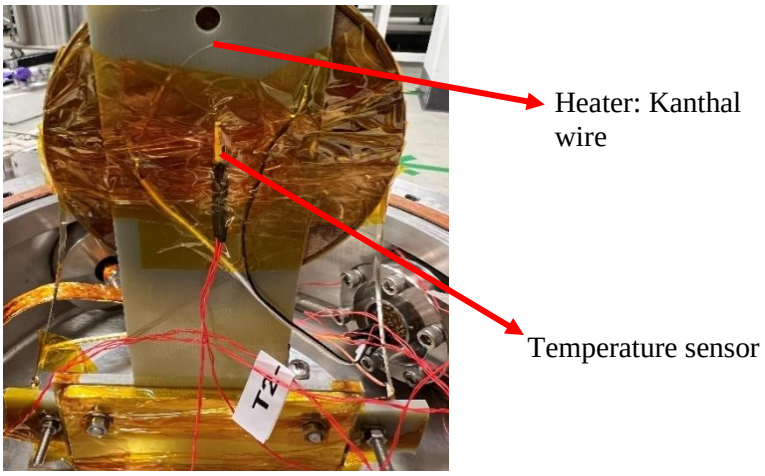

Figure 5. 7. *Calibration setup in the measurement chamber*

As shown in Figure 5.7, the calibration tests were performed using a resistive heater made of Kanthal wire installed in the sample chamber and connected to a DC power source. In the heater calibration procedure, several various DC voltages were applied in the experiments. The voltage drops across the resistive heater for a given current through the heater were measured using voltage taps attached to the heater. ΔT is the temperature difference between inlet and outlet helium streams of the sample chamber. Temperature control of the helium circulation system was performed by a Lakeshore

temperature controller. After cooling the sample chamber down to the set temperature, in the range of 20–40 K, as DC current through the heater was applied, the heat caused a rise of the sample temperature and ΔT started rising. When both the sample temperature and ΔT reached a stable value, ΔT was read along with the helium gas stream characteristics which are sampled to calculate the losses. Finally, when we calculated the HTS AC losses, the background loss and terminal loss were subtracted from total losses during the experiment.

Similarly, the measurement protocol used for calibration procedure described above can be applied for estimating AC losses of HTS coil. Since the mass flow rate cannot be recorded in this machine platform, so in our work instead of using Equation 5.1, a new methodology has been proposed: namely employing the relation between the heat load in the sample chamber Q_{Heater} and the corresponding temperature gradient of the helium stream across the sample chamber ΔT_H, the AC losses of sample coil Q_{HTS} can be calculated accordingly. In the AC loss measurements, the heat in the superconductor is generated due to the AC losses caused by an external AC magnetic field. The sample coil is cooled to the set temperature and the external magnetic field B_{ext} is applied. When the temperature and ΔT reach stable values, ΔT , B_{ext}, and frequency f are recorded. During the calibration process, we recorded the temperature rise ΔT resulted by the heat input for a resistive heater at different applied voltages, as a result, we can obtain the relation between the heat load in the sample chamber and the corresponding temperature gradient of the helium stream across the sample chamber. Therefore, when we put a HTS coil inside the sample chamber, by measuring the temperature difference between inlet and outlet helium streams of the sample chamber, then comparing with the relation we obtained from the heater in the calibration process, the AC losses of sample coil can be estimated accordingly. Finally, the whole process of the AC loss measurement protocol for our new HTS machine platform is illustrated in Figure 5.8.

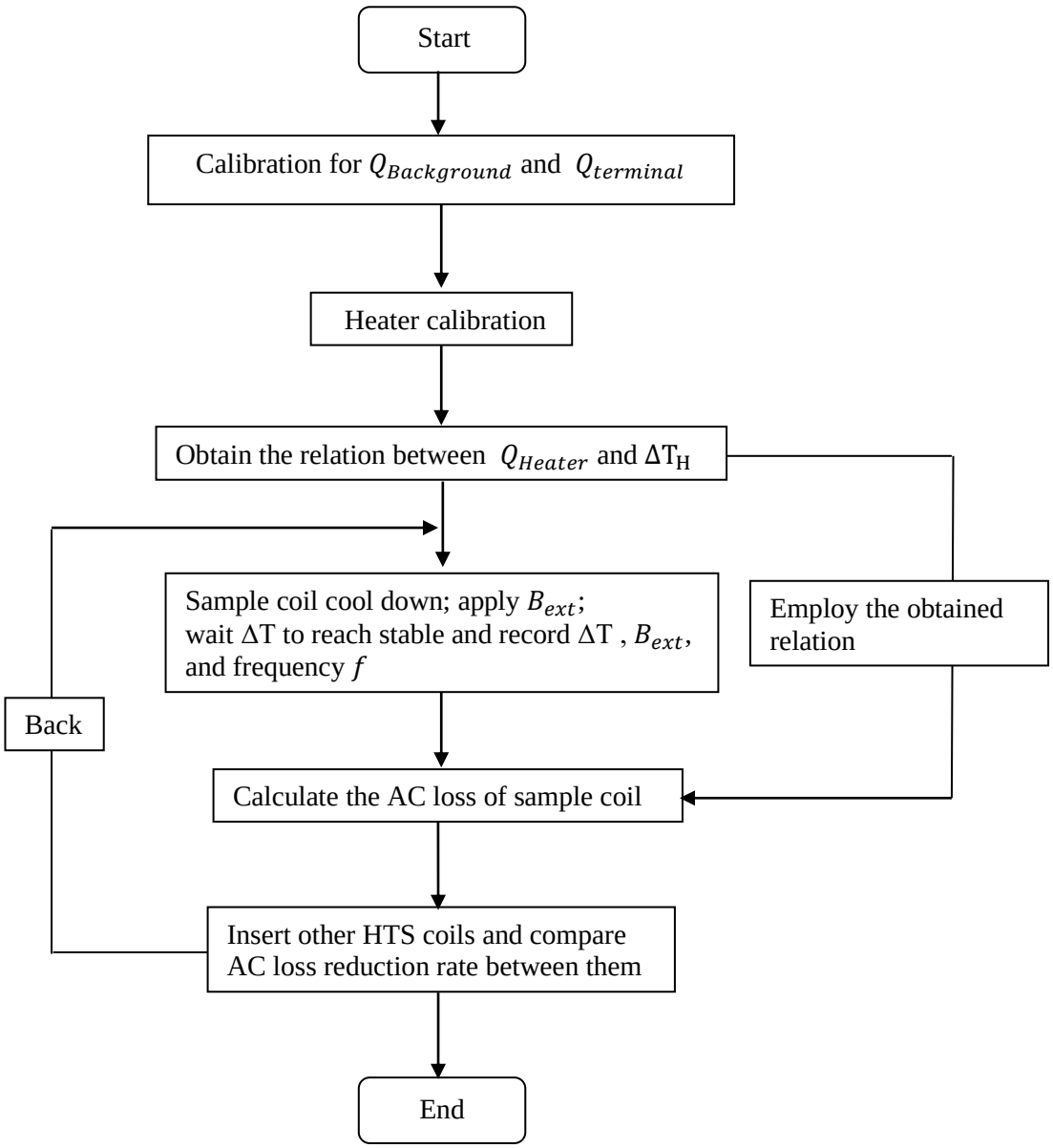

Figure 5. 8. *Flowchart of the AC loss measurement protocol for sample coils*

5.3.4 Challenges of AC loss measurement for HTS coils at temperatures lower than 77 K

As shown in Figure 5.9, a trial of initial testing was conducted using our new fully HTS machine platform according to the proposed measurement principles we presented in Section 5.3.3.

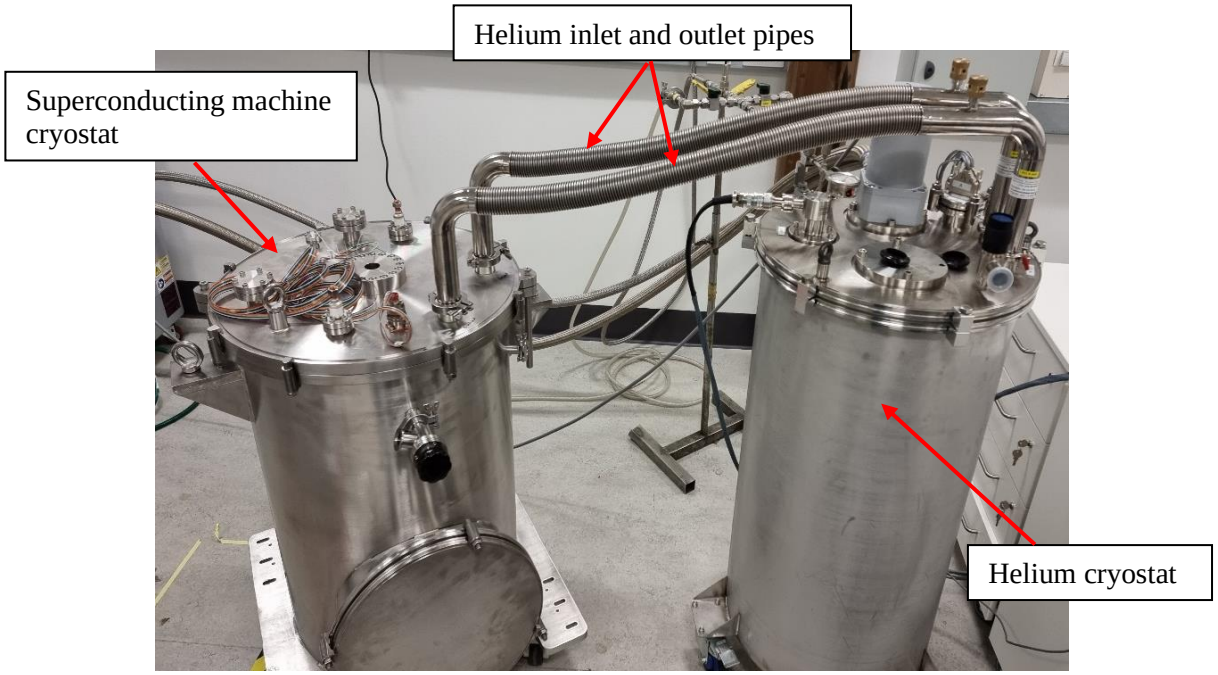

Figure 5. 9. *The initial testing using the new fully HTS machine platform*

However, of many challenges we have faced during the experimental process, the most urgent and problematic is that the sample chamber has slightly expanded at the helium cryogenic temperature, unfortunately thereby causing the leakage between measurement chamber and outer cryostat. As we addressed in Section 5.2.2, it is necessary to find more feasible materials for the follow-on studies, however, this conundrum still remain unsolved. According to [197] and based on several case studies, generally the following materials are suitable at cryogenic temperatures:

- ✓ Austenitic stainless steels e.g. 304, 316, 321
- ✓ Aluminium alloys e.g. 6061, 1100
- ✓ Copper e.g. OFHC, ETP and phosphorous deoxidized
- ✓ Brass
- ✓ Fibre reinforced plastics such as G-10 and G-11
- ✓ Quartz (used in windows)
- ✓ Teflon (depending on the application)
- ✓ Niobium and Titanium (frequently used in superconducting RF systems)
- ✓ Invar (Ni/Fe alloy) (useful in making washers due to its lower coefficient of expansion)
- ✓ Indium (used as an O ring material)
- ✓ Kapton and Mylar (used in Multilayer Insulation and as electrical insulation)

Of the materials above except Teflon, Quartz and Fibre reinforced plastics are other feasible options that do not lend to eddy current losses. However, making the item from one piece with Quartz was very difficult as it need to be machined into a specifically required shape for our sample chamber design. Limited by the technical aspects, it is impossible for our work at this moment. Machining the piece from G-10 also encountered significant challenges since it is an extremely abrasive material and the dust produced during machining is hazardous, which remains a particular problem as the requirement of milling depth is above 150 mm. Also, sourcing the appropriate block of G-10 is not that easy because it is usually woven into fixed standard dimensions of rods or tubes. Hence, useful strategies must be proposed as further improvements to address aforementioned challenges, in order to be successfully prepared for estimating the total AC losses of HTS coils using such new fully HTS machine platform in the future.

5.4 Conclusion

This chapter reports a pioneering testing platform for fully HTS machines developed by the Applied Superconducting Group in University of Strathclyde used for future electric aircraft propulsion. The system is able to provide a machine environment to measure the AC losses of HTS stator windings at temperatures lower than 77 K, by using the cryogenic helium circulation system as the cooling method. The design concept of the cryostat and the measurement protocol were described, and the corresponding testing setup and calibration procedures were also illustrated.

For the testing work, first of all, a stator HTS coil was successfully prepared and can be used to study AC loss at higher operating currents. Then, we conducted the corresponding testing procedures before connecting the helium circulation system to the new HTS machine cryostat. Moreover, it illustrated the calibration procedures and then proposed a methodology for calorimetric estimation of the AC losses for a HTS coil in our new system. Finally, a trial of initial testing was conducted, however due to the unsolved leakage between measurement chamber and outer cryostat, this system have not been properly put into use yet. Further improvements need to carefully consider the material selection of vacuum insulation for the sample chamber to prevent potential heat leak.

To sum up, through focus on calorimetrically quantifying the AC losses of HTS stator windings at lower cryogenic temperatures, the platform will further provide valuable insights into the HTS stator windings design in a rotational machine environment. With temperatures cooled down lower than 77 K, the HTS machines can operate at much higher currents, and achieve the possibilities to become more compact and lightweight, which can be used to further identify AC loss reduction technologies, compared with others we proposed before, thus contributing to the development of a highly efficient fully HTS propulsion machine performance. In the future, various 2G HTS coils as stator armature windings could be easily tested using this platform, with the aim of designing an HTS machine with higher efficiency.

Chapter 6

Conclusion

6.1 Thesis summary

This thesis presented the research on studying the AC loss of 2G HTS for the fully superconducting machine for future electric aircraft propulsion application purposes, including proposing several AC loss reduction strategies for stator armature windings design. Both experiments and models have been carried out and validated in order to investigate the performance of 2G HTS coils in a machine environment. For electrical machine application in electric aircraft, power densities are required to be significantly increased. Meanwhile, care should be taken for the reduction of AC losses to lower the constraint on the cryogenic cooling system. Thus, the AC losses of 2G HTS should be appropriately addressed and evaluated, and this is one of the primary factors for machine design and cryogenic cooling system design. Achieving lower AC losses for HTS coils in the machine environment can push the fully HTS machine forward to possible large-scale electric aircraft propulsion applications.

In Chapter 1, some fundamental theories of superconductivity and AC loss were explained. This chapter demonstrated the understanding of different types of superconductors including LTS and HTS, Type I and Type II superconductors, and 1G HTS and 2G HTS. It also illustrated the theory of critical current, AC loss types, AC loss technical importance, and the AC loss reduction challenges for designing a fully superconducting machine. These theories are the methodological foundation for the following research. Meanwhile, this chapter opened up the challenges that need to be addressed for the design of fully HTS superconducting machines, laying a solid basis

and delivering a helpful guideline for future research efforts.

Chapter 2 illustrated the experimental process for 2G HTS coil measurements. Firstly, this chapter compared two insulation methods including epoxy and non-epoxy materials for insulating 2G HTS tapes. In terms of critical current degradation, Kapton tape and heat shrink tubing were finally chosen for the following research investigations. This chapter then introduced the manufacturing procedure of 2G HTS coils. Two standard 4 mm double pancake HTS coils were prepared for measurements. For the critical current test, they were determined using the 1 μV/cm criterion. The transport loss, magnetization loss and total loss for the coils were measured using both the electrical and calorimetric methods. Last, this chapter introduced a fully HTS machine platform, focusing on calorimetrically quantifying the HTS stator and providing valuable insights into the AC losses of the HTS stator in a rotational machine environment.

Chapter 3 proposed three different AC loss reduction strategies. It successfully performed AC loss measurements and characterized the AC loss reduction rate for different multi-filament cables in transport AC loss as well as total loss in a rotational magnetic field. All the prepared multi-filament cables showed an obvious loss reduction in regard to both a self-field and a real machine environment to different extents. In the first and second strategy, a soldering layer and copper plating were present in the 3S coil and striated coil, respectively. When placed under a rotational magnetic field, the induced coupling losses originating from the soldering stack connections or via copper plating stabilizer could not be effectively suppressed, leading to the reduction rate achieved by these two strategies not being as expected. Therefore, this chapter proposed another new method to make multi-filament HTS cable with increased contact resistivity between filaments by using heat shrink tubing as insulation. Narrow HTS strips were directly stacked and insulated in a heat shrink tube insulation without soldering, hence further reducing or eliminating the coupling

losses, as confirmed by the experiment results.

Chapter 4 presented several 2D models of 2G HTS coils built by the H-formulation. This chapter introduced several FEM models and studied in detail the relationship between empirical data and simulation results. It validated the experimental transport AC loss measurements and confirmed the completeness of the model by the outputs of the AC loss calculation results. The modelling results and the measurements were in close agreement for most of the coils except Coil 3. This chapter then performed loss calculations for a thinner multi-filament coil (4*1 mm) and the simulation results showed further loss reduction up to around 90% compared with standard 4 mm coil. Additionally, this chapter also investigated the existence of soldering stack or copper plating in HTS coils on AC loss and current distribution. The study demonstrated the effectiveness of the AC loss reduction strategies we proposed of using 3S coil, striated coil, and multi-filament coil for design optimization, and offered suggestions for cable manufacture as well as the selection of stacking and insulation materials. The successful implementation of the 2D models in FEM software in this chapter enabled a systematic study of 2G HTS coils and laid a very powerful foundation for optimizing the superconducting machine design.

Chapter 5 reported a pioneering fully HTS machine demonstrator used for future electric aircraft propulsion applications. The system provided a machine environment to measure the AC losses of HTS stator windings at temperatures lower than 77 K, by using the cryogenic helium circulation system as the cooling method. Firstly, this chapter described the design concept of the cryostat as a background information. Then it successfully prepared a stator HTS coil used to study AC loss at higher operating currents. Moreover, this chapter illustrated the corresponding testing procedures. Last, the calibration process and AC loss measurement principles for the machine system were introduced in detail. Focusing on calorimetrically quantifying the electrical HTS stator at lower cryogenic temperatures, this fully HTS machine can

operate at much higher currents and will provide valuable insights into the AC losses of the HTS stator in a rotational machine environment, which can be used to further identify AC loss reduction technologies, thus contributing to the development of a highly efficient fully HTS propulsion machine performance.

6.2 Future work

Firstly, as we addressed in Section 3.5.2, when considering the multi-filament coils used for a practical propulsion system of an electric aircraft, the unavoidable induced harmonic currents in the system might have a significant impact on the total AC losses of the coil, and the eddy current losses will become dominant at higher frequencies. Therefore, further investigations regarding to the coil testing at frequencies of up to few hundreds of Hz or few kHz should be conducted in the future. Moreover, it is necessary to expand further studies in consideration of multi-filament coils with larger size since our experimental coils only consist of small number of turns, and the mechanical stability characteristics and AC loss estimation of the multi-filament coils under larger air-gap magnetic field need to be re-evaluated before applied for electric aircraft propulsion system.

Secondly, in term of the new methodology we proposed to reduce AC loss for multi-filament cables by employing heat shrink tubing as insulation. Section 3.4 demonstrated an example of producing 4*1 mm multi-filament cable, which was damaged during the winding and stacking process. In that work, stacking very thin trips together in a long conductor could lead to an increasing probability of the presence of defects blocking the current path between different filaments, and the potential appearance of imperfections of various types, which makes it extremely risky because the cable is easily damaged. Therefore, the main challenge is to find the balance between appropriate filaments selection and AC loss reduction through more

careful investigations for achieving maximum loss reduction in ways suitable for large-scale manufacture.

Thirdly, although our modelling work regarding to transport AC loss have been effectively validated, however, the total AC loss modelling of 2G HTS coils in a rotational magnetic field remains unsolved and many technical problems need to be addressed with optimized strategies. Further improvements could take a 3D FEM model into account, which can implement both parallel and perpendicular magnetic field components in the model, thereby being able to accurately estimate the total AC loss of 2G HTS coils in a HTS machine environment.

Besides, our experiment confirmed the effectiveness of striation technique for reducing the hysteretic AC losses, but large coupling losses were identified, leading to the total loss reduction of striated sample coil not proportional to the number of striations. Therefore, under the assumption if we increase the number of filaments achieved by the laser striation technique, the effect of copper plating existing in a striated coil with larger number of striations on AC losses should be carefully investigated in future work.

Last, as for the AC loss measurement at temperatures lower than 77 K, the follow-on study will be focused on the suitable insulation material selection for the sample chamber, and be prepared for characterizing the AC loss reduction rate of different HTS coils used as stator armature windings in our new machine platform. The newly designed fully HTS machine demonstrator can operate at higher operating current, higher output voltage, and higher operating frequency, with speed increasing from 300 RPM to 3000 RPM, and operating frequency increasing from 10 Hz to 100 Hz. Therefore, it is to be expected that with the rapid development of HTS technologies, the fully HTS machine will be applied for future electric aircraft propulsion system, ultimately, to maximize the efficiency.

References

[1] G. Bednorz and K. A. Mueller, “Possible High Tc Superconductivity in the Ba-La-Cu-O System,” *Z. Physik B Condensed Matter*, vol. 64, no. 2, pp. 189-193, 1986.

[2] H. Maeda, Y. Tanaka, M. Fukutumi, and T. Asano, “A new high-Tc oxide superconductor without a rare earth element,” *Jpn. J. Appl. Phys.*, vol. 27 L209, no. 2A, 1988.

[3] M.K. Wu, J.R. Ashburn, C.J. Torng, P.H. Hor, R.L. Meng, L. Gao, Z.J. Huang, Y.Q. Wang, and C.W. Chu, “Superconductivity at 93 K in a new mixed-phase Y-Ba-Cu-O compound system at ambient pressure,” *Phys. Rev. Lett.*, vol. 58, no. 9, pp. 908–910, 1987.

[4] J. Schwartz, et al., "High Field Superconducting Solenoids Via High Temperature Superconductors," *IEEE Trans. Appl. Supercond.*, vol. 18, no. 2, pp. 70-81, June 2008.

[5] M. Zhang, W. Wang, Y. R. Chen and T. Coombs, "Design Methodology of HTS Bulk Machine for Direct-Driven Wind Generation," *IEEE Trans. Appl. Supercond.*, vol. 22, no. 3, pp. 5201804-5201804, June 2012.

[6] R. C. Duckworth et al., "On the effect of NiW on the inductance and AC loss of HTS cables," *IEEE Trans. Appl. Supercond.*, vol. 15, no. 2, pp. 1578-1582, June 2005.

[7] M. Polak, E. Demencik, L. Jansak, P. Mozola, D. Aized, C. L. H. Thieme, G. A. Levin, and P. N. Barnes, “ac losses in a $YBa_2Cu_3O_{7-x}$ coil,” *Appl. Phys. Lett.*, vol. 88, no. 23, pp. 232501, 2006.

[8] J. -H. Kim, C. H. Kim, G. Iyyani, J. Kvitkovic and S. Pamidi, "Transport AC Loss Measurements in Superconducting Coils," *IEEE Trans. Appl. Supercond.*, vol. 21, no. 3, pp. 3269-3272, June 2011.

[9] J. Souc, E. Pardo, M. Vojenciak, and F. Gomory, “Theoretical and experimental study of ac loss in high temperature superconductor single pancake coils,” *Superconduc. Sci. Technol.*, vol. 22, no. 015006, 2009.

[10] M. Zhang, Jae-Ho. Kim, S.V. Pamidi, M. Chudy, W. Yuan, and T.A. Coombs, “Study of second generation, high-temperature superconducting coils: Determination of critical current,” *J. Appl. Phys.*, vol. 111, no. 083902, 2012.

[11] J.R. Clem, J.H. Claassen, and Y. Mawatari, “AC losses in a finite z stack using an anisotropic homogeneous-medium approximation,” *Supercond. Sci. Technol.*,

vol. 20, no. 1130, 2007.

[12] W. Yuan, A.M. Campbell, and T.A. Coombs, “Measurements and calculations of transport ac loss in second generation high temperature superconducting pancake coils,” *J. Appl. Phys*, vol. 107, no. 093909, 2010.

[13] K. P. Dahal, “Superconductivity: Chronology of Events and Hallmrk Developments,” *The Himalayan Physics*, vol.1, no.1, May 2010.

[14] J. Rhyner, “Magnetic properties and AC-losses of superconductors with power law current-voltage characteristics,” *Phys. C: Supercond.*, vol. 212, pp. 292–300, 1993.

[15] W. Meissner and R. Ochsenfeld, “Ein neuer effekt bei eintritt der supraleitfähigkeit,” *Naturwissenschaften*, vol. 21, no. 44, pp. 787-788, 1933.

[16] S. S. Kalsi, “Applications of high temperature superconductors to electric power equipment,” *John Wiley & Sons*, 2011.

[17] J. Bardeen, L. N. Cooper, and J. R. Schrieffer, “Microscopic theory of superconductivity,” *Physical Review*, vol. 106, no. 1, pp. 162, 1957.

[18] “BCS Theory of Superconductivity,” *HyperPhysics*, 7 September 2020. Available: http://hyperphysics.phy-astr.gsu.edu/hbase/Solids/bcs.html.

[19] M.-K. Wu et al., “Superconductivity at 93 K in a new mixed-phase Y-Ba-Cu-O compound system at ambient pressure,” *Phys. Rev. Lett.*, vol. 58, no. 9, pp. 908, 1987.

[20] H. Maeda, Y. Tanaka, M. Fukutomi, and T. Asano, "A new high-Tc oxide superconductor without a rare earth element," *Jpn. J. Appl. Phys.*, vol. 27, no. 2A, pp. L209, 1988.

[21] J. Tallon, et al., "High-Tc superconducting phases in the series $Bi_{2.1}(Ca, Sr)_{n+1}Cu_nO_{2n+4+\delta}$," *Nature*, vol. 333, no. 6169, pp. 153-156, 1988.

[22] Z. Sheng and A. Hermann, "Bulk superconductivity at 120 K in the Tl–Ca/Ba–Cu–O system," *Nature*, vol. 332, no. 6160, pp. 138-139, 1988.

[23] A. Schilling, M. Cantoni, J. Guo, and H. Ott, "Superconductivity above 130 K in the Hg–Ba–Ca–Cu–O system," *Nature*, vol. 363, no. 6424, pp. 56-58, 1993.

[24] W. Buckel and R. Kleiner, “Superconductivity: fundamentals and applications,” *John Wiley & Sons*, 2008.

[25] B. Shen, “Study of Second Generation High Temperature Superconductors: Electromagnetic Characteristics and AC Loss Analysis,” *Springer Theses*, Springer, Cham, 2020.

[26] D. Larbalestier, A. Gurevich, D.M. Feldmann, and A. Polyanskii, “High-Tc superconducting materials for electric power applications,” *Nature*, vol. 414, no. 371, 2001.

[27] D. Dew-Hughes, “Flux pinning mechanisms in type II superconductors,”

Philosophical Magazine, vol. 30, no. 2, pp. 293-305, 1974.

[28] H. Johnston, "Flux pinning in action," *Physics World*, 21 October 2011.

[29] H. F. Hess, R. B. Robinson, R. C. Dynes, J. M. Valles, and J. V. Waszczak, "Scanning-Tunneling-Microscope Observation of the Abrikosov Flux Lattice and the Density of States near and inside a Fluxoid," *Phys. Rev. Lett.*, vol. 62, no. 2, pp. 214–216, Jan. 1989.

[30] A. K. Jha and K. Matsumoto, "Superconductive REBCO Thin Films and Their Nanocomposites: The Role of Rare-Earth Oxides in Promoting Sustainable Energy," *Front. Phys.*, Sec. Physical Chemistry and Chemical Physics, 21 June 2019.

[31] M. N. Kunchur, "Current-induced pair breaking in magnesium diboride," *J Phys.: Condens. Matter*, vol. 16, pp. R1183–R1204, 2004.

[32] American Superconductor Corporation, Available: http://www.amsuper.com/, 2005.

[33] K. Sato, "3 - Bismuth-based oxide (BSCCO) high-temperature superconducting wires for power grid applications: Properties and fabrication," Editor(s): Christopher Rey, In Woodhead Publishing Series in Energy, Superconductors in the Power Grid, Woodhead Publishing, 2015.

[34] P. Sunwong, J. S. Higgins and D. P. Hampshire, "Angular, Temperature, and Strain Dependencies of the Critical Current of DI-BSCCO Tapes in High Magnetic Fields," *IEEE Trans. Appl. Supercond.*, vol. 21, no. 3, pp. 2840-2844, June 2011.

[35] Y. Nakamura, et al., "Effect of Bi2223 addition in precursor on the formation and Jc property of Bi2223 tapes sheathed with the Ag–Cu alloy," *Supercond. Sci. Technol.*, vol. 21, no. 035001, 2008.

[36] Y. Yang, et al., "Comparison of magnetically induced and transport current ac losses in silver-sheathed $(Bi,Pb)_2Sr_2Ca_2Cu_3O_{10}$ tapes," *Phys. C: Supercond.*, vol. 269, no. 3-4, pp. 349-353, 1 October 1996.

[37] T. Fukunaga et al., *Advances in Superconductivity VI: Proceedings of the 6th International Symposium on Superconductivity (ISS '93)*, Hiroshima vol. 1-2, October 26–29, 1993.

[38] Y. Iijima, K. Kakimoto, Y. Sutoh, S. Ajimura, and T. Saitoh, "Development of 100-m long Y-123 coated conductors processed by IBAD/PLD method," *Phys. C: Supercond.*, vol. 412, no. 2, pp. 801-806, 2004.

[39] M. Filipenko et al., "Concept design of a high power superconducting generator for future hybrid-electric aircraft," *Supercond. Sci. Technol.*, vol. 33 no. 054002, 2020.

[40] J. H. Durrell, et al., "A trapped field of 17.6 T in melt-processed, bulk Gd–Ba–Cu–O reinforced with shrink-fit steel," *Supercond. Sci. Technol.*, vol. 27, no.

082001, 2014.

[41] A. Patel, et al., “A trapped field of 17.7 T in a stack of high temperature superconducting tape,” *Supercond. Sci. Technol.*, vol. 31, no. 09LT01, 2018.

[42] K. S. Haran et al., "High power density superconducting rotating machines—development status and technology roadmap," *Supercond. Sci. Technol.*, vol. 30, no.123002, 2017.

[43] G. Nerowski, J. Frauenhofer, G. Ries, W. Nick and H.-W. Neumiiller, "Advances and prospects of HTS rotating machine development at Siemens," *IEEE Power Engineering Society General Meeting*, vol. 2, pp. 2052-2055, 2004.

[44] J. R. Bumby, *Superconducting rotating electrical machines*. Oxford University Press, 1983.

[45] H. D. Kim, G. V. Brown, and J. L. Felder, "Distributed turboelectric propulsion for hybrid wing body aircraft", *Proc. 9th Int. Power. Lift Conf.*, July 2008.

[46] D. Sekiguchi et al., "Trial Test of Fully HTS Induction/Synchronous Machine for Next Generation Electric Vehicle," *IEEE Trans. Appl. Supercond*., vol. 22, no. 3, pp. 5200904-5200904, June 2012.

[47] T. Takeda, H. Togawa, and T. Oota, "Development of liquid nitrogen-cooled full superconducting motor," *IHI Eng. Rev.*, vol. 39, pp. 89, 2006.

[48] Z. Huang, et al., "Trial Test of a Bulk-Type Fully HTS Synchronous Motor," *IEEE Trans. Appl. Supercond.*, vol. 24, no. 3, pp. 1-5, June 2014.

[49] T. M. Qu, et al., "Development and testing of a 2.5 kW synchronous generator with a high temperature superconducting stator and permanent magnet rotor," *Supercond. Sci. Technol.*, vol. 27, no. 044026, 2014.

[50] X. Song, et al., "Design Study of Fully Superconducting Wind Turbine Generators," *IEEE Trans. Appl. Supercond.*, vol. 25, no. 3, pp. 1-5, 2015.

[51] P. J. Masson, et al., “Development of a 3D sizing model for all superconducting machines for turbo-electric aircraft propulsion,” *IEEE Trans. Appl. Supercond.*, vol. 23, no. 3, pp. 3600805, 2013.

[52] H. Karmaker, D. Sarandria, M. T. Ho, J. Feng, D. Kulkarni, and G. Rupertus, "High-power dense electric propulsion motor," *IEEE Trans. Ind. Appl.*, vol. 51, no. 2, pp. 1341-1347, 2014.

[53] T. Keim, T. Laskaris, J. Fealey, and P. Rios, "Design and manufacture of a 20 MVA superconducting generator," *IEEE Trans. Power Appar.*, vol. PAS-104, no. 6, pp. 1474-1483, 1985.

[54] "Westinghouse Superconducting Generator Design," Report EPRI EL-577, Project RP429, 1977.

[55] B. B. Gamble and T. Keim, "High-power-density superconducting generator," *Journal of Energy*, vol. 6, no. 1, pp. 38-44, 1982.

[56] K. Yamaguchi et al., "70 MW class superconducting generator test," *IEEE Trans. Appl. Supercond*., vol. 9, no. 2, pp. 1209-1212, June 1999.

[57] S. S. Kalsi, "Development status of superconducting rotating machines," *IEEE Power Engineering Society Winter Meeting*. Conference Proceedings (Cat. No. 02CH37309), vol. 1, pp. 401-403, 2002.

[58] W. Nick, et al., "380 kW synchronous machine with HTS rotor windings—development at Siemens and first test results," *Phys. C: Supercond.*, vol. 372–376, pp. 1506–12, August 2002.

[59] H. Neumüller, et al., "Advances in and prospects for development of high-temperature superconductor rotating machines at Siemens," *Supercond. Sci. Technol.*, vol. 19, no. 3, pp. S114, 2006.

[60] W. Nick, M. Frank, G. Klaus, J. Frauenhofer, and H. Neumuller, "Operational experience with the world's first 3600 rpm 4 MVA generator at Siemens," *IEEE Trans. Appl. Supercond*., vol. 17, no. 2, pp. 2030-2033, 2007.

[61] J. Buck, B. Hartman, R. Ricket, B. Gamble, T. MacDonald, and G. Snitchler, "Factory testing of a 36.5 MW high temperature superconducting propulsion motor," Fuel Tank to Target: Building the Electric Fighting Ship at American Society of Naval Engineers Day, 2007.

[62] K. Sivasubramaniam, et al., "Development of a high speed HTS generator for airborne applications," *IEEE Trans. Appl. Supercond*., vol. 19, no. 3, pp. 1656-1661, 2009.

[63] K. S. Haran, D. Loder, T. O. Deppen and L. Zheng, "Actively Shielded High-Field Air-Core Superconducting Machines," *IEEE Trans. Appl. Supercond*., vol. 26, no. 2, pp. 98-105, March 2016.

[64] S. S. Kalsi, *Chapter 3.19: Ship Propulsion Motor Employing Bi-2223 and MgB2 Superconductors—Research, Fabrication and Applications of Bi-2223 HTS Wires*, Singapore: World Scientific, 2016.

[65] H. Sung, R. Badcock, Z. Jiang, J. Choi, M. Park, and I. Yu, "Design and heat load analysis of a 12 MW HTS wind power generator module employing a brushless HTS exciter," *IEEE Trans. Appl. Supercond*., vol. 26, no. 4, pp. 1-4, 2016.

[66] Airbus, "Airbus, Rolls-Royce, and Siemens team up for electric future Partnership launches E-Fan X hybrid-electric flight demonstrator," Airbus, November 2017. Available: https://www.airbus.com/newsroom/press-releases/en/2017/11/airbus--rolls-royce--and-siemens-team-up-for-electric future-par.html.

[67] NASA, "N3-X, Hybrid & Electric Airplane concepts," NASA, [Online]. Available: https://www1.grc.nasa.gov/aeronautics/hep/airplane-concepts/#n3x.

[68] C. A. Luongo, P. J. Masson, T. Nam, D. Mavris, H. D. Kim, G. V. Brown, M. Waters and D. Hall, "Next Generation More-Electric Aircraft: A Potential

Application for HTS Superconductors," *IEEE Trans. Appl. Supercond.*, vol. 19, no. 3, pp. 1055-1068, 2009.

[69] P. J. Masson and C. A. Luongo, "High power density superconducting motor for all-electric aircraft propulsion," *IEEE Trans. Appl. Supercond*., vol. 15, no. 2, pp. 2226-2229, 2005.

[70] IATA, "Aircraft Technology Roadmap to 2050," Available: https://www.iata.org/contentassets/8d19e716636a47c184e7221c77563c93/technology20roadmap20to20205020no20foreword.pdf.

[71] M. J. Armstrong, C. A. Ross, M. J. Blackwelder, and K. Rajashekara, "Propulsion system component considerations for NASA N3-X turboelectric distributed propulsion system," *SAE International Journal of Aerospace,* vol. 5, no. 2012-01-2165, pp. 344-353, 2012.

[72] J. L. Felder, G. V. Brown, H. DaeKim, and J. Chu, "Turboelectric distributed propulsion in a hybrid wing body aircraft," NASA Langley Research Center, 2011.

[73] G. Brown, "Weights and efficiencies of electric components of a turboelectric aircraft propulsion system," 49th AIAA aerospace sciences meeting including the new horizons forum and aerospace exposition, p. 225, 2011.

[74] Airbus, "Cryogenics and superconductivity for aircraft, explained," 29 March 2021. Available: https://www.airbus.com/en/newsroom/stories/2021-03 cryogenics and-superconductivity-for-aircraft-explained.

[75] M. Feddersen, et al., "AC Loss Analysis of MgB_2-Based Fully Superconducting Machines," *IOP Conf. Ser.: Mater. Sci. Eng.*, vol. 279, no. 012026, July 2017.

[76] W. J. Carr, *AC loss and macroscopic theory of superconductors*, 2nd ed. CRC Press, 2001.

[77] J. J. Rabbers, "AC loss in superconducting tapes and coils," Ph.D. dissertation, University of Twente, Enschede, the Netherlands, 2001.

[78] M. D. Ainslie, "Transport AC loss in high temperature superconducting coils," Ph.D. dissertation, University of Cambridge, UK, 2012.

[79] F. Grilli, E. Pardo, A. Stenvall, D. N. Nguyen, W. Yuan and F. Gömöry, "Computation of Losses in HTS Under the Action of Varying Magnetic Fields and Currents," *IEEE Trans. Appl. Supercond.*, vol. 24, no. 1, pp. 78-110, Feb 2014.

[80] A. A. Golubov, *Handbook of Applied Superconductivity*. IOP Publishing, vol. 1, ch. A2: Type II superconductivity, pp. 37–52, 1998.

[81] J. Sosnowski and H. Malinowski, "Magnetic Characteristics Measurements In Htc Superconductors," *Global Journal of Science Frontier Research Physics & Space Science*, version 1.0, vol. 12, no. 3, April 2012.

[82] S. Takacs, "Coupling Losses in Superconductors with Twisted Filaments,

Stripes, or Striations," *IEEE Trans. Appl. Supercond.*, vol. 17, no. 2, pp. 3151-3154, June 2007.

[83] M. M. Farhoudi, "AC loss in Ag/Bi-2223 tapes in AC field," Master's thesis, University of Wollongong, Wollongong, Australia, 2005.

[84] S. Takács, "Coupling losses in superconducting cables and their expected values in magnetic systems," Review, *Supercond. Sci. Technol*., vol. 10, pp. 733–748, July 1997.

[85] F. Gömöry and J. Sheng "Two methods of AC loss calculation in numerical modelling of superconducting coils," *Supercond. Sci. Technol*., vol. 30 no. 064005, 2017.

[86] K. Funaki, J. Fujikami, M. Iwakuma, H. Kasahara, S. Kawabata, Y. Tanaka, K. Ehara, "Uncertainty considerations in AC loss measurement of multifilamentary superconducting wires performed via a pickup coil method," *Cryogenics*, vol. 50, no. 2, 2010.

[87] M. P. Oomen, "AC loss in superconducting tapes and cables," Ph.D. dissertation, University of Twente, Enschede, The Netherlands, 2000.

[88] M. Staines, et al., "Cooling systems for HTS transformers: impact of cost, overload, and fault current performance expectations," 2nd International Workshop On Cooling Systems For HTS Applications (IWC-HTS). Karlsruhe, Germany, pp. 13–15, 2017.

[89] D. A. Cardwell and D. S. Ginley, *Handbook of superconducting materials*. CRC Press, 2003.

[90] R. Radebaugh, "Cryocoolers for aircraft superconducting generators and motors," *AIP Conf. Proc*., vol. 1434, pp. 171-182, 2012.

[91] A. P. Malozemoff, et al., "High-temperature Superconducting (HTS) AC Cables For Power Grid applications," *Superconductors in the Power Grid: Materials and Applications*, Woodhead Publishing Series in Energy, pp.133-188, 2015.

[92] P. N. Barnes, M. D. Sumption, and G. L. Rhoads, "Review of high-power density superconducting generators: present state and prospects for incorporating YBCO windings," *Cryogenics*, vol. 45, pp. 670–686, 2005.

[93] R. Jansen, G. V. Brown, and J. L. Felder, "Turboelectric Aircraft Drive Key Performance Parameters and Functional Requirements," *51st AIAA/SAE/ASEE Joint Propulsion Conference*, 2015.

[94] National Academies of Sciences Engineering & Medicine, "Commercial Aircraft Propulsion and Energy Systems Research: Reducing Global Carbon Emissions," First Edition, The National Academies Press, 2016.

[95] B. Pan, "Analysis of Eddy Current Loss of 120-kW High-Speed Permanent Magnet Synchronous Motor," *Machines*, vol. 10, no. 5, pp. 346, 2022.

[96] W. Goldacker, et al., "ROEBEL assembled coated conductors (RACC): preparation, properties and progress," *IEEE Trans. Appl. Supercond.,* vol. 17, no. 2, pp. 3398-3401, 2007.

[97] D. C. van der Laan, "$YBa_2Cu_3O_{7-\delta}$ coated conductor cabling for low ac-loss and high-field magnet applications," *Supercond. Sci. Technol*., vol. 22, no. 6, pp. 065013, 2009.

[98] C. A. Luongo, et al., "Next Generation More-Electric Aircraft: A Potential Application for HTS Superconductors," *IEEE Trans. Appl. Supercond.,* vol. 19, no. 3, pp. 1055-1068, June 2009.

[99] M. Henke, et al, "Challenges and opportunities of very light high performance electric drives for aviation," *Energies,* vol. 11, no. 2, pp. 344, 2018.

[100] M. Zhang et al., "AC Loss Measurements for 2G HTS Racetrack Coils With Heat-Shrink Tube Insulation," *IEEE Trans. Appl. Supercond.,* vol. 24, no. 3, pp. 1-4, June 2014.

[101] H. Zhang, Z. Wen, F. Grilli, K. Gyftakis, and M. Mueller, "Alternating Current Loss of Superconductors Applied to Superconducting Electrical Machines," *Energies,* vol. 14, no. 8, pp. 2234, 2021.

[102] Y. Wang, X. Guan, and J. Dai, "Review of AC loss measuring methods for HTS tape and unit," *IEEE Trans. Appl. Supercond.,* vol. 24, no. 5, pp. 1-6, 2014.

[103] C. Schmidt, K. Itoh, and H. Wada, "Second VAMAS AC loss measurement intercomparison: a.c. magnetization measurement of hysteresis and coupling losses in NbTi multifilamentary strands," *Cryogenics*, vol. 37, no. 2, pp. 77–89, 1997.

[104] H. Zhang, "Electromagnetic Characteristics of High Temperature Superconductor Coated Conductors Applied to Electric Machines," Ph.D. dissertation, University of Edinburgh, UK, 2021.

[105] S. Hahn, D. K. Park, J. Bascunan and Y. Iwasa, "HTS Pancake Coils Without Turn-to-Turn Insulation," *IEEE Trans. Appl. Supercond.,* vol. 21, no. 3, pp. 1592-1595, June 2011.

[106] Y. Li, et al., "Feasibility Study of the Impregnation of a No-Insulation HTS Coil Using Solder," *IEEE Trans. Appl. Supercond.,* vol. 28, no. 1, pp. 1-5, Jan. 2018.

[107] Y. Yanagisawa, K. Sato, R. Piao, H. Nakagome, T. Takematsu, T. Takao, H. Kamibayashi, M. Takahashi, H. Maeda, "Removal of degradation of the performance of an epoxy impregnated YBCO-coated conductor double pancake coil by using a polyimide-electrodeposited YBCO-coated conductor," *Phys. C: Supercond.,* vol. 476, pp. 19-22, 2012.

[108] C. Barth, et al., "Degradation free epoxy impregnation of REBCO coils and cables," *Supercond. Sci. Technol*., vol. 26, no. 055007, 2013.

[109] X. Wang, et al., “Turn-to-turn contact characteristics for an equivalent circuit model of no-insulation ReBCO pancake coil,” *Supercond. Sci. Technol.,* vol. 26 no. 035012, 2013.

[110] D. W. Hazelton, “Recent developments in 2G HTS coil technology,” *IEEE Trans. Appl. Supercond.*, vol. 19, no. 3, pp. 2218–2222, June 2009.

[111] G. Messina, M. Yazdani-Asrami, F. Marignetti and A. della Corte, "Characterization of HTS Coils for Superconducting Rotating Electric Machine Applications: Challenges, Material Selection, Winding Process, and Testing," *IEEE Trans. Appl. Supercond.*, vol. 31, no. 2, pp. 1-10, March 2021.

[112] T. Matsushita, “Measurement Methods for Critical Current Density ─ Flux Pinning in Superconductors,” Springer, Berlin, Heidelberg, 2007.

[113] E. F. Talantsev, “On the fundamental definition of critical current in superconductors,” Robinson Research Institute, Victoria University of Wellington, New Zealand, 2017.

[114] S. C. Wimbush and N. M. Strickland, "A Public Database of High-Temperature Superconductor Critical Current Data," *IEEE Trans. Appl. Supercond.,* vol. 27, no. 4, pp. 1-5, June 2017.

[115] S. Mukoyama, et al., “Study on AC loss measurements of HTS power cable for standardizing,” *J. Phys.: Conf. Ser.*, vol. 897, no. 012021, 2017.

[116] W. Yuan, et al, "Measurements and calculations of transport AC loss in second generation high temperature superconducting pancake coils", *J. Appl. Phys.*, vol. 110, no. 113906, 2011.

[117] H. Zhang, et al., “Alternating Current Loss of Superconductors Applied to Superconducting Electrical Machines,” *Energies*, vol. 14, no. 8, pp. 2234, 2021.

[118] R. Pei, A. Velichko, M. Majoros, Y. Jiang, R. Viznichenko, Z. Hong, R. Marchant, A. M. Campbell, and T. A. Coombs, “Ic and AC loss of 2G YBCO tape measurement for designing and fabrication of an HTS motor,” *IEEE Trans. Appl. Supercond.*, vol. 18, no. 2, pp. 1236–1239, Jun 2008.

[119] J. Kokavec, I. Hlasnik, and S. Fukui, “Very sensitive electric method for AC measurement in SC coils,” *IEEE Trans. Appl. Supercond.,* vol. 3, no. 1, pp. 153–155, 1993.

[120] J. Voccio, J.-H. Kim, and S. Pamidi, “Study of AC losses in a 1-m long HTS power cable made from wide 2G tapes,” *IEEE Trans. Appl. Supercond.*, vol. 22, no. 3, pp. 5800304, June 2012.

[121] J. Zhu, Z. Zhang, H. Zhang, M. Zhang, M. Qiu and W. Yuan, "Electric Measurement of the Critical Current, AC Loss, and Current Distribution of a Prototype HTS Cable," *IEEE Trans. Appl. Supercond*., vol. 24, no. 3, pp. 1-4, June 2014.

[122] D. Nguyen, Ph.D. thesis for Florida State University, Tallahassee, Florida, USA,

page 112, 2007.

[123] P. Zhou, G. Ma, and L. Quéval , "Transition frequency of transport ac losses in high temperature superconducting coated conductors," *J. Appl. Phys.*, vol. 126, no. 063901, 2019.

[124] Y. Yang, T. Hughes, C. Beduz, D. M. Spiller, R. G. Scurlock, and W. T. Norris, "The influence of geometry on self-field AC losses of Ag sheathed PbBi2223 tapes," *Phys. C: Supercond.*, vol. 256, no. 3-4, pp. 378-386, 1996.

[125] O. Tsukamoto, et al., "Origins of errors in AC transport current loss measurements of HTS tapes and methods to suppress errors," *IEEE Trans. Appl. Supercond.*, vol. 11, no. 1, pp. 2208-2211, March 2001.

[126] J. -H. Kim, C. H. Kim, G. Iyyani, J. Kvitkovic and S. Pamidi, "Transport AC Loss Measurements in Superconducting Coils," *IEEE Trans. Appl. Supercond*., vol. 21, no. 3, pp. 3269-3272, June 2011.

[127] N. Magnusson, S. Hornfeldt, J.J. Rabbers, B. Haken, and H. Kate, "Comparison between calorimetric and electromagnetic total ac loss measurement results on a bscco/ag tape," *Supercond. Sci. Technol*, vol. 13, no. 291, 2000.

[128] N. Magnusson, N. Schonborg, A. Wolfbrandt, and S. Hornfildt, "Improved experimental set-up for calorimetric ac loss measurements on HTS carrying transport currents in applied magnetic fields at variable temperatures," *Phys. C: Supercond.*, vol. 354, pp. 297–302, 2001.

[129] J. Ekin, *Experimental techniques*, Oxford University Press, 2006.

[130] M. Zhang, "Study of second-generation high temperature superconducting coils," Ph.D. dissertation, University of Cambridge, UK, 2013.

[131] H. Okamoto, F. Sumiyoshi, K. Miyoshi and Y. Suzuki, "The Nitrogen Boil-Off Method for Measuring AC Losses in HTS Coils," *IEEE Trans. Appl. Supercond.*, vol. 16, no. 2, pp. 105-107, 2006.

[132] Y. S. Wang, X. J. Guan and J. Shu, "Review of AC loss measuring methods for HTS tape and unit," IEEE International Conference on Applied Superconductivity and Electromagnetic Devices, pp. 560-566, 2013.

[133] F. Weng, M. Zhang, T. Lan, Y. Wang and W. Yuan, "Fully superconducting machine for electric aircraft propulsion: study of AC loss for HTS stator," *Supercond. Sci. Technol*., vol. 33, no.104002, 2020.

[134] F. Weng, M. Zhang, A. Elwakeel, T. Lan, N. McNeill and W. Yuan, "Transient Test and AC Loss Study of a Cryogenic Propulsion Unit for All Electric Aircraft," *IEEE Access*, vol. 9, pp. 59628-59636, 2021.

[135] M. Zhang, et al., "AC Loss Estimation of HTS Armature Windings for Electric Machines," *IEEE Trans. Appl. Supercond.*, vol. 23, no. 3, pp. 5900604-5900604, June 2013.

[136] M. Zhang, W. Yuan, J. Kvitkovic and S. Pamidi, "Total AC loss study of 2G

HTS coils for fully HTS machine applications," *Supercond. Sci. Technol*., vol. 28, no. 11501111, 2015.

[137] F. Grilli and A. Kario, "How filaments can reduce AC losses in HTS coated conductors: a review," *Supercond. Sci. Technol*., vol. 29, no. 083002, 2016.

[138] H. W. Neumuller, W. Nick, B. Wacker, M. Frank, G. Nerowski, J. Frauenhofer, W. Rzadki, and R. Hartig, "Advances in and prospects for development of high-temperature superconductor rotating machines at Siemens," *Supercond. Sci. Technol*., vol. 19, no. 3, pp. S114–S117, 2006.

[139] J. H. Kim et al., "Investigation of the Over Current Characteristics of HTS Tapes Considering the Application for HTS Power Devices," *IEEE Trans. Appl. Supercond*., vol. 18, no. 2, pp. 1139-1142, June 2008.

[140] D. Golovanov, L. Papini, D. Gerada, Z. Xu, and C. Gerada, "Multidomain Optimization of High-Power-Density PM Electrical Machines for System Architecture Selection," *IEEE Trans. Appl. Supercond*., vol. 65, no. 7, pp. 5302-5312, 2018.

[141] J. Šouc, et al., "Theoretical and experimental study of AC loss in high temperature superconductor single pancake coils," *Supercond. Sci. Technol*., vol. 22, no. 01500611, 2008.

[142] Z. Hong, W. Yuan, M. Ainslie, Y. Yan, R. Pei and T. A. Coombs, "AC Losses of Superconducting Racetrack Coil in Various Magnetic Conditions," *IEEE Trans. Appl. Supercond*., vol. 21, no. 3, pp. 2466-2469, June 2011.

[143] E. H. Brandt and M. Indenbom, "Type-II-superconductor strip with current in a perpendicular magnetic field," *Phys. Rev. B*, vol. 48, no. 12893, 1993.

[144] E. Zeldov, J. Clem, M. McElfresh and M. Darwin, "Magnetization and transport currents in thin superconducting films," *Phys. Rev. B*, vol. 49, no. 9802, 1994.

[145] W. Goldacker, et al., "Roebel cables from REBCO coated conductors: A one-century-old concept for the superconductivity of the future," *Supercond. Sci. Technol*., vol. 27, no. 9, 2014.

[146] D. C. Van der Laan, et al., "Engineering current density in excess of 200 A/mm-2 at 20 T in CORC magnet cables containing RE-123 tapes with 38 um tick substrates," *Supercond. Sci. Technol*., vol. 28, no. 124001, 2015.

[147] M. Marchevsky, E. Zhang, Y. Xie, V. Selvamanickam and P. G. Ganesan, "AC Losses and Magnetic Coupling in Multifilamentary 2G HTS Conductors and Tape Arrays," *IEEE Trans. Appl. Supercond*., vol. 19, no. 3, pp. 3094-3097, June 2009.

[148] S. Terzieva, et al., "Investigation of the effect of striated strands on the AC losses of 2G Roebel cables," *Supercond. Sci. Technol*., vol. 24, no. 045001, 2011.

[149] Z. Li, et al., "Development of a Novel Soldered-Stacked-Square (3S) HTS Wire

Using 2G Narrow Tapes With 1 mm Width," *IEEE Trans. Appl. Supercond.*, vol. 27, no. 4, pp. 1-4, June 2017.

[150] M. Wang, et al., “An effective way to reduce AC loss of second-generation high temperature superconductors,” *Supercond. Sci. Technol*., vol. 32, no. 01LT01, 2019.

[151] S. Ashworth and M. Suenaga, “The calorimetric measurement of losses in HTS tapes due to ac magnetic fields and transport currents,” *Phys. C: Supercond.*, vol. 315, pp. 79–84, 1999.

[152] T. Hardono, C. D. Cook and J. X. Jin, "Measurements of AC losses in HTSC wires exposed to an alternating field using calorimetric methods," *IEEE Trans. Appl. Supercond*., vol. 9, no. 2, pp. 813-816, June 1999.

[153] D. E. Daney, H. J. Boenig, M. P. Maley, D. E. McMurry and B. G. DeBlanc, "AC loss calorimeter for three-phase cable," *IEEE Trans. Appl. Supercond*., vol. 7, no. 2, pp. 310-313, June 1997.

[154] M. D. Sumption, E. W. Collings, and P. N. Barnes, “AC loss in striped multifilamentary YBCO coated conductors leading to designs for high frequencies and field-sweep magnitudes,” *Supercond. Sci. Technol.*, vol.18, pp. 122–134, 2005.

[155] D. W. Hazelton, Y. Y. Xie, Y. Qiao, E. Zhang, and V. Selvamanickam, U. Balachandran, Ed., “Superpower’s second generation HTS conductor design for stability and low ac losses,” Advances in Cryogenic Engineering: Transactions of the International Cryogenic Materials Conference - ICMC, vol. 52, pp. 859–868, 2006.

[156] S. P. Ashworth and F. Grilli, “A strategy for the reduction of ac losses in YBCO coated conductors,” *Supercond. Sci. Technol.*, vol. 19, pp. 227–232, 2006.

[157] P. Calvert, “Inkjet printing for materials and devices,” *Chem. Mater.*, vol. 13, pp. 3299–3305, 2001.

[158] F. A. List, T. Kodenkandath and M. W. Rupich, "Fabrication of Filamentary YBCO Coated Conductor by Inkjet Printing," *IEEE Trans. Appl. Supercond*., vol. 17, no. 2, pp. 3355-3358, June 2007.

[159] N. Magnuson, B. Bersos, and S. Hornfeldt, “Setup for calorimetric measurements of the ac loss in HTS tapes due to longitudinal magnetic fields and transport currents,” *Phys. C: Supercond.*, vol. 372–376, pp. 1762–1765, 2002.

[160] M. Polak, E. Usak, L. Jansak, E. Demencik, G. A. Levin, P. N. Barnes, D. Wehler, and B. Moenter, “Coupling losses and transverse resistivity of multifilament YBCO coated superconductors,” *J. Phys.: Conf. Ser.*, vol. 43, pp. 591–594, 2006.

[161] N. Amemiya, S. Kasai, K. Yoda, Z. Jiang, G. A. Levin, P. N. Barnes, and C. E. Oberly, “AC loss reduction of YBCO coated conductors by multifilamentary

structure," *Supercond. Sci. Technol.*, vol. 17, no. 12, pp. 1464–1471, 2004.

[162] M. Majoros, B. A. Glowacki, and A. M. Campbell, "Transport ac losses and screening properties of Bi-2223 multifilamentary tapes covered with magnetic materials," *Phys. C: Supercond.*, vol. 338, pp. 251–262, 2000.

[163] A. B. Yahia, X. Li, M. Majoros, M. D. Sumption and V. Selvamanickam, "AC Loss Reduction in Multifilamentary Coated Conductors With Transposed Filaments," *IEEE Trans. Appl. Supercond.*, vol. 27, no. 4, pp. 1-5, June 2017.

[164] J. Šouc, et al., "Low AC loss cable produced from transposed striated CC tapes," *Supercond. Sci. Technol.*, vol. 26, no. 7, 2013.

[165] D. Abraimov et al., "Significant reduction of AC losses in YBCO patterned coated conductors with transposed filaments," *Supercond. Sci. Technol.*, vol. 21, no. 8, 2008.

[166] J. C. Prestigiacomo, R. C. Y. Auyeung, and M. S. Osofsky, "Modeling the resistive critical current transitions of striated superconducting tapes," *IEEE Trans. Appl. Supercond.*, vol. 26, no. 8, Dec. 2016.

[167] A. Godfrin, et al., "Influence of the Striation Process and the Thickness of the Cu-Stabilization on the AC Magnetization Loss of Striated REBCO Tape," *IEEE Trans. Appl. Supercond.*, vol. 27, no. 6, pp. 1-9, Sept. 2017.

[168] Advanced Polymers, Vention Medical Company, Salem, NH, USA.

[169] E. Lavopa, P. Zanchetta, M. Sumner and F. Cupertino, "Real-Time Estimation of Fundamental Frequency and Harmonics for Active Shunt Power Filters in Aircraft Electrical Systems," *IEEE Trans. Appl. Supercond.*, vol. 56, no. 8, pp. 2875-2884, Aug. 2009.

[170] Z. Hong, A.M. Campbell, and T.A. Coombs, "Numerical solution of critical state in superconductivity by finite element software," *Supercond. Sci. Technol.*, vol. 19, pp. 1246–1252, 2006.

[171] G. Barnes, M. McCulloch, and D. Dew-Hughes, "Computer modelling of type II superconductors in applications," *Supercond. Sci. Technol.*, vol. 12, no. 518, 1999.

[172] T.A. Coombs, A.M. Campbell, A. Murphy, and M. Emmens, "A fast algorithm for calculating the critical state in superconductors, " *Int J for Computation and Maths. in Electrical and Electronic Eng.*, vol. 20, no. 1, pp. 240-252, 2001.

[173] N. Amemiya, S. Murasawa, N. Banno, and K. Miyamoto, "Numerical modelings of superconducting wires for ac loss calculations," *Phys. C: Supercond.*,vol. 310, pp. 16–29, 1998.

[174] G. Meunier, Y. Le Floch and C. Guerin, "A nonlinear circuit coupled t-t/sub 0/-/spl phi/ formulation for solid conductors," *IEEE Trans. Magn.*, vol. 39, no. 3, pp. 1729-1732, May 2003.

[175] R. Brambilla, F. Grilli, and L. Martini. "Development of an edge-element model

for ac loss computation of high-temperature superconductors," *Supercond. Sci. Technol.*, vol. 20, no. 1, 2007.

[176] S. Stavrev, et al., "Comparison of numerical methods for modeling of superconductors," *IEEE Trans. Magn.*, vol. 38, no. 2, pp. 849-852, March 2002.

[177] F. Grilli, et al., "Finite-element method modeling of superconductors: from 2-D to 3-D," *IEEE Trans. Appl. Supercond.*, vol. 15, no. 1, pp. 17-25, March 2005.

[178] S. Wimbush, N. Strickland, and A. Pantoja, *Critical current characterisation of Fujikura FESC 2G HTS superconducting wire*, Available: https://doi.org/10.6084/m9.figshare.c.2861821.v15.

[179] F. Gomory, et al., "AC losses in coated conductors," *Supercond. Sci. Technol.*, vol. 23, no. 3, pp. 034012, 2010.

[180] Y. Liu and K.N. Tu, "Low melting point solders based on Sn, Bi, and In elements," *Materials Today Advances*, vol. 8, no. 100115, pp. 2590-0498, 2020.

[181] D. R. Lide, *Properties of solids: Properties of superconductors – CRC handbook of chemistry and physics*, CRC Press, Boca Raton, pp. 64-94, 2004.

[182] M. Polak, E. Usak, L. Jansak, E. Demencik, G. A. Levin, P. N. Barnes, D. Wehler, and B. Moenter, "Coupling losses and transverse resistivity of multifilament YBCO coated superconductors," *J. Phys.: Conf. Ser.*, vol. 43, pp. 591–594, 2006.

[183] J. Ma, et al., "Impact of Stabilizer Layers on the Thermal-Electromagnetic Characteristics of Direct Current Carrying HTS Coated Conductors under Perpendicular AC Magnetic Fields," *IEEE Trans. Appl. Supercond.*, vol. 30, no. 4, pp. 1-6, June 2020.

[184] J. F. Maguire, et al., "Progress and Status of a 2G HTS Power Cable to Be Installed in the Long Island Power Authority (LIPA) Grid," *IEEE Trans. Appl. Supercond.*, vol. 21, no. 3, pp. 961-966, June 2011.

[185] S. Honjo, et al., "Status of Superconducting Cable Demonstration Project in Japan," *IEEE Trans. Appl. Supercond.*, vol. 21, no. 3, pp. 967-971, June 2011.

[186] S. Pamidi, C. H. Kim, J. Kim, D. Crook, and S. Dale, "Cryogenic helium gas circulation system for advanced characterization of superconducting cables and other devices," *Cryogenics*, vol. 52, no. 4–6, pp. 315–320, 2012.

[187] J. T. Kephart, et al., "High temperature superconducting degaussing from feasibility study to fleet adoption," *IEEE Trans. Appl. Supercond.*, vol. 21, no. 3, pp. 2229–2232, Jun. 2011.

[188] U. K. Sinha, et al., "Development and test of world's first industrial high temperature superconducting (HTS) power cable," *IEEE Power Engineering Society Winter Meeting*, Conference Proceedings (Cat. No.01CH37194), vol. 2, pp. 442-447, 2001.

[189] M. J. Cheadle, et al., "DC Superconducting Cable Using MgB_2 Wires," *IEEE*

Trans. Appl. Supercond., vol. 23, no. 3, pp. 6200805-6200805, June 2013.

[190] J. Kvitkovic, P. Patil, S. V. Pamidi, and J. Voccio, “Characterization of 2G superconductor magnetic shields at 40–77 K,” *IEEE Trans. Appl. Supercond*., vol. 21, no. 3, pp. 1477–1480, Jun. 2011.

[191] J. Kvitkovic, D. Davis, M. Zhang, and S. Pamidi, “Influence of interlayer separation on magnetic shielding properties of 2G HTS sheets made of 46 mm wide RABiTS tape,” *IEEE Trans. Appl. Supercond.*, vol. 23, no. 3, Jun. 2013.

[192] C. H. Kim, S. Kim, L. Graber, and S. Pamidi, “Cryogenic Thermal Studies on Terminations for Helium Gas Cooled Superconducting Cables,” *Physics Procedia*, vol. 67, pp. 201-207, 2015.

[193] B. K. Fitzpatrick, J. T. Kephartl and E. M. Golda, "Characterization of Gaseous Helium Flow Cryogen in a Flexible Cryostat for Naval Applications of High Temperature Superconductors," *IEEE Trans. Appl. Supercond*., vol. 17, no. 2, pp. 1752-1755, June 2007.

[194] J. T. Kephart, B. K. Fitzpatrick, P. Ferrara, M. Pyryt, J. Pienkos and E. M. Golda, "High Temperature Superconducting Degaussing From Feasibility Study to Fleet Adoption," *IEEE Trans. Appl. Supercond*., vol. 21, no. 3, pp. 2229-2232, June 2011.

[195] P. J. Ferrara, M. A. Uva and J. Nowlin, "Naval Ship-to-Shore High Temperature Superconducting Power Transmission Cable Feasibility," *IEEE Trans. Appl. Supercond*., vol. 21, no. 3, pp. 984-987, June 2011.

[196] J. Kvitkovic, D. Davis, M. Zhang and S. Pamidi, "Magnetic Shielding Characteristics of Second Generation High Temperature Superconductors at Variable Temperatures Obtained by Cryogenic Helium Gas Circulation," *IEEE Trans. Appl. Supercond.*, vol. 25, no. 3, pp. 1-4, June 2015.

[197] J. G. Weisend II, “Principles of cryostat design,” *Cryostat Design*, Principles and Engineering International Cryogenics Monograph Series (ICMS), Springer, pp. 1–45, 2016.